Electrospinning living bacteria into alginate-based nanofibers for biomedical applications

ELECTROSPINNING LIVING BACTERIA INTO ALGINATE-BASED NANOFIBERS FOR BIOMEDICAL APPLICATIONS

A Dissertation Presented

by

EMILY DIEP

Submitted to the Graduate School of the
University of Massachusetts Amherst in partial fulfillment
of the requirements for the degree of

DOCTOR OF PHILOSOPHY

February 2024

Department of Chemical Engineering

ELECTROSPINNING LIVING BACTERIA INTO ALGINATE-BASED NANOFIBERS FOR BIOMEDICAL APPLICATIONS

A Dissertation Presented

by

EMILY DIEP

Approved as to style and content by:

____
Jessica D. Schiffman, Chair

____
Lauren B. Andrews, Member

____
Jungwoo Lee, Member

____
D. Julian McClements, Member

____
Dimitrios Maroudas, Interim Department Head
Chemical Engineering Department

DEDICATION

To Ma Phi

ACKNOWLEDGMENTS

I would like to express my deepest appreciation and gratitude to my advisor Dr. Jessica D. Schiffman. Her guidance and support have been essential to not only the completion of my doctoral studies but also the development of the scientist and the person I am today. I am indescribably thankful for all the opportunities she encouraged me to pursue including controlling the directions of my research project, publishing papers, and going to conferences. Most of these opportunities terrified me, but she always knew when I needed a good push. Her enthusiasm and passion will forever inspire me to celebrate both successes and failures. No matter how big or small, these were opportunities to learn and grow.

I would like to thank my committee members for their support throughout my project. Dr. Lauren Andrews was kind enough to donate most of the bacteria used throughout this dissertation. She and her group were an incredible resource for all things bacteria-related. Dr. Jungwoo Lee has seen me through my qualification exam, my prospectus, and now my dissertation defense. His interest in and insights on alginate and the gastrointestinal tract were pivotal to this work. I want to thank Dr. D. Julian McClements for his contagious enthusiasm for probiotics and functional food. His work laid the groundwork for the gut delivery application of this dissertation and was an inspiration for one of the nanofiber formulations.

I would like to extend my sincere thanks to Dr. Nina Shapley and Dr. Benjamin J. Glasser from the Chemical Engineering Department at Rutgers University for my first experiences in research that encouraged me to pursue a PhD. Special thanks to Dr. Hao Chen with whom I conducted undergraduate research.

Many thanks to the former and current members of the Schiffman Lab Group: Dr. Aydin Cihanoglu, Dr. Kerianne M. Dobosz, Dr. Mengfei Huang, Dr. Priyanka Kaushik, Dr. Vanda Liadinskaia, Dr. Xiangxi (Zoey) Meng, Dr. Kelsi Rehmann, Prerana Rathore, Thilo Heckmann, Irene K. Kurtz, Brandon Barajas, Shao-Hsiang Hung, Rushabh Shah, Jichao Song, Hyerim Ban, Meng-Chen Chiang, Deepa Reddy Konuganti, Xi (Lindsay) Ning, and our mascot Finn. It was a pleasure to share a lab with you all. Thank you for all the conversations and hang-out sessions. I would like to thank the undergraduate students who have contributed to this work: Sarah Koprek, Anthony Dee, and Norah Nguyen.

Thanks to Jim Chambers, Shane Duclos, Dave Follette, Dennis Glick, Louis Raboin, Marie Wallace, Amity Lee, Anshalee Guarnieri, and Jessica Washer for their technical and logistical assistance. I am grateful for funding support from the Spaulding Smith Fellowship, PPG Fellowship, Soft Materials for Life Sciences Traineeship by the National Science Foundation, and Tillwick and Eldridge Award for Excellence as a Teaching Assistant award.

Words cannot express my gratitude to my parents, Andrew Diep and Phuong Le Diep, for their enduring support. To Paulina Diep (my sister and best friend) and Jashlie Anne Melgar (my best friend and sister), I don’t ever say it, but I love you. Thank you for pretending to know what I was talking about every time I talked about anything science. And thanks to my friends Jovelle Melgar, William E. Peralta, James O. Pasion, Megan Orense, Ariel Verzosa, and Dr. Allen C. Chang for their company.

ABSTRACT

ELECTROSPINNING LIVING BACTERIA INTO ALGINATE-BASED NANOFIBERS FOR BIOMEDICAL APPLICATIONS

FEBRUARY 2024

EMILY DIEP, B.S., RUTGERS UNIVERSITY

Ph.D., UNIVERSITY OF MASSACHUSETTS AMHERST

Directed by: Professor Jessica D. Schiffman

Bacteria play a pivotal role in daily life: from digesting nutrients to fighting off infections in the human body to degrading pollutants in the environment. In order to exploit the benefits that bacteria have to offer, the encapsulation systems are needed to keep bacteria alive and deliver them to various environments. Alginate is a polysaccharide derived from seaweed and a commonly used biomaterial. In particular, alginate nanofibers would be beneficial for the encapsulation and release of probiotic bacteria due to the biocompatibility of the biopolymer and high surface area to volume ratio of the nanofiber mat. Additionally, the flexible and porous nature of the nanofiber mat can easily be integrated into biomedical technologies like wound dressings. In my dissertation, I have developed probiotic-loaded, alginate-based nanofibers mats and demonstrated their use as an oral probiotic delivery and as an antimicrobial wound dressing.

The electrospinning of aqueous alginate solution into polymer nanofibers is challenging due to their high viscosity, surface tension, and conductivity; these factors were overcome using a biocompatible carrier polymer, polyethylene oxide (PEO), and an FDA-approved surfactant, polysorbate 80 (PS80). The effects of including PEO and PS80

in the precursor electrospinning solutions were systematically investigated to determine the influence of precursor solution properties on the formation and morphology of the electrospun nanofibers. The formation of smooth nanofibers was confirmed by scanning electron microscopy while Fourier transform infrared spectroscopy and thermogravimetric analysis were used to determine the chemical and mass composition of the electrospun fibers which differed from the composition of the precursor solution due to carrier polymer enrichment during electrospinning.

With the confirmation of alginate content in the electrospun nanofibers, I proceeded to crosslinking the alginate using calcium ions to create water-stable, biocompatible nanofibers. Aqueous and glycerol-based calcium crosslinking systems were explored as an alternative co-solvent to ethanol to create chemically resilient, alginate-based nanofibers. The alginate-to-carrier polymer and surfactant content in the nanofibers was influenced by the crosslinking solutions used. Furthermore, the nanofibers were generally stable in acidic environments and swelled in higher pH environments indicating their potential use in gut delivery.

A probiotic, *Lactococcus lactis*, was encapsulated within the alginate-based nanofibers using a coaxial electrospinning setup to achieve high bacteria loading ($>10^9$ colony forming units/g of as-spun electrospun mat). The aqueous and glycerol-based crosslinking systems allowed the encapsulated bacteria to survive. The encapsulated bacteria in these crosslinked alginate fibers were able to inhibit the growth of pathogenic *Staphylococcus aureus* for wound dressing applications. For the delivery of probiotics into the gut, antacid was formulated into the fibers to reduce acidic insult in a simulated stomach phase and demonstrate the targeted release of bacteria into the intestines.

Overall, this work provides important insights into the development and understanding of calcium crosslinked alginate nanofiber scaffolds while showing potential applications of such nanofibers for the encapsulation and delivery of beneficial biological materials.

TABLE OF CONTENTS

LIST OF TABLES

Table Page

LIST OF FIGURES

Figure Page

ABBREVIATIONS

$CaCl_2$: calcium chloride

$CaCO_3$: calcium carbonate

CFU: colony forming units

CMC: critical micelle concentration

DI water: deionized water

DMSO: dimethyl sulfoxide

E. coli: *Escherichia coli*

EDTA: Ethylenediaminetetraacetic acid

FDA: Food and Drug Administration

FTIR: Fourier Transform Infrared

GFP: Green-Fluorescent protein

GRAS: Generally regarded as safe

L. lactis: *Lactococcus lactis*

MW: molecular weight

OD: Optical density

OD600: Optical density at 600 nm wavelength

PEO: Polyethylene oxide

PVA: Polyvinyl alcohol

PS80: Polysorbate 80

S. aureus: *Staphylococcus aureus*

SA: Sodium alginate

SEM: Scanning electron microscopy

TGA: Thermal gravimetric analysis

UV-Vis: Ultraviolet-visible

CHAPTER 1

INTRODUCTION

Adapted from:

Diep, E.; Schiffman, J. D. Electrospinning Living Bacteria: A Review of Applications from Agriculture to Health Care. *ACS Appl. Bio Mater.* **2023**, *6* (3), 951–964. https://doi.org/10.1021/acsabm.2c01055.

1.1 Motivation

Bacteria, while infamously known for pathogenic infections, play a major positive role in everyday life – from helping with digestion to creating electricity.[1,2] In general, bacteria grow easily in nutrient-rich liquid media or in fermented foods like yogurt, kombucha, sauerkraut, kimchi, etc.[3] While ideal for bacterial growth, liquid cultures are only viable for a few days and tend to be difficult to maintain and transport.[4] Smaller frozen stocks of bacteria are easier to transport than liquid vats, remain viable for up to 3 years, and reduce chances of contamination.[5,6] Unfortunately, ice formation can puncture and kill bacterial cells. Moreover, maintaining low temperatures during transport and long-term storage is a costly challenge.[7] Dried bacteria can be used as powders that facilitates their transport, storage, and processing into various supplements.[5,8] Conventional drying methods lead to bacterial death due to heat and dehydration[5] whereas freeze drying or spray drying allow the bacteria to go into a dormant state while maintaining higher viability.[9] For freeze drying or spray drying, bacteria can be suspended in a solution with polymers or polysaccharides that form a protective encasing around bacteria cells to further improve their viability. Cell encapsulation technologies have been explored to address many of the aforementioned bacteria viability challenges.

Bacterial encapsulation is a technique that protects the bacteria by forming a physical barrier around the cell to support its structure and reduce contact with damaging agents.[10] For example, during freeze-drying, bacteria that were encapsulated within rice proteins had higher viability after processing, during storage at various temperatures, and in simulated gastrointestinal tract environments. While different approaches – spray drying, extrusion, emulsion, microfluidics, and 3D printing – are effective methods of encapsulating living microbes into polymer materials, additional drying can be required to store the bacteria over long periods of time.[6,11–15]

Alternatively, electrospinning allows live bacteria to be encapsulated within multifunctional, polymer nanofibers at room temperature.[16–20] The electrospinning process does not require the use of heating, freezing, or organic solvents which can harm encapsulant materials. Thus, suspensions of bacteria are blended into solutions compromised of various synthetic and naturally-derived polymers for electrospinning. Biopolymers dissolved in aqueous solutions are commonly used as they promote the viability of encapsulated cells within the fibers.[21] Thus, biologicals like cells,[18,22,23] proteins,[24] antibiotics,[25,26] and drugs[27–30] have been encapsulated via electrospinning; the high surface area of the cargo-loaded nanofiber mats enabled excellent delivery characteristics.[31] In conjunction with their excellent flexibility and porosity, nanofiber mats with encapsulated biologics hold great potential in wound dressing, protective coatings, and biological scaffolds.

1.2 Electrospinning

1.2.1. Basic setup and mechanism

The term "electrospinning" comes from a combination of the words "electrostatic" and "spinning" where "electrostatic" refers to the application of an electric field onto a precursor polymer solution to “spin” or form a polymer fiber.[32] As such, the electrospinning setup (**Figure 1**) often consists of a polymer solution or melt contained within a syringe with a metallic needle tip, a pump used to extrude the polymer at a constant rate, a metallic collector plate, and a voltage supply connecting the needle tip to the collector plate.[33,34] When the electric field is applied, the precursor solution becomes charged.[34] A buildup of charges on the surface of the polymer solution causes the droplet of the precursor to deform into a Taylor cone and eject a jet of polymer. Stabilizing forces, such as the viscosity of the precursor solution, prevent the electrospinning jet from fracturing into beads. The radial electric forces cause the jet to bend which evolves into coiling and whipping of the jet which helps to expel solvent from the nanofiber. Eventually, randomly collected nanofibers are deposited onto the collector plate as a nonwoven mat.

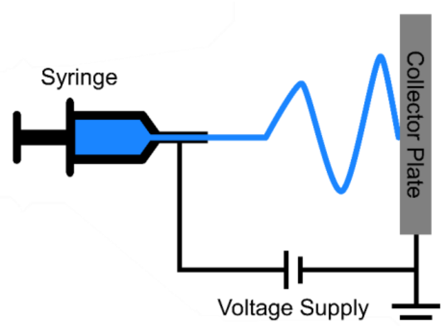

Figure 1: Illustration of the single needle electrospinning setup where an electric field is used to draw polymer nanofibers from a precursor solution. Adapted with permission from ref. 35. Copyright 2023 American Chemical Society.

1.2.2. Brief overview of electrospinning parameters

Both precursor solution components and properties as well as experimental parameters (needle tip-to-collector distance, needle diameter, humidity, temperature, etc.) influence the diameter and morphology of electrospun nanofibers.[28,33,34,36,37] These electrospinning factors are summarized in **Table 1**. Generally, each precursor solution depending on the polymer(s) and solvent(s) used have a set of optimal conditions under which fibers can form.[38] That is to say, there is no set numerical value of concentration, viscosity, conductivity, etc. under which all precursor solutions can be electrospun.

Table 1: Electrospinning parameters and properties summary

		Contribution to electrospinning	Effect of parameter or property	Ref
Solution Property	Polymer	Viscoelastic nature allows the precursor solution to be deformed by the electric field into a stable electrospinning jet and subsequent nanofiber	Low polymer concentration may not have enough polymer to form nanofiber High polymer concentration leads to thicker fibers until extremely high concentrations leads to high viscosity, surface tension, and needle clogging that prevents fiber formation	[39,40]
Solution Property	Molecular weight	Influences intermolecular interactions and/ or entanglement	Low molecular weight is challenging to electrospun due to lack of intermolecular interactions High molecular weight increases intermolecular interaction but increases viscosity	[41,42]
Solution Property	Solvent	Can be used to solvate polymer	Influences polymer behaviors (entanglement, flexibility, etc) and affect solution properties (viscosity, surface tension, conductivity, etc)	[37,43]
Solution Property	Viscosity	Measurement of internal friction in the polymer solution which has been correlated to the amount of polymer entanglements in solution	Nanofibers do not typically form without entanglements or intermolecular interactions High viscosities are difficult to overcome by the electric field	[44–46]
Solution Property	Surface Tension	Surface tension must be overcome by the electric field force for polymer chains to be pulled from solution	Low surface tension cannot stabilize the jet allowing too much solution to be pulled from the droplet High surface tension forces pull the electrospinning jet into spherical shapes which cause beading along the fiber	[46]
Solution Property	Conductivity	A measurement of free charges in the solution that can carry the force of the electric field	Strong repulsive charges can prevent polymer entanglement and break the electrospinning jet Low conductivity solutions are unaffected by the electric field	[45,46]
Electrospinning parameter	Flow rate & Needle size	Dictates the amount of polymer solution introduced to the electrospinning system	Beading can be caused when insufficient amounts of polymer High flow rates can increase fiber diameter or lead to wet fibers Needle diameter can be correlated to fiber diameter size and affects clogging or lack thereof during pumping	[44–47]
Electrospinning parameter	Tip-to-collector Distance	Distance over which entangled polymer chains are bent, whipped, and dried into a solidified nanofiber	Wet fibers form at close distances due to incomplete drying Far distances increase the amount of whipping and stretching but also decrease the strength of the electric field	[46,47]
Electrospinning parameter	Voltage	Driving force that draws entangled polymer chains from the electrospinning droplet	Must provide sufficient force for pulling polymer chains from solution without breaking the electrospinning jet	[39,44–47]
Electrospinning parameter	Temperature & Humidity	Determine drying conditions that are dependent on the solvent used	Faster drying can truncate an electrospinning jet, leading to a thicker fiber Slow drying rates can lead to thin fibers as the jet can stretch thinner. However, if the drying rate is too slow, fibers may never solidify	[44,48,49]

1.3 Encapsulation of bacteria via electrospinning

In the next sections, encapsulation of live bacteria cells due to the sink-like flow (illustrated in **Figure 2**) that forms during electrospinning is explained for two types of electrospinning setups. It is important to note that electrospinning factors like polymer selection, solvent selection, bacterial precursor solution concentration, applied voltage, and electrospinning environment are electrospinning parameters that have been found to influence either the loading or viability of electrospun bacteria, which will also be discussed.

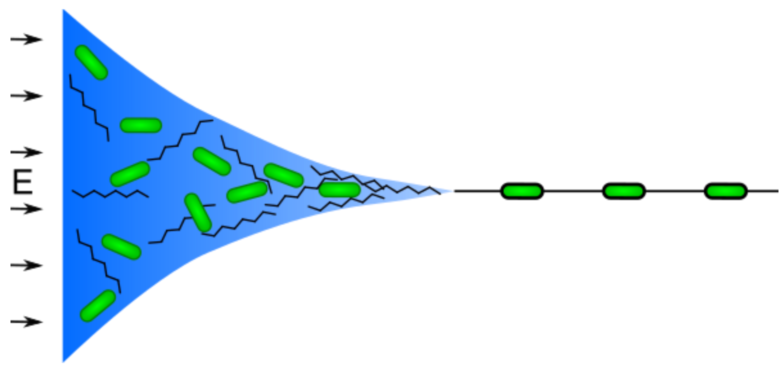

Figure 2: Illustration of sink-like flow forms during electrospinning that leads to the encapsulation of bacteria. This illustration was adapted with permissions from ref. 50. Copyright 2022 John Wiley & Sons, Inc.

1.3.1. Sink-like flow encapsulation using single needle electrospinning

Drug molecules,[30] proteins,[24,40] and DNA[33] cannot be electrospun on their own due to lack of entanglement and/or viscoelastic behavior. Instead, a carrier polymer can be used in the precursor solution wherein the polymer helps "carry along" the "non-electrospinnable" molecules during electrospinning. Larger materials like pigments, particles, and cells are pulled into a sink-like flow [18] that forms when the electrospinning jet is ejected from the precursor solution to be enveloped within the polymers during fiber formation. The concentration of encapsulants are usually directly proportional to the initial loading of encapsulants in the precursor solution.[51,52] For a more direct flow of encapsulants into the polymer solution, a more complex, coaxial electrospinning setup can be used.

1.3.2. Encapsulation via coaxial electrospinning

The coaxial electrospinning setup (**Figure 3**) extrudes two or more solutions from needles coaxially aligned and nested within each other.[53] During electrospinning, the polymer solutions may mix at the needle tip to create a blended fiber or be electrospun together into a layered fiber. Similar to the carrier polymer, the outer needle solution (also called the shell or sheath solution) is recommended to be an "electrospinnable" solution (discussed in the next section) such that the inner solution (also called the core solution) is carried along using interfacial forces. Not only is this an acceptable method for the encapsulation of materials, but control of respective flow rates also enables the controlled loading/ release of materials from the nanofibers.[54] Layered encapsulations, like coaxially electrospinning can provide, have led to improved stability and gastric survival of microencapsulated probiotics.[55]

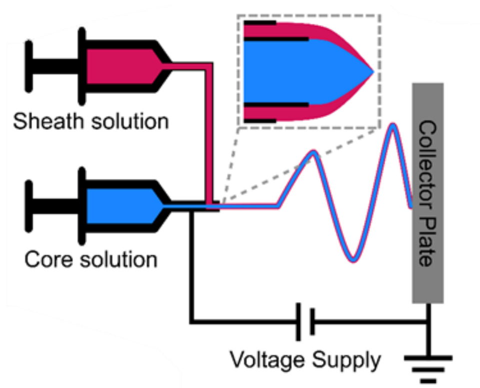

Figure 3: Illustration of coaxial electrospinning setup where a core solution and sheath or shell solution are drawn into a singular polymer nanofiber by the electric field. Adapted with permission from ref. 35. Copyright 2023 American Chemical Society.

1.3.3. Polymer and solvent selection

The most common way of fabricating nanofiber mats that contain bacteria is to blend the bacteria into the precursor solution that will be electrospun.[33,35] As such, the bacteria come into direct contact with the components of the precursor solution. Biocompatible polymers dissolved in aqueous solutions are often used for the electrospinning of bacteria as these components support bacteria viability. Synthetic, natural, and mixture of synthetic and natural polymer solutions have been used to encapsulate live bacteria using electrospinning.[21] While natural polymers can have inherent biocompatible properties, synthetic polymer are superior for mechanical properties leading to a grow field of electrospun composite fibers. As for solvents, most bacteria electrospinning studies use water.[19,35,56,57] One study encapsulated live bacteria into an organic solvent-based precursor solution using a coaxial electrospinning setup.[58] It was still necessary to suspend the bacteria in an aqueous solution to support their viability before being extruded into the core needle. A polymer dissolved in organic solvent was extruded from the sheath needle that encased the core solution. While some bacteria viability was detected, the researchers incubated the nanofibers in a nutrient-rich broth to regenerate the bacterial activity which was reduced after contact with the organic solvent.

1.3.3.1. Alginate

Alginate, a copolymer of β-(1–4) linked D-mannuronic acid units and α-(1–4)-linked L-guluronic acid units, is a polysaccharide primarily derived from algae but also produced by bacteria that is particularly advantageous for the encapsulation of bacteria due to its biocompatibility and for delivery into the gut due to its pH-controlled crosslinks and mucoadhesive properties.[59,60] Multivalent ions form a complex with the carboxylic acid groups along the alginate chain as shown in **Figure 4**. In fact, food grade alginate has been used as packaging for electrolyte drinks for runners in place of paper cups, as well as in cocktails and desserts as bursting favor bubbles.[61,62] For the delivery of specific materials like drugs into the intestines, calcium alginate structures remain stable in low pH environments like that of the stomach and swell in high pH environments like that of the intestines for targeted release.[63,64]

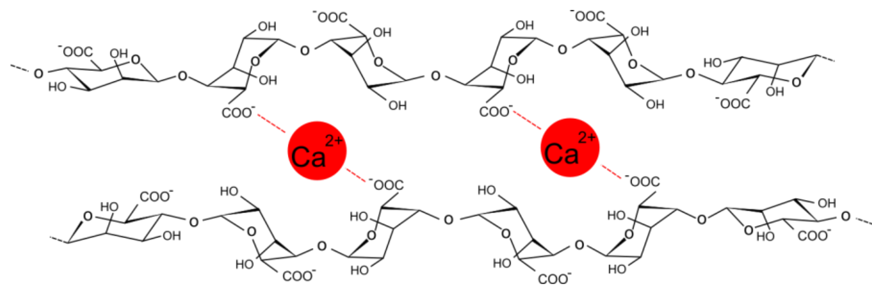

Figure 4: Schematic of egg-box model representing the ionic crosslinking of alginate chains with calcium ions.

Typically, alginate solutions are extruded into calcium-based gelling solutions to form calcium alginate hydrogel capsules. For drug delivery systems, the drug is blended into the alginate solution before gelation.[64,65] For example, a drug used for the treatment of hypertension, nicardipine HCl, was incorporated into the alginate solution before gelling to create drug-loaded calcium alginate beads.[66] The study showed that alginate gels can swell slightly at low pH allowing some of the drugs to diffuse out of the gel. However, the drug is completely released at pH > 7 due to both swelling and then erosion of the beads. Calcium alginate structures have also been used for the “triggerable” delivery of an antimalarial drug in the gastrointestinal tract of a Yorkshire pig model. Ethylenediaminetetraacetic acid (EDTA), a chelation agent, was used to release crosslinks in vitro in simulated gastric fluid and in vivo in pig model simulations and trigger the release of the drug.[67]

While calcium alginate can be processed into various form factors, the spherical particle or bead morphology has been widely used for biomedical and pharmaceutical applications including the encapsulation of proteins, drugs, and live cells.[11,68,69] Beads vary in size from a few microns to several nanometers in diameter usually formed by extrusion, emulsion, or aerosolization.[70] Larger microbeads affect sensory perception during ingestion and also may burst during mastication leading to a search for smaller encapsulation methods.[69] Drying these hydrogel capsules lower water content while increasing shelf life and stability.[71,72] However, drying can cause bacteria to die either by dehydration or injury.[11,73] Furthermore, spherical beads have a limited surface area to volume ratio compared to other morphologies.[74] Nanomaterials like electrospun nanofibers have been explored for drug delivery purposes due to their higher surface area to volume ratio.

Alginate is challenging to electrospin due to its charge, rigidity, and high viscosity. Organic solvents help to increase alginate chain flexibility to enable electrospinning. However, organic solvents tend to be toxic and are typically avoided for the encapsulation of live cells. Instead, several studies have electrospun alginate from aqueous solutions by using carrier polymers and surfactants. Carrier polymers like PEO and polyvinyl alcohol (PVA) form entanglements between and around alginate chains to carry the alginate along during electrospinning.[41,75] Surfactants lower surface tension and alter the conductivity of the precursor solution to produce smooth nanofibers.[23,76] After electrospinning, the alginate-based nanofibers can be ionically crosslinked with biocompatible calcium ions thus avoiding the use of damaging agents like free radicals or UV light. Typically, an ethanol co-solvent systems prevent the dissolution of the nanofibers during crosslinking in aqueous solutions.[41,77,78] Thus, the research of crosslinked alginate nanofibers for encapsulation of live cells has been limited.[23,79]

1.3.4. Bacterial loading in the precursor solution

The concentration of bacteria in the precursor solution can influence the encapsulant concentration in the final fiber. For the encapsulation of *Lactobacillus plantarum* in polyethylene oxide,[52] increasing the bacteria loading in the precursor solution (colony forming units or CFU/mL) by 10-fold led to 1000-fold increase in the bacteria concentration of the nanofiber mat (CFU/mg). Similarly, Kurečič et al.[80] found that increasing the bacterial loading of *Staphylococcus epidermis* from 1.1×10^9 CFU/mL to 1.6×10^9 CFU/mL lead to the bacteria loading increasing from $6.9 \pm 1.8 \times 10^5$ CFU/g to $2.0 \pm 0.3 \times 10^6$ CFU/g of their carboxymethylcellulose and PEO composite nanofiber. They also reported that the higher bacterial suspension led to a change in solution viscosity and conductivity. While solution properties are known to influence the formation and morphology of electrospun fibers,[23,28] more should be studied regarding their effects on the encapsulation of materials during electrospinning. Additionally, viability likely depends on the strain of bacteria encapsulated because some strains of bacteria could be more resistant to mechanical or oxidative stresses.[18]

1.3.5. Influence of the electric field on bacterial viability

The cells are pulled into a sink-like flow by the electric field during the formation of the electrospinning jet.[18,22–25] Despite the high voltage, multiple studies have shown high bacteria viability after electrospinning. During electrospinning, the current or flow of electrons traveling through the precursor solution, polymer nanofiber, and encapsulated bacteria remains low due to the high resistivity of the polymer and allow some bacteria to survive.[39,81] Some amount of cell death can still be expected due to osmotic stresses as moisture is wicked away as the fiber is whipped.[82] A handful of studies attempted to correlate applied voltage with bacteria viability in the encapsulated nanofiber. When Škrlec et al.[52] used an applied voltage of 15 kV (with a separation distance of 15 cm), the cells had a higher viability than when 20 kV was used, which led to a 2 log reduction compared to theoretical loading. However, other studies[83,84] showed that applied voltage did not significantly affect the viability of *Escherichia coli* (*E. coli*) Nissle electrospun into polyethylene glycol-polylactide and *Lactobacillus plantarum* in PVA. The effect of electrospinning voltage on the viability of bacteria may depend on the strain of bacteria and/or components of the precursor solution. Additional concerns surrounding death caused by the electric field, which applies a radial force causing the fiber to bend and whip.[34] Reznik et al.[85] determined this whipping force to be 5×10^3 g cm^{-1} s^{-2} which is smaller than the force a cell of *E. coli* can withstand which was determined to be 3×10^6 g cm^{-1} s^{-2}.[18]

1.3.6. Electrospun bacteria – a short literature review

Electrospun nanofibers have shown excellent capabilities for encapsulation high loading of probiotic bacteria and keeping viability throughout storage. The largest area of research for electrospun bacteria is intended for the gut delivery of probiotic bacteria. However, there is a rising interest in the delivery of beneficial bacteria to other areas of the body like the skin or the vagina as well as the encapsulation of bacteria for environmental uses like water purification, plant growth promotion, and alternative electricity production. A summary of electrospun bacteria for these various applications is provided in **Table 2**.

Table 2: Summary of electrospun bacteria. This table is reproduced with permission from ref. 35. Copyright 2023 American Chemical Society.

Probiotic strain	Precursor solution(s)	Bacterial loading in nanofibers	Ref
Oral Probiotic Applications			

Bifidobacterium animalis	Sheath: PVA in water *Core: Skim milk	Not quantified	[22]
Escherichia coli K12	SA/PEO/PS80 in water	2.74×10^5 CFU/g	[23]
Escherichia coli Nissle	Sheath: Polyethylene glycol-polylactide in dichloromethane/dimethylformamide *Core: Polyvinylpyrrolidone or glycerol	5×10^5 CFU/mg	[83]
Lactobacillus plantarum	PVA and fructoolgiosaccharides in water	8.88 log(CFU/mL)	[84]
Clostridium butyricum	Hydroxypropyl-beta-cyclodextrin	$>10^8$ CFU	[86]
Lactobacillus acidophilus *Lactobacillus rhamnosus* *Bifidobacterium bifidum* *Bifidobacterium animalis*	SA and corn starch in water	>9 log(CFU/mL) starting loading in gastric fluid	[87,88]
Lactobacillus acidophilus	Gum arabic and PVA in water	>9.97 log(CFU/g)	[89]
Lactobacillus paracasei	SA and PVA in water	8.57 log(CFU/g)	[79]
Wound dressing applications			
Staphylococcus epidermidis	Carboxymethylcellulose and PEO in water	$6.9 \pm 1.8 \times 10^5 – 2.0 \pm 0.3 \times 10^5$ CFU/g	[80]
Enterococcus mundtii	PVA/ polyvinylpyrrolidone/ glycerol in water	>8 log(CFU/g)	[90]
Vaginal probiotic application			
Lactobacillus acidophilus	PVA and polyvinylpyrrolidone in water	8.87 – 9.28 log(CFU) per g of fiber	[17]
Lactobacillus acidophilus *Lactobacillus delbrueckii ssp. Bulgaricus* *Lactobacillus casei* *Lactobacillus gasseri* *Lactobacillus paracasei* *Lactobacillus plantarum* *Lactobacillus reuteri* *Lactobacillus rhamnosus* *Lactobacillus salivarius* *Lactococcus lactis*	PEO in water	9.18 ± 0.21 log (CFU/mg) 5.91 ± 0.15 log (CFU/mg) 7.33 ± 0.19 log (CFU/mg) 9.20 ± 0.11 log (CFU/mg) 8.02 ± 0.18 log (CFU/mg) 8.70 ± 0.38 log (CFU/mg) 9.32 ± 0.04 log (CFU/mg) 7.41 ± 0.16 log (CFU/mg) 6.75 ± 0.07 log (CFU/mg) 8.19 ± 0.33 log (CFU/mg)	[19]
Lactobacillus plantarum	PEO in water	7.6×10^6 CFU/mg	[52]
Lactobacillus gasseri *Lactobacillus rhamnosus*	PVA in water	$>10^7$ CFU/g	[91]
Lactobacillus crispatus *Lactobacillus gasseri* *Lactobacillus jensenii*	PEO and sucrose in water	>10 log(CFU/g)	[92]
Seed coatings			
Methylobacterim aminovorans	PVA in water	6.6×10^5 CFU/g	[93]

Pantoea agglomerans ISIB55 *Burkholderia caribensis ISIB40*	PVA in water with and without glycerol	>7.42 ± 0.02 log (CFU/g) >7.23 ± 0.02 log (CFU/g)	94
Bradyrhizobium japonicum SEMIA 5079 and *Bradyrhizobium elkanii SEMIA 587*	PVA in water	4.29×10^5 CFU/seed	95
Bifidobacterium subtilis and *Serratia marcescens*	PVA, polyvinylpyrrolidone, and glycerol in water	5.7 ± 0.48 log (CFU/seed)	96
Bioremediation			
Pseudomonas aeruginosa	Sheath: Polyvinylpyrrolidone and polyvinylidene fluoride-co-hexafluoropropylene in tetrahydrofuran and dimethylformamide *Core: Water	Not quantified	58
Pseudomonas aeruginosa	PVA or PEO in water	10^7-10^8 CFU/mL per 10 mg of polyvinyl alcohol web 10^8 CFU/mL per 10 mg of polyethylene oxide web	97
Lysinibacillus sphaericus	Cyclodextrin in water and skim milk	6.0×10^2 CFU/mL after storage at 4 °C for 24 hr	98
Microbial Fuel Cells			
Electroactive consortia	PEO in water	Not quantified	99
Shewanella oneidensis	Sheath: Poly(ε-caprolactone) in chloroform/dimethylformamide *Core: PEO in phosphate buffer saline	Not quantified	100

* The probiotic strain was blended into the core precursor solution during coaxial electrospinning

Few studies have investigated the gut fate of probiotic-loaded nanofibers. PEO and PVA are commonly electrospun for the encapsulation of bacteria.[56] As water-soluble polymers, the release of the bacteria from these polymer nanofibers would occur rapidly in aqueous environments like that of the internal human body. Other functional polymers can be incorporated into the precursor solution to affect the release of probiotics from the fibers. *Lactobacillus acidophilus* encapsulated within a mixture of gum arabic and PVA electrospun nanofibers showed survivability after exposure to simulated gastric fluid for 150 min.[89] While typically used as an emulsifier or thickening agent in food products, gum arabic has been used in a variety of encapsulation technologies for delivery into the gut. Other polymers like alginate have proven useful for the delayed release of materials into the intestines.[64,101,102] More specifically, alginate hydrogels contract in acidic environments to protect encapsulants from acid damage in the stomach. In the intestines, swelling of the alginate structure due to higher pH releases encapsulants.[69,103,104] Several strains of bacteria have been electrospun into alginate-based nanofibers.[23,79,87,88] Alginate-based encapsulations improved the acid tolerance and viability of probiotics in simulated gastrointestinal systems as compared to free cells.[79,87] Furthermore, alginate favorably binds with the intestinal mucosa to prolong the delivery of drugs.[59,60]

CHAPTER 2

DISSERTATION OBJECTIVES

2.1 Broad Scope

Living bacteria are used in biotechnologies that lead to improvements in healthcare, agriculture, and energy.[35] Electrospinning bacteria into flexible and functional electrospun polymer fabrics maintain their viability and enable further use.[33] Blending bacteria into the polymer solution allows the bacteria to be encapsulated within the nanofiber during electrospinning without the use of extreme heat or temperature differences typically used to store bacteria for long periods of time. Research[17,33] has shown that electrospinning is effective for encapsulating large quantities of viable bacteria in dry, stable fibers. Several polymers, both synthetic and natural, have been electrospun.[21] Alginate is a fascinating polymer favored for its biocompatibility and gelatin under mild conditions using calcium ions. Furthermore, alginate exhibits pH-dependent behavior which can control the delivery of viable bacteria directly to the gut microbiota.[63,64] I electrospun bacteria into alginate-based nanofibers for biomedical applications through four objectives briefly summarized below. Materials and methods are outlined in **Chapter 3**. Subsequent Chapters contain results, discussion, and future work.

2.2 Objective 1: Formation of alginate-based electrospun nanofibers

First, the formation of alginate-based nanofibers was initiated using a carrier polymer and surfactant. Alginate has a rigid structure that makes it a challenge to electrospin from aqueous solutions. I proposed using biocompatible polyethylene oxide as a carrier polymer and FDA-approved polysorbate 80 as a surfactant to electrospin high content alginate nanofibers. Solution characteristics were monitored to determine their effects on the fiber formation, diameter, and morphology of electrospun fibers. Scanning electron microscopy (SEM) was used to image the fibers. Fourier transform infrared (FTIR) analysis and thermogravimetric analysis (TGA) confirmed the chemical composition of the nanofiber.

2.3 Objective 2: Encapsulation of live bacteria into alginate-based nanofibers

Second, live bacteria were introduced into the system for encapsulation. The bacterial suspension changes the properties of the precursor solution requiring the system to be reoptimized. Once the bacteria are encapsulated, the bacterial loading within the nanofiber can be determined. Both single needle and coaxial electrospinning setup were employed to maximize the bacteria loading in the electrospun fiber. Furthermore, a few strains were encapsulated including the lab standard *E. coli* K12 and probiotics *E. coli* Nissle and *Lactococcus lactis* (*L. lactis*).

2.4 Objective 3: Calcium crosslinking of alginate-based nanofibers

Third, the alginate-based fibers can be crosslinked with calcium ions to stabilize the nanofiber structure in aqueous environments. Since current methods of crosslinking alginate nanofibers require the use of ethanol, ethanol-free crosslinking systems were explored in order to support the viability of encapsulated bacteria. The challenge in this objective was preventing dissolution of the water soluble alginate chains out of the electrospun nanofiber during crosslinking in aqueous solutions while using only generally regarded as safe (GRAS) agents. Both crosslinking pH and a glycerol co-solvent were explored. After crosslinking, the stability of the nanofiber structure was determined in pure water, acidic buffer, and phosphate buffer saline.

2.5 Objective 4: Applications of bacteria-loaded fibers

After confirming the viability and loading of probiotics in the electrospun and crosslinked nanofibers, applications of these bacteria-loaded nanofibers were explored. *L. lactis* has been shown to inhibit the growth of methicillin-resistant *S. aureus* (MRSA). By electrospinning *L. lactis* into polymer nanofibers, the antimicrobial functionalities can be incorporated into wound dressings to prevent pathogenic infection. The antimicrobial activity of electrospun *L. lactis* was demonstrated using an overlay assay against three different strains of *S. aureus* including clinically relevant MRSA.

For gut delivery, the survivability of the encapsulated bacteria against acid insult was improved by formulating antacid into the nanofibers. In acidic environments like the stomach, protonated carboxylic acids along the alginate chain form hydrogen bonds causing alginate hydrogels to contract. In higher pH environments like the intestines where the gut microbiota resides, the alginate structures tend to swell releasing any encapsulants. The pH-dependent release of probiotics from the alginate nanofibers was demonstrated using a simulated gastrointestinal tract.

CHAPTER 3

MATERIALS AND METHODS

3.1 Materials

All chemicals were used as received without further purification. Low viscosity alginic acid sodium salt from brown algae (SA, ν = 4-12 cP, 1 wt% in H_2O at 25°C) was purchased from Sigma Aldrich (St. Louis, MO). The molecular weight (MW) and ratio of mannuronic acid to guluronic acid (M/G ratio) were reported to be 58.9 kDa and 2.65, respectively.[105] Brain heart infusion (BHI), calcium carbonate ($CaCO_3$), calcium chloride ($CaCl_2$), carbenicillin, glutaraldehyde, glycerol, Mueller Hinton Broth (MHB), poly(ethylene oxide) (PEO, Mw = 600 kDa), polysorbate 80 (PS80), potassium phosphate (KH_2PO_4), propidium iodide (PI), sodium chloride (NaCl), sodium phosphate dibasic (Na_2HPO_4), tryptone, yeast extract, were purchased from Sigma Aldrich (St. Louis, MO).

Hydrochloric acid (HCl; percent purity: 36.5-38.0%), agar, 200 proof ethanol, potassium chloride (KCl), and sodium hydroxide (NaOH) were purchased from Fisher Scientific (Hampton, NH). Deionized (DI) water was obtained from a Barnstead Nanopure Infinity water purification system (Thermo Fisher Scientific, Waltham, MA).

3.2 Bacteria

E. coli K12 MG1655 with GFP, *E. coli* Nissle with YFP, *L. lactis* ATCC 11454, *S. aureus* 12600, *S. aureus* SH1000 also known as methicillin-sensitive *S. aureus* (MSSA), MRSA IDRL-6169 were kindly gifted by Dr. Lauren Andrews (Department of Chemical Engineering, University of Massachusetts Amherst, Amherst, MA) and Dr. Robin Patel (Infectious Disease Research Laboratory, Mayo Clinic, Rochester, MN).

3.3 Creation of Precursor Solution

To create the SA/PEO/PS80 electrospinning solution, separate SA and PEO solutions were gently dissolved into sterile DI water by rotation (20 rpm) in the Roto-Therm™ Incubated Tube Rotator (Benchmark Scientific, Sayreville, NJ) for 24 hr at room temperature (25°C). Precursor solutions were made by mixing combinations of SA, PEO, PS80, and/or $CaCO_3$ together using the Roto-Therm™ (20 rpm, 24 hr, 25°C) to ensure even mixing.

3.4 Single electrospinning setup

The precursor solution was then loaded into a 5 mL Luer-Lock syringe (Norm-Ject Tuttligen, Germany) capped with an 18-gauge hypodermic needle (Exelint, Redondo Beach, CA) secured to a horizontal syringe pump (Cole Parmer, Vernon Hills, IL). (**Figure 1**) Alligator clips connected the high voltage supply (Gamma High Voltage Research, Ormond Beach, FL) to the metallic syringe needle and a copper collector plate (15 cm × 15 cm × 0.32 cm) covered in aluminum foil for easy sample removal. Unless otherwise stated, fibers were electrospun using a solution flow rate of 2 mL/hr, applied voltage of 17.5 kV, tip-to-collector distance of 18 cm, temperature of 25°C, and relative humidity of 20-30%.

3.5 Coaxial electrospinning setup

Both core and shell solutions were loaded into 5 mL syringes and connected to a homemade coaxial needle with a blunt 18-gauge inner needle and a blunt 14-gauge outer needle. (**Figure 3**) Horizontal syringe pumps were used to advance the solution from the syringes. The copper collector plate (15 cm × 15 cm × 0.32 cm) which was covered in aluminum foil for ease of sample removal was placed 18 cm from the tip of the coaxial needle. A high voltage supply connected to both the metallic needle and the collector plate via alligator clips applied 17.5 kV to the system. Solution flow rates of core and shell solutions were varied. The temperature and relative humidity were kept constant across all experiments at 25°C and 20-30%, respectively.

3.6 Characterization of electrospinning solutions

Surface tension measurements were made using a tensiometer (Optical Contact Angle 20, Dataphysics Inc., GmbH, Germany) that utilized the drop pendant method. Droplets of either SA, PEO, SA/PEO, SA/PEO/PS80, or SA/PEO/PS80 with bacteria solutions were suspended in air from an 18-gauge needle. The needle gauge was selected because it matches that used for electrospinning. The droplet was recorded until reaching equilibrium; analysis of surface tension was conducted using the integrated system software (SCA20, Dataphysics Inc., GmbH, Germany). Conductivity was measured using a conductivity probe (Tetracon 325, Vernon Hills, IL). Surface tension and conductivity experiments were conducted in triplicate.

3.7 Fourier-Transform Infrared (FTIR) Spectroscopy & Thermogravimetric Analysis (TGA)

A Bruker Alpha II FTIR spectrometer (Bruker Optics, Billerica, MA) was used to determine the functional groups present in fiber samples. Spectra of electrospun fibers were compared to spectra acquired from dried SA films, dried PEO dry films, liquid PS80, and dried SA/PEO/PS80 (2.8/1.2/3 wt%) mixture films. The mass composition of samples was analyzed by Q50 Thermogravimetric Analyzer (TA Instruments, New Castle, DE).[106] Samples (5-10 mg) were weighed while heating from 20-600°C at a scan rate of 10°C/min in nitrogen gas (25 mL/min).[107]

3.8 Scanning Electron Microscopy of electrospun nanofibers

As-spun and crosslinked fibers were sputter-coated (Cressington208 Sputter Coater, Watford, UK) with 3 nm of platinum before imaging with FEI Magellan 400 XHR-SEM (ThermoFisher Scientific, Hillsboro, OR). The diameters of 50 random fibers from five micrographs were measured using ImageJ 1.52a software (National Institutes of Health, Bethesda, MD) to determine the average fiber diameter.[108] Fiber diameter was measured as consistent widths across fibers excluding bulges that might have been bacterial cells (length ~ 1-2 µm & width ~ 0.5 µm) which were previously measured. The change in the average fiber diameter post-crosslinking was determined using **Equation 1**:

$$\textbf{Relative fiber diameter}\ (\%) = \frac{\mathbf{d_{CA-X}}}{\mathbf{d_{As-spun}}} * \mathbf{100}\% \qquad \textbf{Equation 1}$$

where $\mathrm{d_{CA-X}}$ and $\mathrm{d_{As-spun}}$ represent the average fiber diameter of crosslinked and as-spun fibers, respectively.

3.9 Preparation of bacteria

Overnight cultures of *E. coli* K12 MG1655, *E. coli* Nissle, or *L. lactis* were grown in Luria Bertani (LB) broth (10 g/L tryptone, 10 g/L NaCl, 5 g/L yeast extract in DI water) with carbenicillin (1 µg/mL), LB broth with kanamycin (50 µg/mL), or BHI broth, respectively, for 16 h at 37 °C. Cells were harvested by centrifugation at 2500g for 5 min at 25 °C (Sorvall™ ST 40R, ThermoFisher Scientific, Waltham, MA). Bacteria pellets were washed three times with phosphate buffer saline (PBS, 8 g/L NaCl, 0.2 g/L KCl, 1.44 g/L Na_2HPO_4, 0.24 g/L KH_2PO_4 in DI water, adjusted to a pH of 7.4 using HCl) before being resuspended in sterile DI water to a desired concentration.

3.10 Fluorescence Microscopy of bacteria

Visualization of the fluorescent proteins produced by the encapsulated bacteria or fluorescent beads was captured using a Zeiss Axio Imager A2 M Microscope (Carl Zeiss Microscopy, White Plains, NY). Additionally, dead bacteria were revealed by dead staining with PI before imaging. Bacteria viability was calculated by the following equation:

$$\textbf{Bacteria viability}\ (\%) = \frac{\mathbf{A_{live}}}{\mathbf{A_{live}+A_{dead}}} * \mathbf{100}\% \qquad \textbf{Equation 2}$$

where A_{live} and A_{dead} represent the area coverage of live bacteria and dead bacteria, respectively.

3.11 Determination of bacteria loading in solutions and as-spun fibers

The single plate-serial dilution spotting (SP-SDS) drop plate method was used to determine cell viability within the precursor solutions and fiber mats.[109] To determine bacterial loading of a solution, solutions were serial diluted. To determine bacterial loading within as-spun nanofibers, the fibers were dissolved in the relevant bacterial media before serial dilution. Samples of 20 µL from dilutions were plated on agar plates. Plates were incubated for 16 h at 37 °C. Each bacterium that grew into a distinct, visible colony was counted as a colony forming unit (CFU).

3.12 Fixation of bacteria

For SEM imaging of bacteria cells, overnight cultures of bacteria were incubated. The bacterial suspension was adjusted to OD600 = 0.3-0.4 by diluting with respective media, inoculated onto filter paper (10 µL), and dried at room temperature for 1 hr. The bacteria-loaded filter paper was fixed using 2.5 w/v% of glutaraldehyde in PBS for 2 hr at room temperature[110] and then rinsed in DI water twice. After fixation, samples were dehydrated in 30%, 50%, 75%, 85%, 95%, 100% alcohol-water gradients for 5 min in each solution.[111] Samples were oven dried 70°C before mounting to SEM stubs with carbon tabs.

3.13 Crosslinking of electrospun nanofibers

As outlined in **Table 3**, five crosslinking systems were evaluated. Electrospun nanofibers were submerged in acidic (pH 3.0), neutral (pH 7.0), or basic (intrinsic pH 10.3) solutions containing 2 wt% $CaCl_2$ (aq) for 60 s followed by rinsing in sterile DI water for 60 s to remove excess salt. The resulting crosslinked fibers were designated as CA-3, CA-7, and CA-10 to denote calcium ion crosslinked alginate nanofibers and their respective crosslinking solution pH value.

Table 3: Names and crosslinking compositions used to create the five crosslinked alginate nanofibers explored in this study, as well as the as-spun fibers. This table is reproduced with permission from ref. **[112]**. Copyright 2023 American Chemical Society.

Sample name	Pretreatment	Pretreatment time (s)	Composition of the crosslinking solution	Crosslinking solution pH	Crosslinking time (s)
As-spun[a]	n/a	n/a	n/a	n/a	n/a
CA-3	n/a	n/a	2 wt% $CaCl_2$ (aq)	Adjusted to pH 3 using HCl	60
CA-7	n/a	n/a	2 wt% $CaCl_2$ (aq)	Adjusted to pH 7 using HCl	60
CA-10	n/a	n/a	2 wt% $CaCl_2$ (aq)	Intrinsic pH 10.3	60
CA-PE[b]	Ethanol	60	2 wt% $CaCl_2$ in 1:5 ethanol:water	Intrinsic pH 10.4	10
CA-E	n/a	n/a	2 wt% $CaCl_2$ in 1:5 ethanol:water	Intrinsic pH 10.4	60
CA-G	n/a	n/a	2 wt% $CaCl_2$ in 1:1 glycerol:water	Intrinsic pH 7.8	60

[a] Altered from previous work[23]
[b] Literature control[21,41,75,78,113]

As a literature control, as-spun fiber samples were pretreated in 100% ethanol for 60 s followed by crosslinking in 2 wt% $CaCl_2$ in 1:5 ethanol:water for 10 s before being rinsed for 60 s in DI water.[41] These samples were named CA-PE fibers to denote the pretreatment and use of ethanol as a co-solvent. As an alternative co-solvent system, 2 wt% $CaCl_2$ was dissolved in a 1:1 glycerol:water solution. These samples, referred to as CA-G fibers, were crosslinked in the glycerol co-solvent for 60 s followed by rinsing in DI water for 60 s.

3.14 Mass loss analysis of crosslinked nanofibers

To calculate the change in mass that resulted from crosslinking, as-spun fibers and crosslinked fibers were lyophilized (FreeZone 2.5 Plus, Labconco, Kansas City, MO) for 16 hr before being weighed (AX105 Analytical SemiMirco balance, Mettler Toldeo, Vernon Hills, IL). The fiber mass retained after crosslinking was calculated using **Equation 3**:

$$\textbf{Fiber mass retention}\ (\%) = \frac{\mathbf{m_{CA-X}}}{\mathbf{m_{As\ spun}}} * \mathbf{100}\% \qquad \textbf{Equation 3}$$

where m_{CA-X} and $m_{As-spun}$ represent the mass of crosslinked fibers and as-spun fibers, respectively.

3.15 Stability of crosslinked nanofibers in various environments

To test their stability in different pH values and salt environments, crosslinked fibers were submerged in DI water, potassium chloride acid buffer (HCl/KCl acid buffer; 7.45 g/L KCl, 772 mg/L HCl in DI water adjusted to pH 2.0 using HCl), and phosphate-buffered saline (PBS). Samples were removed at 1 min, 60 min, and 120 min and dried at room temperature before SEM imaging.

3.16 Determining bacterial viability after crosslinking via fluorescence microscopy

Bacteria were electrospun directly onto 22 × 22 glass coverslips attached to the aluminum foil and collector plate using tape. Excess nanofiber mats from the aluminum foil could also be peeled from the foil and layered on top the electrospun mat on glass to increase the sample size/mass. As-spun fiber mats on glass slips were submerged in a PI stain (30 μM) for 15 min. If needed, mats were crosslinked in respective crosslinking solutions also containing PI stain (30 μM). As a control, overnight cultures of bacteria were incubated at 37°C. The overnight culture (250 μL per well) was added to a 6-well plate containing a glass coverslip (Fisherfinest Premium Cover Glass, Fisher Scientific, Pittsburgh, PA) and M9 solution (4.750 mL per well) and incubated for 2 hr such that bacteria could adhere to the coverslip. After incubation, the coverslips with bacteria were either submerged in PI stain or crosslinking solution containing PI stain. The samples were imaged using fluorescence microscopy of 15 random images per sample to determine the area coverage of live, fluorescent cells compared to the area coverage of PI dead-stained cells. Bacteria viability was calculated using **Equation 2**.

3.17 Determining bacteria loading after crosslinking

After electrospinning, bacteria-loaded nanofibers were weighed (2-5 mg) and crosslinked. The crosslinked fibers were then submerged in centrifuge tubes containing bacteria media, vortexed for 1 min, and incubated (37°C, 250 rpm, 1 hr) to release the bacteria from crosslinked fibers. The media was sampled, diluted, and plated to determine the amount of encapsulated bacteria from the original weight of fibers before crosslinking.

3.18 Overlay assay for the determination of antimicrobial activity of *L. lactis* against *S. aureus* strains

The overlay assay is based off a method described by Fleming et al.[114] and adapted by Millette et al.[115] but adjusted for a 6-well plate setup. First, 5 mL of BHI agar was added to each well in a 6-well plate. After electrospinning, several layers of bacteria-loaded nanofiber mats were sandwiched between autoclave sterilized Whatman Grade 3 filter paper and hole punched into 6 mm diameter circles. Punched nanofiber mats were separated from the filter paper and crosslinked if necessary. The nanofiber mats were then placed on the agar surface in separate wells. The well plate was incubated for 24 hr prior to overlay. For the overlay, *S. aureus* strains were grown overnight in MHB. Soft agar made of 0.5% of agar with 2.1 w/v% of MHB was autoclaved at 15 min at 120°C and 1 bar and then cooled to 50°C in a water bath. The soft agar was inoculated with 20 µL of the overnight culture of *S. aureus* per mL of soft agar. Each well is then overlaid with 1 mL of bacteria suspended in agar before being incubated at 37°C. After 24 hr of incubation, positive inhibition is recognized as a clear zone around the sample.

3.19 Release of fluorescent beads in a simulated gastrointestinal tract (GIT)

Green fluorescent beads were encapsulated in the alginate-based nanofibers to investigate the release of cargo from the crosslinked nanofibers. Green fluorescent beads (5 mg/mL) were blended into the previously described precursor solution (2.5 wt% SA, 1.5 wt% PEO, and 3 wt% PS80), and the solution was electrospun using the aforementioned parameters. Approximately 20 mg (XP204 Analytical Balance, Mettler Toledo, Vernon Hills, IL) of as-spun fibers were loaded into a stainless steel mesh (Smellshark, Zhengzhou City, CN), crosslinked as described in **Table 1**, and submerged sequentially in the GIT solutions consisting of an acidic stomach stage (HCl/KCl acid buffer, 30 mL, 2 hr)[116] and a neutral intestinal stage (PBS, 30 mL, 4 hr).[103,117]

Release studies were conducted on a shake plate (100 rpm) in an incubator (37°C) to imitate the mechanical agitation and temperature environment of the GIT.[118,119] At predetermined time points, samples were extracted from the GIT solution for optical density (OD; 515 nm) measurements acquired using a UV-Vis spectrometer (Genesys

10s, Thermo Scientific, Waltham, MA). The removed sample volume was subsequently replaced by the respective buffer solution. Cumulative release, or the mass percentage of dissolved fiber mass at a specified time over the total mass of as-spun fiber before crosslinking, was calculated.

.

3.20 Acid survivability of free cells

Overnight cultures of bacteria in respective media, with antibiotic if applicable, were grown in an incubator at 37°C with 250 rpm shaking. Bacteria were diluted to a predetermined concentration. 50 uL of the bacterial suspension was next inoculated into test tubes containing either 5 mL of BHI (5 mL) as the control sample or 5 mL of HCl/KCl acidic buffer (pH 2.0) to represent the acidic environment of the gastrointestinal tract.[120] Immediately after inoculation, a 100 µL sample wass removed, serial diluted, and plated on agar similar to the drop plate test. The test tubes were then incubated at 37°C. After 2 hr of incubation, samples were again taken from each test tube, serial diluted, and plated on agar. The agar plates were incubated overnight before colony counting to determine the number of surviving cells compared to the control.

3.21 Acid survivability of electrospun cells

After electrospinning, bacteria-loaded nanofibers were weighed, crosslinked if necessary, and submerged in a well plate containing 5 mL of HCl/KCl acidic buffer. The well plates were incubated at 37°C for 2 hr. Nanofiber mats were then removed from acidic solution and submerged in bacteria media. The crosslinked fibers were vortexed for 1 min and incubated (37°C, 250 rpm, 1 hr) to release the bacteria from crosslinked fibers. The media was sampled, diluted, and plated to determine the amount of encapsulated bacteria from the original weight of fibers before crosslinking.

3.22 Release of *L. lactis* into a simulated GIT

L. lactis was coaxially electrospun into alginate-based nanofiber as previously described in this Chapter. Between 5-10 mg (XP204 Analytical Balance, Mettler Toledo, Vernon Hills, IL) of as-spun fibers were crosslinked using CA-PE, CA-10 and CA-G crosslinking systems outlined in **Table 3.** Next, the nanofiber mats were sequentially incubated (37°C) in the GIT solutions consisting of an acidic stomach stage (HCl, pH = 2.5, 2 mL, 2 hr) and a neutral intestinal stage (NaOH, pH = 7.0, 2 mL, 2 hr).[103] At predetermined timepoints, the GIT solution was sampled (20 μL) and plated on BHI agar. After plates were incubated for 24 hr, colony counts were used to determine the amount of viable bacteria cells released throughout the model.

3.23 Statistical Analysis

Significant differences between samples were determined either using t-test (Microsoft Excel Version 2304) between two samples or using one-way ANOVA with Tukey post-hoc test on OriginPro 2022 (OriginLab, Northampton, MA) between multiple samples. Fiber diameter and relative fiber diameter are expressed as mean ± standard deviation. Fiber mass retention and release profiles are reported as mean ± standard error of at least three replicates. Standard deviation and standard error are represented as error bars in figures. Statistical significance was set to $p < 0.05$.

CHAPTER 4

ELECTROSPINNING ALGINATE-BASED NANOFIBERS USING FDA-APPROVED SURFACTANT POLYSORBATE 80

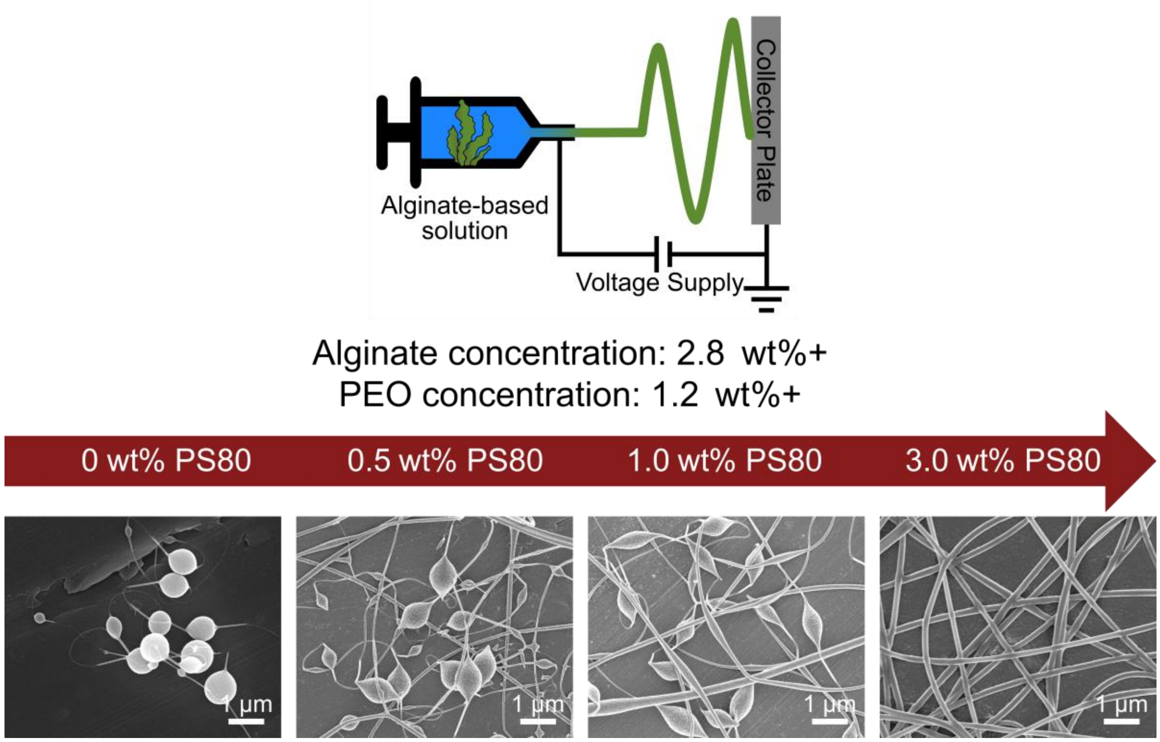

This chapter was adapted with permission from

Diep, E.; Schiffman, J. D. Encapsulating Bacteria in Alginate-Based Electrospun Nanofibers. *Biomater. Sci.* **2021**, *9* (12), 4364–4373. https://doi.org/10.1039/D0BM02205E.

4.1 Abstract

In this chapter, the alginate-based nanofibers will be electrospun from GRAS materials and solvents. First, the carrier polymer PEO initiates fiber formation during electrospinning though the fibers appear heavily beaded, indicating high surface tension in the precursor solution. In order to produce smooth, uniform fibers, an FDA-approved surfactant, PS80, is introduced to the precursor solution in incremental amounts. At

concentrations as low as 0.5%, PS80 significantly lowers the surface tension of the precursor solution. However, some beading is still present along the fibers. Increasing the surfactant concentration to 3% reduces both the surface tension and the conductivity of the solution such that bead-free fibers were produced. By systematic study of precursor solution properties on the electrospun nanofiber, we better understand the electrospinning system and can easily adapt the precursor system for the incorporation of active ingredients that would be useful in biomedical applications. Lastly, FTIR and TGA were conducted to reveal the chemical and mass composition of the as-spun nanofiber.

4.2 Introduction

Natural polymers, like alginate, are ideal for use in biomaterials due to their biocompatibility and water solubility. Alginate hydrogels have been used as implants, tissue scaffolds, and wound dressing, by crosslinking the alginate using with calcium ions.[64] Biological cargo like drugs, proteins, and cells can also be safely encapsulated within these biocompatible alginate hydrogels.[23,65,69,104,121] The formation of alginate hydrogels into nanomaterials that have high surface area to volume ratio for drug delivery purposes has been challenging due to the high viscosity of aqueous alginate solutions. Fortunately, electrospinning and its well-studied, highly tunable system can be employed to make nanofiber mats from polymer solutions by using high voltage.

As electrospinning is dependent on the balance between fiber stabilizing forces like polymer entanglement and the fiber drawing forces of the electric field,[122] the viscosity of the solution has been used as a measurement for polymer entanglement and as an indicator of “electrospinnability.”[123] When the polymer concentration in solution is low, chains hardly interact leading to a regime of low viscosity changes with increasing polymer concentration (**Figure 5.a**). As concentration continues to increase, the polymer chains eventually begin to overlap causing the viscosity to greatly increase (**Figure 5.b**). Finally, at entanglement concentration, increasing polymer concentration rapidly increases solution viscosity due to strong interactions between the polymer chains (**Figure 5.c & 5.d**). In the field of electrospinning, concentrations well above the entanglement concentration are usually required to form nanofibers. A study by McKee et al.[124] showed that electrospinning smooth fibers occur at 2-2.5 times the entanglement concentration for their copolymer system. Therefore, the viscosity of an electrospinning solution as it pertains to the relevant polymer concentration and entanglement concentration necessary for fiber formation has been used in several studies.[44–46,123]

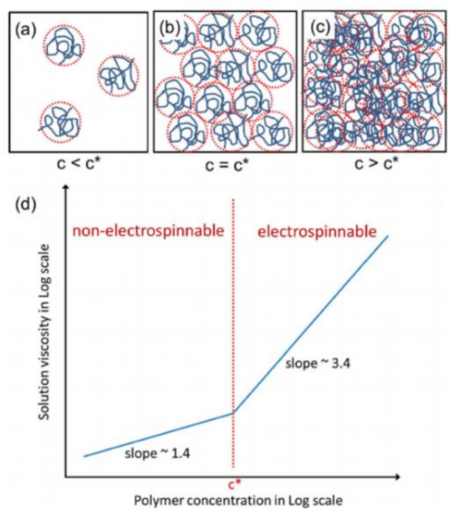

Figure 5: As polymer concentration increases, the polymer chains experience different regimes at low concentration where the chains do not interact with each other (a), at an overlap concentration where they begin to touch and interact (b), and at an entanglement concentration where the chains entangle around each other (c) causing a steep increase in viscosity as concentration increases (d). This figure is used with permission from ref. **[123]**. Copyright 2019 Han & Steckl. Published by Wiley.VCH Verlag GmbH & Co. KGaA.

As viscosity is a measurement of internal friction caused by intermolecular interactions, polymers that are higher in molecular weight tend to have higher viscosities due to more opportunities for interaction due to size. The ring structure of alginate units gives it a high molecular weight and high viscosity. Despite this high viscosity, alginate cannot be electrospun from a purely aqueous solution (**Figure 6**).[41,75,76] The rigid structure of alginate due to its hydrocarbon rings prevents entanglements as chains cannot wrap tightly around each other.[125] Therefore, the traditional entanglement concentration of electrospinning cannot be applied to electrospinning alginate-only solutions. Furthermore, charges along the alginate chain similarly prevent entanglement due to strong repulsive forces that are brought to the surface of the electrospinning jet when the electric field is applied.[75,125,126] Lastly, the interaction between carboxylic acids and water molecules are strong enough to maintain high surface tension that prevents chains from being drawn into solid nanofibers.[125,126]

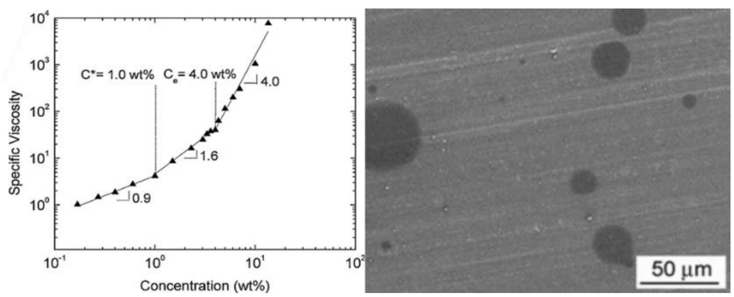

Figure 6: Bonino et al.[41] showed that electrospinning alginate does not form fibers even when the precursor solution exceeds entanglement concentration. This figure was adapted with permission from ref. 41. Copyright 2011 Elsevier.

Though the electrospinning of alginate has posed several challenges, researchers [41,75–77,79,125–131] have been able to remedy entanglement and surface tension challenges to allow nanofiber formation. To increase entanglement, two methods can be used: introducing a solvent to increase alginate flexibility or adding a flexible polymer that can form entanglements between alginate chains.[129–131] Most organic solvents used to alter alginate chain flexibility are not safe for human consumption and are, therefore, not suitable for blend electrospinning of bacteria. Carrier polymers like PVA and PEO are used to wrap around these rigid structures and allow fiber formation.[132,133] While both these polymers are biocompatible, PEO allows for high contents of alginate to be spun compared to polyvinyl alcohol.[76] The long, flexible chains of PEO shield the strong negative charges of the alginate chain that can prevent jet formation.[132,134] Both alginate and PEO also have mucoadhesive properties which can help prolong the residence time of the probiotic bacteria in the gut.[52,59,60] However, alginate/PEO fibers tend to form beads along the fiber attributed to high surface tension.[41,76]

Surfactant has been used to decrease this surface tension and promote fiber formation. Since alginate is a natural polymer, its polymer properties like molecular weight and M/G ratio are dependent on the source of alginate. Therefore, variable recipes are used to electrospin smooth fibers based on the polymer characteristics of alginate. Examples of precursor solutions used to electrospin alginate-based nanofibers are listed in **Table 4**. While these published studies have pioneered key parameters for electrospinning alginate into nanofibers, few[79] have demonstrated their ability to encapsulate living cells and most feature cytotoxic solvents.

Table 4: Summary of electrospun alginate highlighting different alginate sources and recipe compositions.

Study	Alginate Source and reported properties	Precursor solution composition	Ref.
Electrospinning alginate-based nanofibers: From blends to crosslinked low molecular weight alginate-only systems	FMC Biopolymers MW = 196 kDa, MW/Mn = 1.6, 66:34 G:M blocks	8.0/1.6/2.0 wt% SA/PEO/Pluronic F127 in water	41
Controlled synthesis and structural stability of alginate-based nanofibers	Sigma-Aldrich Viscosity ~3500 cP (2% solution, 25 ◦C)	3.6/0.4/0.5 wt% SA/PEO/Triton X-100 in water and dimethyl sulfoxide	129
Alginate-lavendar nanofibers with antibacterial and anti-inflammatory activity to effectively promote burn healing	Sigma-Aldrich	3.2/0.8/1.5 wt% SA/PEO/Pluronic F127 in water and dimethylformamide	130
Gelatin/alginate composite nanofiber membranes for effective and even adsorption of cationic dyes	Kangtong Marine Fiber Corporation	2.7/0.3/0.8 wt% SA/PEO/Triton X-100 in water and ethanol	131

In this chapter, we systematically investigated precursor solutions that enabled the electrospinning of smooth alginate-based nanofibers. Due to its bulky uronic groups, alginate has a rigid structure that limits chain entanglements and subsequent electrospinning.[41,76,132] PEO was selected as a carrier polymer because it is biocompatible and can also act as a mucoadhesive for prolonged probiotic presence in the gut.[52] Another precursor additive, the nonionic surfactant, Triton X-100,[41] was previously reported to enable the formation of bead-free fibers by reducing the surface tension of precursor solution. We focused on using only GRAS solvents and additives to manufacture smooth fibers. Therefore, FDA-approved surfactant polysorbate 80 was used electrospin smooth nanofibers.

4.3 All Materials and Methods are described in Chapter 3.

4.4 Results and Discussion

4.4.1. Enabling alginate fiber formation via the addition of PEO

Bead-free alginate-based nanofibers were developed by electrospinning a solution of SA, PEO, and PS80. Attempts were first made to electrospin pure solutions of SA; however, as expected and consistent with previous works,[41,76,125,126] the rigid structure, high surface tension (47.35 N/m for 4 wt% SA), and high conductivity (8.17 mS/cm for 4 wt% SA) of a pure aqueous SA solution prevented fiber formation. A solution of PEO (4 wt%; MW: 600 kDa) was added to the 4 wt% SA solution in a 30 to 70 ratio to create a 2.8/1.2 wt% SA/PEO solution. Preliminary studies (**Appendix A**) found that the viscosities of the precursor solutions using higher molecular weight PEO (900 kDa and 1,000 kDa) were too high for the voltage supply to overcome for electrospinning. This concentration of SA/PEO was used as a starting point as it has been electrospun in other studies.[41,76]

The onset of fiber formation can be seen by the thin fibers in **Figure 7.a**. Beading, also seen in the figure, can be caused by several factors including low polymer concentration,[47] low viscosity,[135] slow solution flow rate,[46] low applied voltage,[39] and low surface tension.[41,45,76] In our case, we hypothesized that the reason for beading was due to high surface tension which has been shown by other studies to be common for alginate systems.[41,76,125,126,129] As the electric field pulls the solution into a conical jet, surface tension forces attempt to decrease the surface area per unit of mass turning the jet into spherical shapes that create the beaded fiber morphology.[135] Introducing surfactant into the precursor solution decreased the surface tension and allowed for the formation of smooth fibers as covered in the Section 4.4.2.

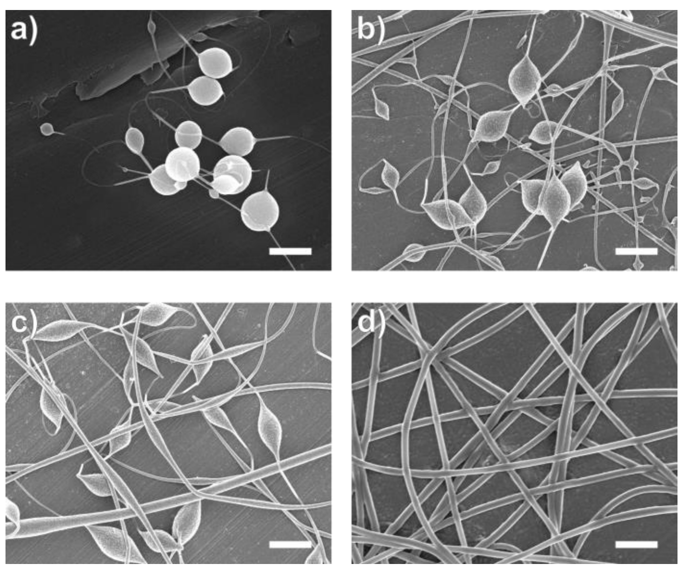

Figure 7: Scanning electron micrographs of fibers electrospun from SA/ PEO (2.8/1.2 wt%) solutions (a) without any surfactant, as well as with (b) 0.5 wt%, (c) 1 wt%, and (d) 3 wt% PS80. Scale bars are 1 μm. This figure is reproduced with permission from ref. 23. Copyright 2021 The Royal Society of Chemistry.

4.4.2. Effect of surfactant on alginate-based nanofibers

To study the effects of PS80 on fiber formation and morphology, SA and PEO solutions were electrospun from solutions without surfactant and with PS80 surfactant. We explored the use of a nonionic surfactant, PS80 because it is an FDA approved surfactant already used in oral delivery.[136] To decrease beading, 0.5 wt%, 1 wt%, and 3 wt% of PS80 surfactant was mixed into the SA/PEO solution. The addition of PS80 to create the 2.8/1.2/0.5 wt% SA/PEO/PS80 solution reduced the surface tension by 19% to ~41.93 mN/m, compared to the surfactant-free solution. Continuous fibers that were 125 ± 37 nm in diameter were formed at the smallest incorporation of surfactant, but elongated beads were still present (**Figure 7.b**). Increasing the surfactant concentration to 1.0 wt% produced more spindle-like beads but did not significantly alter the average diameter (**Figure 7.c**).

Further increasing the surfactant concentration to 3.0 wt% yielded smooth fibers with an average fiber diameter of 167 ± 24 nm (**Figure 7.d**). As the surface tension decreased, the fiber diameter (and consequently the fiber mass) is more consistent along the length of the fiber leading to smaller, less spherical beads and thicker fiber diameters.[135] The presence of surfactant, in any amount, was able to significantly decrease the surface tension of the precursor solution compared to the solution without surfactant. However, statistical analysis (detailed in **Chapter 3**) proved that the surface tension did not significantly change between the varying amounts of surfactant, from 0.5-3.0 wt% (**Table 5**).

Table 5: Characteristics of precursor solutions and respective electrospun alginate-based fibers. This table is reproduced with permission from ref. 23. Copyright 2021 The Royal Society of Chemistry.

Precursor solution composition Polymer (wt%)			Solution properties		Fiber characteristics	
			Conductivity[a]	Surface tension[a]	Fiber diameter[b]	Bead formation
SA	PEO	PS80	(mS/cm)	(mN/m)	(nm)	(yes/no)
4.0	n/a	n/a	8.17 ± 0.21[x]	47.35 ± 2.82[y]	n/a	n/a
2.8	1.2	n/a	5.38 ± 0.14[y]	51.70 ± 0.66[x]	n/a	Yes
2.8	1.2	0.5	5.58 ± 0.04[y]	41.92 ± 0.91[z]	125 ± 37	Yes
2.8	1.2	1.0	5.44 ± 0.05[y]	40.37 ± 0.58[z]	127 ± 38	Yes
2.8	1.2	3.0	5.04 ± 0.10[y]	39.65 ± 0.63[z]	167 ± 23	No

[a]Values are reported as mean ± standard error
[b]Values are reported as mean ± standard deviation

While several different operating parameters were investigated to determine the conditions under which fiber formation occurs, the solution flow rate (2 mL/hr), tip-to-collector distance (17 cm), and applied voltage (17.5 kV) at room temperature (25°C) and relatively humidity (20-30%) will be used for the remainder of this study unless otherwise specified. For example, a flow rate of 1 mL/hr was sufficient for the formation of fibers; however, a flow rate of 2 mL/hr was chosen as a greater mass of fiber mat was obtained from this flow rate. At shorter tip-to-collector distances, less time is available for evaporation before the polymer solution/nanofiber reaches the collection plate leading to the production of a wet fiber. At lower applied voltages, no visible mats were produced.

Similar trends of increasing the surfactant concentration to reduce beading in SA/PEO electrospun fibers have been reported in other studies. Saquing et al.[76] found that lower concentrations of Triton X-100 (0.1 wt% and 0.3 wt%) produced beaded fibers with an 80 to 20 ratio of SA to PEO, whereas higher concentrations (0.5 wt%, 1 wt%, 1.5 wt%) produced bead-free fibers. Similar to our study, all these concentrations were well above critical micelle concentration (CMC). At this concentration, surfactant molecules have saturated the surface of the liquid allowing excess molecules in the bulk solution to form micelles. Therefore, increasing the surfactant concentration should not significantly affect surface tension values after reaching the CMC.[137] Yet, changes in morphology were reported.

Diverse sources of alginate and varying molecular weights of PEO were used across several studies leading to the electrospinning of different weight ratios and concentrations. It is interesting that various concentrations of surfactant can be used to form smooth fibers even though the surface tension should not significantly change after reaching CMC; this led us to hypothesize that the surfactant concentration might have a compounding effect on solution properties, which would affect fiber formation.

4.4.3. Effect of conductivity on alginate-based nanofibers

We next determined the conductivity of the precursor solutions because sodium alginate dissolved in water has a high conductivity due to its ionic nature. Notably, high conductivity can prevent fiber formation by causing strong repulsive forces between polymer chains that prevent entanglements during electrospinning.[41,75,76,126,132] One of the reasons that a linear copolymer, like PEO, is used to electrospin alginate is because the PEO chains wrap around the rigid alginate chains to interrupt interactions between alginate and sodium ions lowering the conductivity of the solution.[132] We observed this effect, too. Mixing the SA solution with the PEO solution decreased its conductivity from 8.17 mS/cm (4 wt% SA) to 5.38 mS/cm (2.8/1.2 wt% SA/PEO) (**Table 5**). Though this change was statistically significant, bead-free fibers were not formed upon the addition of PEO into the solution. While the lowest addition of 0.5 wt% PS80 did not have a statistical effect on the conductivity of the solution, additional amounts of PS80 significantly decreased the solution conductivity from 5.58mS/cm (0.5 wt% PS80) to 5.44 mS/cm (1.0 wt% PS80) and to 5.04 mS/cm (3.0 wt% PS80). Increasing the concentration of surfactant above the CMC leads to the formation of micelles in the bulk solution. These micelles tend to have lower conductivity than their single-molecule counterparts thereby decreasing the conductivity of the solution as surfactant concentration increases.[138,139]

Decreasing conductivity has been previously shown to be able to suppress beading. While electrospinning relies on charges within the polymer solution to form the Taylor cone, a highly conductive solution can also be detrimental to the formation of fibers. For example, Zhang et al.[46] reported that when they added protein to their precursor solution, it increased solution conductivity and was a source of instability that caused fiber beading. Furthermore, increases in conductivity decreases the tangential electrostatic force within the polymer droplet which hinders Taylor cone and subsequent fiber formation.[33,134] In a SA/PEO/Triton X-100 solution, Saquing et al.[76] found that even a low concentration (1 wt%) of sodium chloride salt which increases solution conductivity began to decrease fiber formation. Fang et al.[126] electrospun a mixture of alginate and calcium chloride salt where the crosslinking of calcium ions with alginate chains allowed for entanglement-like interactions that promoted electrospinning.

Conductivities of solutions used in the aforementioned study remained relatively low due to the mixed solvent system used (i.e., a combination of DI water, ethanol, and DMF). Solvents like glycerol[125] and dimethyl sulfoxide[129] also alter interactions between alginate molecules in solution and aid in fiber formation. In our system, we used an aqueous solution to ensure that the final product would be safe for consumption as a delivery vehicle for probiotics. In sum, both the lower surface tension and lower conductivity of the precursor solution aided in the suppression of the beading in our system allowing us to form smooth fibers using 2.8/1.2/3 wt% SA/PEO/PS80 solution (**Figure 7.d**).

4.4.4. Chemical characterization of alginate-based nanofibers

In **Figure 8**, we confirmed the chemical composition of the electrospun fibers by acquiring FTIR spectra and comparing them to control spectra of SA, PEO, PS80, and SA/PEO/PS80. Characteristic peaks of each compound also appeared in the FTIR spectra of the SA/PEO/PS80 fibers and control films, thus indicating that all three components were present. Characteristic peaks in the pure SA spectra included hydroxyl groups (3500-3000 cm^{-1} broad peak followed by 2800 cm^{-1} sharp peak), asymmetric stretches of carboxylate anions (1566 cm^{-1} and 1408 cm^{-1} peaks), and ester bonds (1026 cm^{-1} strong peak).[128] Similarly, the PEO spectra exhibited strong peaks at 2878 cm^{-1} and 1098 cm^{-1} indicating terminal hydrogens and ester groups, respectively. The series of peaks in the 1460-1180 cm^{-1} range of the PEO spectra were attributed to secondary hydrogens along the PEO backbone.[140] Different from SA and PEO, the PS80 spectra showed a peak at 1700 cm^{-1} representing a carbonyl group.[141] Indeed, fibers were comprised of alginate, PEO, and PS80.

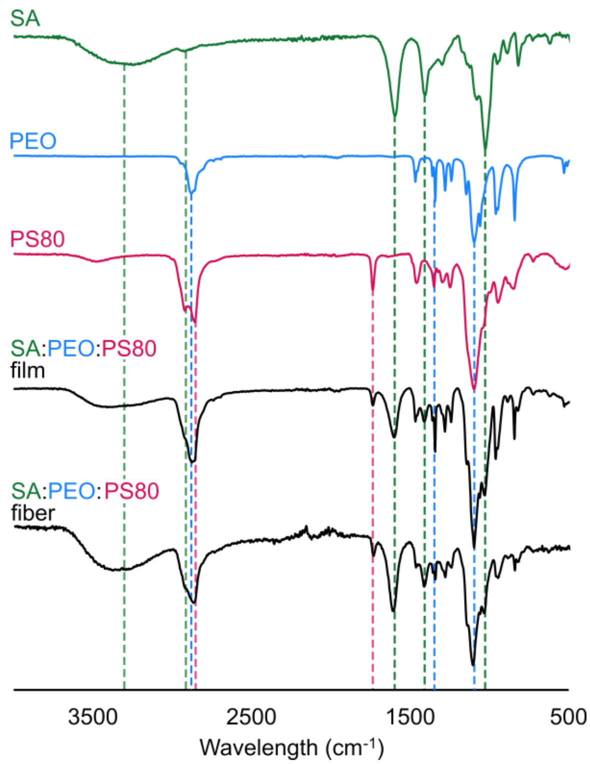

Figure 8: FTIR spectra of SA, PEO, PS80, and SA/PEO/PS80 films as compared to the spectra of SA/PEO/PS80 as-spun nanofibers. SA, PEO, PS80, and SA/PEO/PS80 nanofiber spectra are reproduced with permission from ref. **[112]**. Copyright 2023 American Chemical Society.

4.4.5. Mass composition of electrospun nanofibers

TGA thermograms (**Figure 9** with data listed in **Table 6**) were used to confirm and quantify the composition of alginate in the as-spun fiber for crosslinking. Nanofiber mats spun from 2.5/1.5/3% SA/PEO/PS80 (this composition will be explained in **Chapter 5**) experienced their first major degradation between 200°C-265°C with a peak at 230°C, which correlates primarily to the breaking of glycosidic bonds between uronic acid groups along the alginate chain.[25,107] The second major degradation event of the as-spun fibers occurred between 355°C and 405°C corresponding to the breaking of C-O-C bonds present in both PEO and PS80.[142,143] After the degradation of PEO and PS80, the remnant mass is likely carbonaceous and inorganic residue formed during thermal degradation which is common in alginate structures.[144,145]

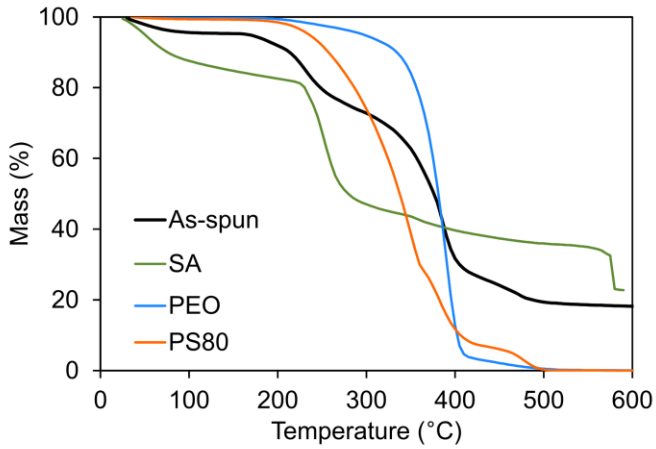

Figure 9: TGA graphs of SA, PEO, PS80, and as-spun SA/PEO/PS80 nanofibers. This figure is reproduced with permission from ref. [112]. Copyright 2023 American Chemical Society.

Table 6: Thermal degradation data of raw SA, PEO, and PS80, as well as as-spun nanofibers. This table is reproduced with permission from ref. [112]. Copyright 2023 American Chemical Society.

Sample	Water loss (%)	Residue (%)	Range (°C)[a]	Peak (°C)[b]	Mass loss (%)[c]	Reason for mass loss
SA film	17.3	44.6	235-275	250	38.0	Glycosidic bond breaking[d] Dehydration[d] Decarboxylation[d] Decarbonylation[d]
PEO film	2.5	3.1	360-405	390	94.4	C-O-C bonds breaking[e]
PS80	0.7	1.2	305-380 390-425 470-505	375 400 500	71.2 20.0 6.8	Olefinic bond breaking[f] C-O-C bond breaking[e]
As-spun fibers	8.0	25.7	210-265 365-405	230 385	18.5 35.9	Alginate degradation[d] C-O-C bond breaking[ef]

[a] Degradation temperature ranges are reported from the onset temperature to offset temperature.[146]

[b] Peak degradation temperature represents the temperature of maximum mass loss as determined by local maxima on the first derivative thermogram.[142,146]

[c] Mass loss (%) refers to the change in mass between the onset and offset temperatures.[106]

d 25,107,144

e 107,142

f 143

The mass composition of the as-spun fibers, calculated as the difference in mass between onset and offset points of each degradation event, was determined to be 15.6 wt% SA and 40.2 wt% PEO/PS80 with 28.8 wt% residue. These results are consistent with a study by

Kianfar et al.[106] that reported PEO enrichment in a nanofiber electrospun from a chitosan and PEO mixture due to the ease of electrospinnability of PEO compared to chitosan.

4.5 Conclusion

In summary, smooth, alginate-based nanofibers were electrospun despite challenges of high surface tension and conductivity which were alleviated by the addition of carrier polymer and surfactant. In particular, the carrier polymer PEO and FDA-approved surfactant PS80 were chosen to produce biocompatible nanofiber. After the addition of PEO to SA precursor solution, large beads interconnected by wispy fibers indicated high surface tension in the precursor solution. PS80 lowered the surface tension; however, concentrations lower than 3% of PS80 did not produce a smooth nanofiber. No significant difference was found between the surface tension of the precursor solutions with 0.5%, 1%, 2%, and 3% PS80. Conductivity measurements revealed a significant decrease with the addition of 3% PS80 which stabilized the electrospinning jet such that smooth nanofibers were formed. Chemical composition revealed the fiber indeed contained at least 15.6% alginate when electrospun from a solution of 2.5/1.5/3% SA/PEO/PS80.

In conclusion, surface tension and conductivity were identified as key precursor solution properties involved in the electrospinning of alginate. PEO and PS80 are GRAS components that can affect these properties to facilitate fiber formation. The presence of alginate was confirmed in the nanofibers using FTIR and TGA despite the enrichment of PEO that occurred during electrospinning.

CHAPTER 5

ENCAPSULATING BACTERIA IN ALGINATE-BASED ELECTROSPUN NANOFIBERS

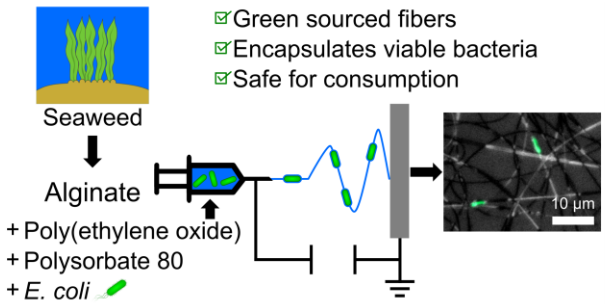

Adapted from:

Diep, E.; Schiffman, J. D. Encapsulating Bacteria in Alginate-Based Electrospun Nanofibers. *Biomater. Sci.* **2021**, *9* (12), 4364–4373. https://doi.org/10.1039/D0BM02205E.

&

Diep, E.; Schiffman, J. D. Electrospinning Living Bacteria: A Review of Applications from Agriculture to Health Care. *ACS Appl. Bio Mater*. 2023, *6* (3), 951-964. https://doi.org/10.1021/acsabm.2c01055.

5.1 Abstract

To deliver beneficial bacteria to various environments, live bacteria were encapsulated within alginate-based nanofibers was achieved through using both single needle and coaxial needle electrospinning. Mixing *E. coli* K12 into the precursor solution for single needle electrospinning led to the formation of beaded fibers where bacteria encapsulation was not disguisable. To compensate for the addition of bacteria, the SA/PEO/PS80 weight ratio was reoptimized to be 2.5/1.5/3 using the information and characterization techniques from the previous chapter. Smooth fibers with bulges around the live

microbes (2.74×10^5 CFU/g of mat) were formed, as confirmed using fluorescence and scanning electron microscopy. We also found that coaxial electrospinning was able to significantly increase the bacteria-loading in these fibers to over 10^9 CFU/g. Probiotics *E. coli* Nissle and *L. lactis* were coaxially electrospun into alginate-based nanofibers. Effects of core/shell flow rate on bacteria loading within the as-spun nanofiber was investigated. However, inherent differences between bacterial strains appear to influence the loading capacity in the coaxially electrospun fiber. This work demonstrates the use of electrospinning to encapsulate live bacteria in alginate-based nanofibers for the potential delivery of probiotics to the gut.

5.2 Introduction

Bacterial encapsulation is a technique that protects the bacteria by forming a physical barrier to support the cell structure and reduce contact with damaging agents.[10] Additionally, encapsulations can act as a delivery vehicle to transport bacteria wherever they are useful. For example, during freeze-drying, bacteria that were encapsulated within rice proteins had higher viability after processing, during storage at various temperatures, and in simulated gastrointestinal tract environments. The freeze-dried bacteria take on a powder form that is easily compressed into tablets for the oral supplementation of probiotics in the gut.

Electrospinning is particularly useful for the encapsulation of bacteria into polymer nanofibers because heating, freezing, and organic solvents which can harm encapsulant materials are not needed. Thus, suspensions of bacteria are blended into various synthetic and naturally-derived polymer solutions for electrospinning. Biopolymers dissolved in aqueous solutions are commonly used as they promote the viability of encapsulated cells within the fibers.[21] However, the high voltage poses a threat toward the viability of the encapsulated bacteria. The major reasons for cell death during electrospinning are attributed to cell rupture due to electrical forces, mechanical forces, and dehydration.[18,19,147] However, numerous studies have shown that bacteria cells survive the applied voltages used during electrospinning.[18,52,56,83,84] During electrospinning, the current or flow of electrons traveling through the precursor solution, polymer nanofiber, and encapsulated bacteria remains low due to the high resistivity of the polymer.[39,81] Therefore, the current does not disrupt the cell membrane of the bacteria which would lead to cell death. Additional concerns surrounding death caused by the electric field, which applies a radial force causing the fiber to bend and whip.[34] Reznik et al.[85] determined this whipping force to be 5×10^3 g cm^{-1} s^{-2} which is smaller than the force a cell of E. coli can withstand which was determined to be 3×10^6 g cm^{-1} s^{-2}.[18]

A handful of studies attempted to correlate applied voltage with bacteria viability in the encapsulated nanofiber. When Škrlec et al.[52] used an applied voltage of 15 kV (with a separation distance of 15 cm) the cells had a higher viability than when 20 kV was used, which led to a 2-log reduction compared to theoretical loading. However, other studies[83,84] showed that voltage did not significantly affect the viability of *E. coli* Nissle electrospun into polyethylene glycol-polylactide and Lactobacillus plantarum in polyvinyl alcohol. The effect of electrospinning voltage on the viability of bacteria may depend on the strain of bacteria and components of the precursor solution.

In this chapter, the addition of *E. coli* K12 as a model bacterium was incorporated into the precursor solution before electrospinning. We continued studying the effects of precursor solution properties on the formation of smooth, bacteria-load nanofibers. Due to a shift in surface tension and conductivity, the concentration of the precursor solution was reoptimized to produce smooth nanofibers with bulges that accommodated the encapsulated bacteria. SEM, fluorescent microscopy, and drop plate techniques were used to confirm the encapsulation of live bacteria cells in the alginate-based nanofibers. Next, known probiotics *E. coli* Nissle and *L. lactis* were also electrospun by single and coaxial electrospinning. *E. coli* Nissle proved to be a more robust bacterium than *E. coli* K12 leading to higher bacterial loading in the nanofiber despite having the same concentration in the precursor solution. However, bacterial loading could be further increased by coaxial electrospinning wherein the bacterial suspension extruded from the inner needle can be carried along as the polymer-based precursor solution is electrospun from the outer needle.

5.3 All Materials and Methods are described in Chapter 3.

5.4 Results and Discussion

5.4.1. Developing precursor solution for encapsulation of bacteria

The previously described optimized 2.8/1.2/3 wt% SA/PEO/PS80 solution was loaded with 10^8 CFU/mL of *E. coli* K12 and electrospun into beaded fibers with an average diameter of 100 ± 23 nm. We measured the rod-shaped *E. coli* K12 cells using SEM (**Figure 10.a**), and they were roughly 2.44 ± 0.57 µm in length by 0.65 ± 0.07 µm in diameter. The beads present along these bacteria loaded fibers were 0.81 ± 0.25 µm in length and 0.23 ± 0.04 µm in width (**Figure 10.b**); therefore, we did not suspect that these beads were bacteria.

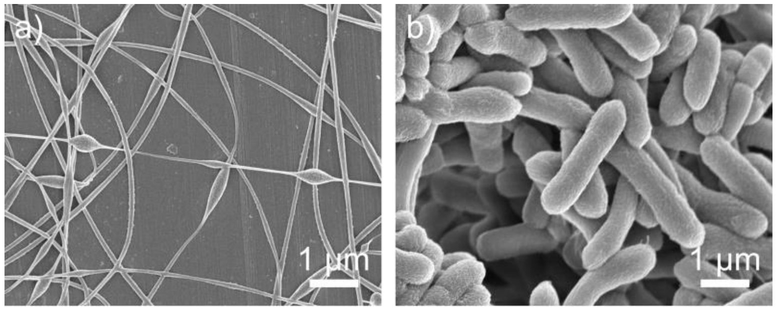

Figure 10: Scanning electron micrographs of fibers electrospun with 10^8 CFU mL^{-1} of *E. coli* encapsulated in (a) 2.8/1.2/3 wt%, (b) 2.8/1.2/5 wt%, and (c) 2.5/1.5/3 wt% SA/PEO/PS80 precursor solutions. This figure is reproduced with permission from ref. 23. Copyright The Royal Society of Chemistry 2021.

5.4.1.1. Comparison between bacteria-free and bacteria-loaded precursor solution

Conductivity and surface tension of bacteria-loaded solutions were determined to explore their role in fiber beading. These results were compared to the solution properties of the previously optimized bacteria-free solutions, as shown in **Table 7**. The change in conductivity due to the addition of bacteria in the 2.8/1.2/3 wt% SA/PEO/PS80 solution, though statistically insignificant, was likely due to the negative charge carried on the surface of the *E. coli*.[148] Škrlec et al.[52] saw a similar increase in conductivity due to the addition of *L. plantarum* in their PEO precursor solution and attributed it to extracellular proteins and ions. Increases in solution conductivity can cause thinner fibers as additional repulsive charges stretch the electrospinning jet.[46] This would explain the decrease in average fiber diameter due to the addition of the bacteria. As previously mentioned, increased conductivity also causes beading along electrospun nanofibers due to Taylor Cone instability.[135] The surface tension of the bacteria-loaded solution was found to be 41.25 mN/m. From our previous studies, high surface tension could also have caused the beading. Though neither the change in solution conductivity nor surface tension was statistically significant, we propose changing these solution properties could compensate for the addition of *E. coli* and produce smooth fibers due to previous indications that these properties influence fiber morphology.

Table 7: Characteristics of bacteria-loaded precursor solutions and bacteria electrospun into alginate-based fibers. This table is reproduced with permission from ref. 23. Copyright 2021 The Royal Society of Chemistry.

Precursor solution composition				**Solution properties**		**Fiber characteristics**	
Polymer (wt%)			***E. coli* concentration**	**Conductivity**[a]	**Surface tension**[a]	**Fiber diameter**[b]	**Bead formation**
SA	**PEO**	**PS80**	**(CFU/mL)**	**(mS/cm)**	**(mN/m)**	**(nm)**	**(yes/no)**
2.8	1.2	3.0	10^8	5.28 ± 0.03^x	41.25 ± 0.24^x	100 ± 23	Yes
2.8	1.2	5.0	10^8	5.09 ± 0.05^y	39.50 ± 0.34^x	305 ± 110	Yes
2.5	1.5	3.0	10^8	4.74 ± 0.04^z	40.43 ± 0.56^x	273 ± 64	No

[a]Values are reported as mean ± standard error
[b]Values are reported as mean ± standard deviation

5.4.1.2. Increasing surfactant concentration of bacteria-loaded precursor solution

Increasing the PS80 concentration would lower both surface tension and conductivity as proven in the previous section (**Section 5.4.1.1**). By increasing the surfactant from 3 to 5 wt% PS80, the 2.8/1.2 wt% SA/PEO solution with bacteria electrospun into flattened and webbed structures indicative of wet fibers (**Figure 11.a**). These fibers were 305 ± 110 nm in diameter, which was much larger than any of our previously spun fibers. Surface tension was reduced to 39.50 mN/m compared to the 3 wt% PS80 with bacteria, which could explain the production of wet fibers. The force of the electric field that aims to pull entangled polymers out from the electrospinning droplet to form nanofibers is countered by the force of surface tension which stabilizes the electrospinning jet. High surface tension may cause beading, but the low surface tension cannot hold the jet together.[39,45,46] Therefore, excess amounts of solution, both polymer and solvent, is removed from the electrospinning droplet and lands on the collector. In this case, the produced fibers would be larger due to increased mass flow rate and can be wet due to increased amounts of solvent being pulled into fibers.[39]

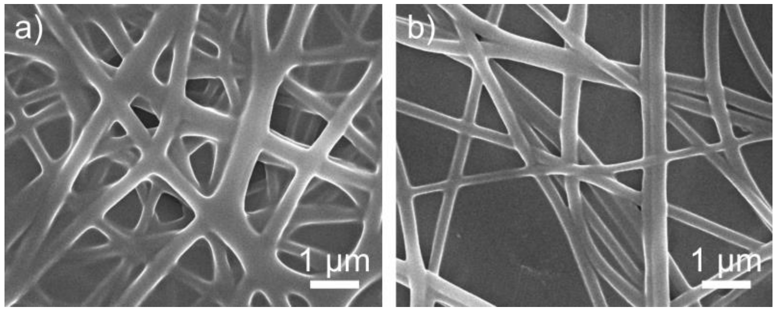

Figure 11: Scanning electron micrographs of fibers electrospun with 10^8 CFU mL^{-1} of *E. coli* encapsulated in (a) 2.8/1.2/5 wt% and (b) 2.5/1.5/3 wt% SA/PEO/PS80 precursor solutions. This figure is reproduced with permission from ref. 23. Copyright The Royal Society of Chemistry 2021.

5.4.1.3. Increasing carrier polymer concentration of bacteria-loaded precursor solution

Alternatively, conductivity and surface tension can be altered by changing the SA to PEO ratio. PEO chains can interfere with the interaction between sodium ions and alginate chains which are the major contributors to the conductivity in this system.[41,75,76,126,132] Therefore, decreasing the concentration of alginate while increasing the PEO concentration will decrease the solution conductivity. When the ratio of SA to PEO was changed to 2.5 to 1.5, the resulting conductivity of the 2.5/1.5/3 wt% SA/PEO/PS80 solution with 10^8 CFU/mL of *E. coli* K12 was 4.74 ± 0.08 mS/cm, which was significantly lower than all other bacteria loaded solutions. Consequently, the surface tension was also altered to a value of 40.43 mN/m though this was not significantly different from the 2.8/1.2/3 wt% SA/PEO/PS80 solution with or without bacteria. We suspect lower solution conductivity stabilizes the electrospinning jet while surface tension allows a moderate amount of polymer and solvent to be drawn into dry fibers enabling this solution to produce smooth, bead-free fibers with encapsulated *E. coli* K12 (**Figure 11.b**). The optimized fibers containing bacteria were 273.40 ± 62.53 nm in diameter. Fluorescence microscopy was used to detect the live, green fluorescent protein

(GFP) producing bacteria within the electrospun nanofiber while the bacterial cell presents as bulges along the nanofiber in the SEM image (**Figure 12**).[23] The 2.5/1.5/3% SA/PEO/PS80, which will be used for the remainder of this work, was also capable of single needle and/or coaxial electrospinning of probiotics *E. coli* Nissle and *L. lactis* though no solution characterization was conducted for solutions with these bacteria.

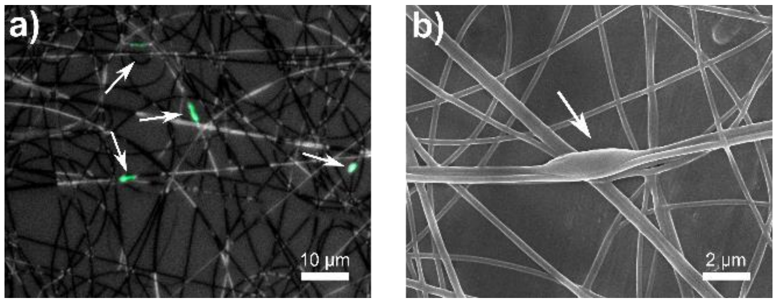

Figure 12: (a) Fluorescent micrograph and (b) SEM of GFP-producing *E. coli* electrospun into alginate-based nanofibers. The arrows indicate the location of the cells. This figure is reproduced with permission from ref. 23. Copyright The Royal Society of Chemistry 2021.

5.4.2. Bacteria viability throughout electrospinning

Against high voltage, dehydration, and osmotic stresses, live bacteria have been encapsulated with high viability and loading through electrospinning. To further prove the viability of the bacteria throughout the electrospinning process, we determined the bacteria loading in the precursor solution before mixing, after mixing, and after electrospinning quantified for *E. coli* K12, *E. coli* Nissle, and *E. coli* Nissle with 1% glycerol single needle electrospun into 2.5/1.5/3% SA/PEO/PS80 nanofibers.[149] (**Figure 13**) In our studies, 17.5 kV was applied across a tip-to-collector distance of 17 cm. After passing through the electric field, the bacteria loading was statistically equivalent to the loading in the precursor solution before and after mixing for all samples. This experiment demonstrates that despite the applied voltage,[150] the amount of charge that travels through the bacteria remains low and does not lead to cell inactivation.[39,81]

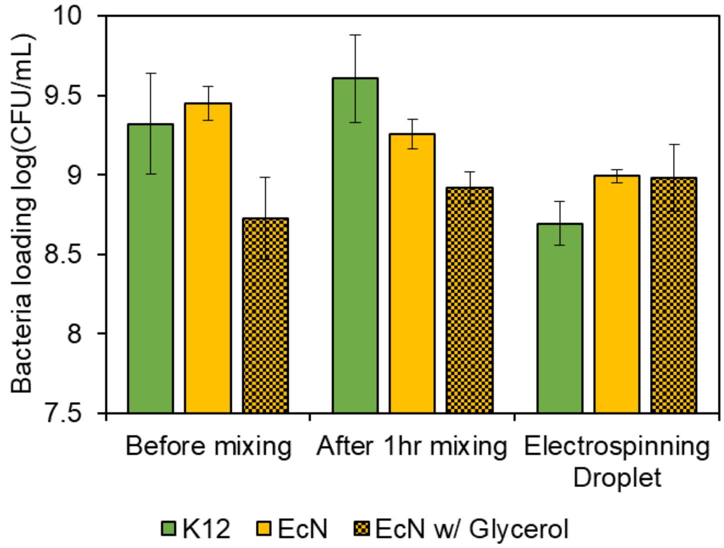

Figure 13: Bacterial loading in the precursor solution immediately after inoculation (0 hr), after mixing (1 hr), and after electrospinning (Droplet) as well as in fiber mats electrospun from 2.5/1.5/3 wt% SA/PEO/PS80 solutions loaded with 10^8 CFU/mL of *E.* coli K12 (K12; green), *E. coli* Nissle (EcN; yellow), and *E. coli* Nissle with 1 wt% glycerol (EcN w/ Glycerol; yellow with black pattern). Error bars denote standard error (n=3). K12 data is reproduced with permission from ref. 23. Copyright The Royal Society of Chemistry 2021.

5.4.3. Bacteria loading in single needle electrospun fibers

Next, the number of live bacteria encapsulated in the electrospun nanofibers was determined by dissolving the nanofibers and drop plating the solution. As shown in **Figure 14**, bacterial loading of > 10^5 CFU/g was achieved in each sample. The loading of all electrospun bacteria in this dissertation can be found in Appendix B. While the loading of *E. coli* Nissle appears larger than that of *E. coli* K12, the statistical difference between the three samples was not significant.

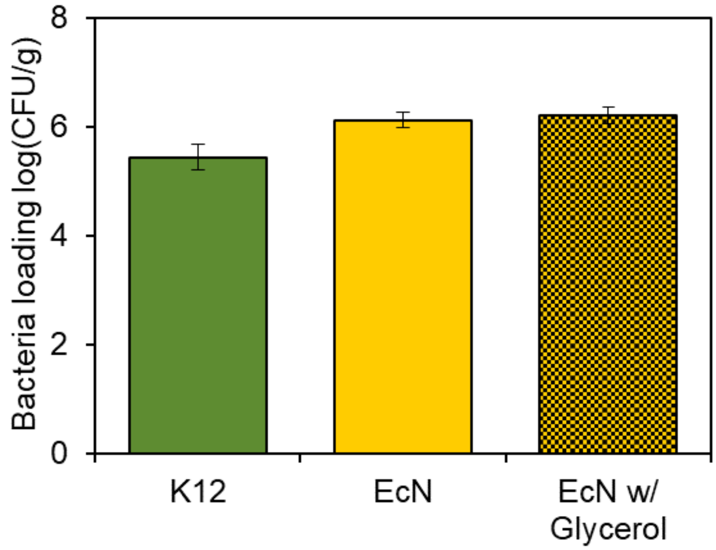

Figure 14: Bacterial loading in single needle electrospun SA/PEO/PS80 nanofibers containing *E. coli* K12 (K12), *E. coli* Nissle (EcN), and *E. coli* Nissle with 1% glycerol (EcN w/ Glycerol) reported as mean ± standard error of technical triplicates. All samples were determined to be statistically equivalent in bacterial loading by statistical analysis detailed in **Section 3.22**. K12 data is reproduced with permission from ref. 23. Copyright The Royal Society of Chemistry 2021.

In an attempt to increase bacteria loading, 1 wt% of glycerol was added to the precursor solution. Glycerol can be used by bacteria as a carbon source or as a cryoprotectant that prevents ice formation that kills bacteria during long-term storage.[7] The addition of glycerol during the electrospinning of *E. coli* electrospun into polyvinyl alcohol in another study greatly improved the bacterial viability after electrospinning.[18] Additionally, alginate has been electrospun with glycerol as a plasticizer to make alginate chains more flexible and easy to entangle.[125] Since no statistical significant differences were found between the bacteria loading due to the addition of glycerol, we did not continue with the incorporation of glycerol in the as-spun nanofiber.

5.4.4. Coaxial electrospinning of probiotics *E. coli* Nissle and *L. lactis*

Increasing the bacterial loading beyond 10^8 CFU/mL in the precursor solution prevented the electrospinning of fibers likely due to changes in surface tension and conductivity. Rather than reoptimizing the precursor solution concentration, the coaxial electrospinning setup (**Figure 3**) was adapted such that higher suspensions of bacteria (inner needle) could be electrospun into a precursor solution (outer needle). Equal volumes of a suspension of 10^{10} CFU/mL of *E. coli* Nissle or *L. lactis* and a solution of 5 wt% sodium alginate (aq) were mixed together to reduce interfacial tension variance that can occur where both solutions meet at the coaxial needle tip.

After electrospinning, fluorescence microscopy and SEM imaging were used to confirm the encapsulation of cells within the alginate-based nanofibers. The fluorescent proteins which are produced by metabolically active bacteria can be monitored using fluorescence microscopy to locate encapsulated bacteria and confirm their viability. In these micrographs (**Figure 15.a**), fluorescent *E. coli* K12 cells appeared to be encapsulated within the nanofibers. The distinct rod shape of *E. coli* was oriented length-wise along the fiber due to a sink-like flow in the electrospinning jet.[18] SEM micrographs were also able to confirm the encapsulation of bacteria. Bulges appeared along the length of the fiber which were 2.52 ± 1.14 μm in length and 0.86 ± 0.05 μm in width (**Figure 15.b**). These dimensions closely resemble that of our *E. coli* K12 (2.44 μm × 0.65 μm).

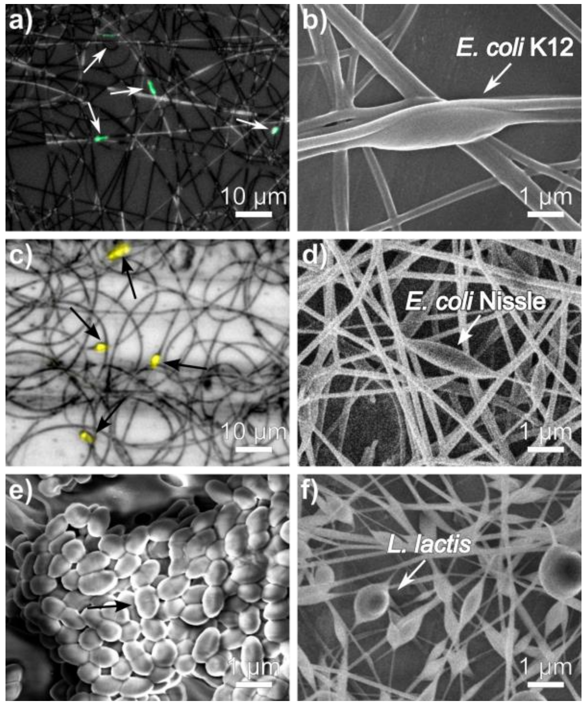

Figure 15: Various (a & c) fluorescent or (b, d, e, & f) SEM micrographs of electrospun (a & b) *E. coli* K12, (c & d) *E. coli* Nissle, and (e & f) *L. lactis* in alginate-based nanofibers. Arrows indicate locations of bacterial cells in each image. Panels (a) and (b) are adapted with permission from ref. 23. Copyright The Royal Society of Chemistry 2021.

Similar images were taken of coaxial electrospun *E. coli* Nissle (**Figure 15.c & 15.d**) which was engineered to produce yellow fluorescent proteins and *L. lactis* (**Figure 15.e & 15.f**). The production of fluorescent proteins confirmed the viability of the *E. coli* while SEM imaging showed the smooth, uniform nanofibers. The *L. lactis* strain was not engineered to produce fluorescent proteins; therefore, SEM micrographs can be used to compare the bacteria and bead sizes but not cell viability.

Using the coaxial setup (**Figure 3**), the bacterial loading in the electrospun nanofiber can be influenced by the flow rate of the solutions. A higher flow rate of the inner solution containing bacteria suspended in SA solution led to significantly higher loadings in the as-spun nanofiber for both bacteria. (**Figure 16**) *L. lactis* had a significantly higher loading than *E. coli* Nissle likely due to inherent differences between bacteria strains. Though flow rate did not significantly influence the loading of electrospun *E. coli* Nissle and *L. lactis*, control of coaxial flow rates has been shown to influence fiber diameter and material release.[54,123,151]

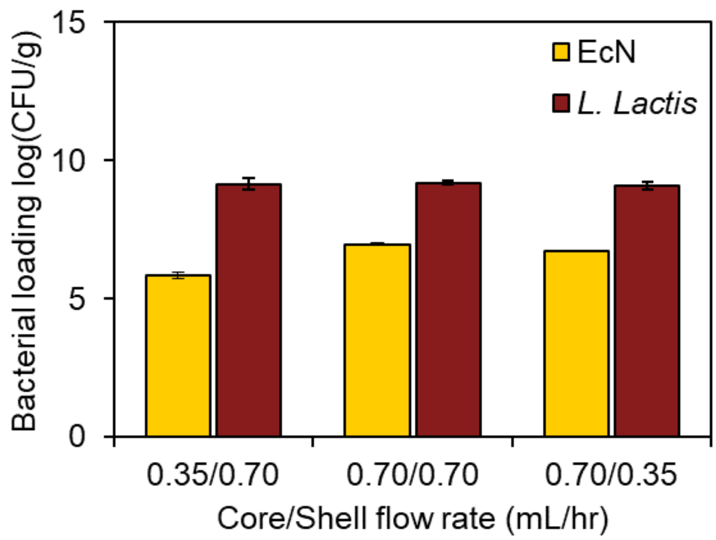

Figure 16: Bacteria loading of *E. coli* Nissle and *L. lactis* in coaxially electrospun into alginate-based nanofibers at varying core/shell solution flow rates reported as mean ± standard error of three technical triplicates.

5.5 Conclusions

This study aimed to encapsulate live bacteria into alginate-based nanofibers to demonstrate the potential of using these materials to deliver probiotics to the gut. First, we optimized the morphology of SA/PEO fibers using the surfactant PS80. The addition of surfactant decreased both the surface tension and the conductivity of the precursor solution to form smooth fibers from a SA/PEO/PS80 (2.8/1.2/3 wt%) solution. Next, a suspension of *E. coli* was blended into this polymer solution to be encapsulated during electrospinning. Fibers with a beaded morphology were electrospun from this bacteria-loaded solution. The polymer concentration was modified to compensate for the addition of bacteria into the solution and smooth fibers were once again produced. The electrospun solution of 2.5/1.5/3 wt% SA/PEO/PS80 encapsulated 2.74×10^5 CFU/g of viable *E. coli* K12 and 8.47×10^5 CFU/g of *E. coli* Nissle. To achieve higher bacteria loading, coaxially electrospinning was conducted on known probiotics *E. coli* Nissle and *L. Lactis* for bacteria loadings up to 9.05×10^6 CFU/g and 1.29×10^9 CFU/g, respectively. The thorough understanding of how surfactant and cargo loading impact precursor solution properties and subsequently biopolymer fiber formation can facilitate the ease of encapsulating living active agents into biopolymer fibers, thus broadening their application space. The need to deliver living microorganisms using a flexible, porous, and biocompatible textiles will continue to expand in years to come.

CHAPTER 6

ETHANOL-FREE CROSSLINKING OF ALGINATE-BASED FIBERS

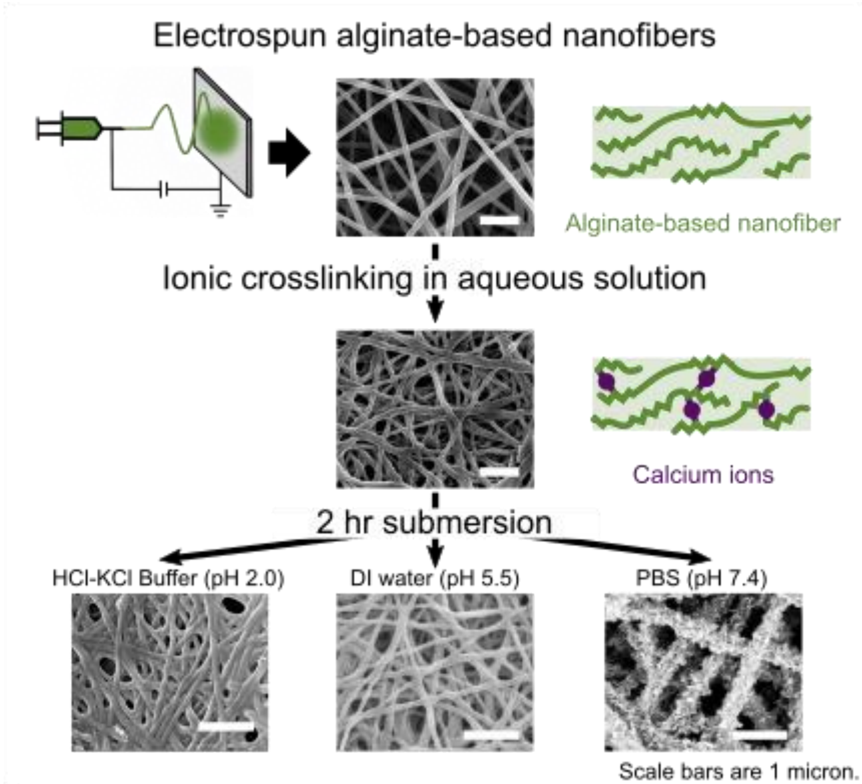

This chapter was adapted with permission from

Diep, E.; Schiffman, J. D. Ethanol-free Cross-Linking of Alginate Nanofibers Enables Controlled Released into a Simulated Gastrointestinal Tract Model. *Biomacromolecules*. **2023**, *24* (6), 2908-2917. https://doi.org/10.1021/acs.biomac.3c00274.

6.1 Abstract

The use of alginate nanofibers in certain biomedical applications, including targeted delivery to the gut, is limited because an ethanol-free, biocompatible crosslinking method has not been demonstrated. Here, we developed water-stable, alginate-based nanofibers by systematically exploring post-electrospinning crosslinking approaches that used calcium ions dissolved in (1) a glycerol/water co-solvent system and (2) acidic, neutral,

or basic aqueous solutions. Scanning electron microscopy proved that the fibers crosslinked in glycerol co-solvent or pH-optimized solutions had maintained the same morphology as the ethanol-based literature control. Notably, crosslinked fibers were generally smaller in diameter than the as-spun fibers due to both chemical interactions and mass loss during crosslinking, which was supported by mass measurements, FTIR, and TGA. During stability tests wherein the crosslinked fibers were exposed to three aqueous solutions, the crosslinked fibers were stable in water and acid buffer, yet swelled in phosphate buffer saline, making them useful scaffolds for pH-controlled release applications. Proof-of-concept release experiments were conducted using a simulated gastrointestinal tract model. As desired, the cargo remained encapsulated within the crosslinked nanofibers when exposed to an acidic solution that modeled the stomach. Upon exposure to a solution that mimicked the intestines, the cargo was released. We suggest that these crosslinked, alginate-based nanofiber mats hold the potential to be broadly used in biomedical and environmental applications.

6.2 Introduction

Natural polymers, like alginate, are ideal for use in biomaterials due to their biocompatibility and water solubility. Alginate is a polysaccharide composed of (1,4)-β-D-mannuronic acid and (1,4)-α-L-guluronic acid that can be derived from abundantly-found brown seaweed. Significant research has been conducted to construct hydrogels that could be used as implants, tissue scaffolds, and wound dressing, by crosslinking the alginate using aqueous solutions containing calcium ions.[64] The calcium ions from ionic bonds with carboxylate functional groups along the alginate chains to create a water-stable structure. [152,153] For wound dressing and tissue engineering applications, crosslinked alginate hydrogels create a physicochemical environment similar to extracellular matrices that promote healing and/or support tissue cell adherence and growth. [30,33,154] Biological cargo like drugs, proteins, and cells can also be safely encapsulated within the biocompatible alginate hydrogels.[23,65,69,104,121] Calcium alginate hydrogels are particularly beneficial in the oral delivery of biologicals because the gel collapses in low pH environments like that of the stomach and swells to release cargo in higher pH environments, like that of the intestines.[64,72]

Relative to well-documented hydrogels and capsules, alginate nanofiber scaffolds offering high surface area, porosity, and flexibility have been much less studied.[21,33,64,67,155,156] The formation of alginate into fine micro- or nanostructures has been challenging due to its rigid chain structure and high viscosity in aqueous solutions.[41,64,76,157] While not optimal for biocompatible applications, organic solvents have been demonstrated to increase the flexibility and entanglement of alginate chains for electrospinning purposes.[33,129–131] Other researchers have demonstrated that by adding biocompatible carrier polymers, like polyethylene oxide or polyvinyl alcohol (PVA) to the precursor solutions, entanglements are formed around the alginate chains that facilitate electrospinning.[43,75,76,158] Glycerol, which has been used as a plasticizer for alginate hydrogels, has been shown to increase alginate chain flexibility to facilitate electrospinning.[159,160,126] The use of a surfactant is also a common approach to lowering the surface tension of the alginate precursor solution and assisting in the formation of smooth fibers.[41,76,113,161]

In Chapter 0, we fabricated bacteria-loaded, alginate-based nanofibers by electrospinning alginate with GRAS additives and solvents. [23] The precursor solution featured PEO, as the biocompatible carrier polymer, and polysorbate 80, as an FDA-approved surfactant, to produce smooth fibers. Despite the demonstrated success of electrospinning alginate-based nanofibers, GRAS crosslinking methods are necessary to stabilize the fibers for their utilization in aqueous environments, such as biological media. Unfortunately, GRAS crosslinking methods for electrospun alginate nanofibers were not studied in our previous work nor in other literature reports.[23,41,75,129,162–164]

Previously, researchers crosslinked alginate-based fibers by submerging them in aqueous solutions containing calcium nitrate tetrahydrate; however, this caused the alginate chains to rearrange and partially dissolve into a film rather than maintaining the electrospun nanofiber morphology.[77] In other studies where nanofiber structures were maintained, ethanol was used as a co-solvent in the crosslinking solution which prevented the dissolution of the fibers.[41,78,165] Notably, ethanol is not ideal for the encapsulation/delivery of biologics as it can cause cell death and promote oxidative stress that damages proteins and DNA.[166–171] Despite these promising preliminary studies, more work is needed to establish biocompatible methods of transforming as-spun alginate nanofibers into structures that are stable in aqueous media.

In this chapter, we explored five different solutions to transform alginate-based nanofibers post-spinning into chemically robust biomaterials. The influence of solution pH and co-solvent systems on the crosslinking of the alginate-based nanofibers, rather than the published crosslinking method that relies on ethanol, was investigated. We hypothesized that changing the pH value could influence the behavior and hydrogen bonding between alginate chains in the nanofibers during crosslinking to hinder the dissolution of alginate into the aqueous crosslinking solution. Similarly, glycerol is known to form hydrogen bonds between alginate chains that may help to maintain the nanofiber structure during crosslinking. Changes in the chemical and mass composition of the fibers before and after crosslinking were also investigated via FTIR spectroscopy, TGA, and mass measurements. SEM imaging tracked the fiber morphology of the crosslinked fibers through submersion in aqueous environments of varying pH and salt concentrations.

6.3 All Materials and Methods are described in Chapter 3.

6.4 Results and Discussion

6.4.1. Crosslinking of alginate-based nanofibers

Alginate-based nanofibers (**Figure 17**) electrospun from a 2.5/1.5/3 wt% solution of SA/PEO/PS80 were smooth and uniform with a fiber diameter of 146.4 ± 18.1 nm. This precursor solution was a slightly modified composition from **Section 5.4.3** that optimized these as-spun (non-crosslinked) fibers.[23] After electrospinning, as-spun fibers were ionically crosslinked using calcium chloride solutions as outlined in **Table 3**. A crosslinking time of 60 s was chosen based on the overall treatment time of the previously published, ethanol-based crosslinking method. As a reminder, CA-3, CA-7, and CA-10 samples are fibers crosslinked in 2% $CaCl_2$ (aq) at pH values of 3, 7, and 10.3, respectively. Notably, the inherent pH of 2% $CaCl_2$ dissolved in DI water was 10.3. CA-PE nanofibers were pretreated in ethanol for 60 s before being crosslinked in 2% $CaCl_2$ in 1:5 ethanol:water co-solvent system. To decouple the effects of the ethanol pretreatment, fibers were also crosslinked in the 2% $CaCl_2$ in 1:5 ethanol:water solution for 60 s. This sample was labeled CA-E. Glycerol was proposed as an alternative co-solvent that would be more compatible with biological cargo. CA-G samples were created by crosslinking as-spun fibers in 2% $CaCl_2$ in 1:1 glycerol:water.

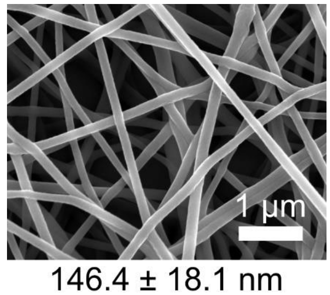

Figure 17: SEM micrographs of electrospun2.5/1.5/3% SA/PEO/PS80 nanofibers. The scale bar is 1 µm, and the mean diameter ± standard deviation is provided below the micrograph. This figure is reproduced with permission from ref. [112]. Copyright 2023 American Chemical Society.

6.4.2. SEM analysis of crosslinked nanofibers

Our crosslinked fibers did not dissolve while using the ethanol-based literature (control) method or the new ethanol-free systems. (**Figure 18**) Some fibers appeared flattened (less cylindrical), compacted (increased fiber density in the z-direction), and aggregated (aligned along the lengths of the fiber) as compared to the as-spun fibers but do not indicate total loss of nanofiber structure. These morphologies are also commonly reported for electrospun fibers that have been crosslinked[77,172] or submerged in liquids.[173]

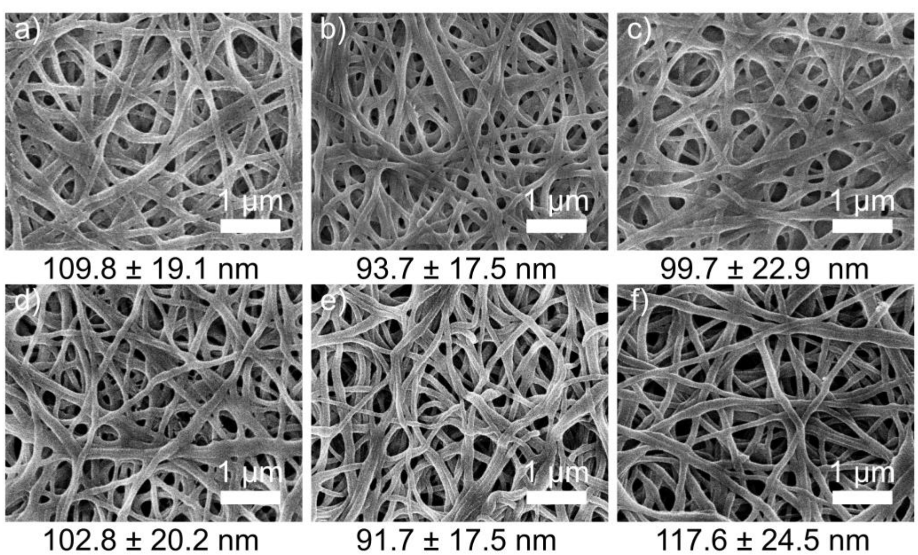

Figure 18: SEM micrographs of (a) CA-3 crosslinked nanofibers, (b) CA-7 crosslinked nanofibers, (c) CA-10 crosslinked nanofibers, (d) CA-PE crosslinked nanofibers, (e) CA-E crosslinked nanofibers, and (f) CA-G crosslinked nanofibers. Scale bars are 1 µm, and the mean diameters ± standard deviations are provided below each micrograph. Panels (a), (b), (c), (d), and (f) are reproduced with permission from ref. [112]. Copyright 2023 American Chemical Society.

Previous studies have noted that crosslinking alginate-based nanofibers with aqueous calcium solutions (without ethanol) caused the nanofiber structure to become compromised. For example, Leung et al.[77] reported the loss of fiber structure due to partial dissolution and fiber webbing after the fibers were submerged in an aqueous calcium nitrate crosslinking solution. Despite spraying the alginate nanofiber mat with an aqueous solution of calcium chloride rather than submersion, Wongkanya et al.[164] also reported damage to the macrostructure of fibers after crosslinking due to fusion of the fibers. Previous reports[41,78,172] suggest that using ethanol to crosslink the alginate content in electrospun nanofibers assists in maintaining the nanofiber morphology until crosslinking is complete.

6.4.3. Relative fiber diameter and mass retention analysis of crosslinked nanofibers

Relative fiber diameters (calculated using **Equation 1**) are displayed in **Figure 19**. Fiber diameters after crosslinking were smaller than that of the as-spun fiber. The fiber mass retained after crosslinking (calculated using **Equation 3** and shown in **Figure 19**) to determine if mass lost during crosslinking contributed to the decrease in fiber diameter. Despite having statistically equivalent mass retention, CA-3 and CA-7 had statistically different average diameters from the CA-10 and CA-PE nanofibers. Differences in fiber diameter can then be attributed to chemical interactions present in each crosslinking system. In the acidic environment of the CA-3 crosslinking system, the carboxylate groups on the alginate chain are protonated causing hydrogen bonding between chains. According to a proposed model that was based on microstructural analysis by Zazzali et al.,[174] strong intermolecular interactions between protonated alginate chains quickly consolidate into a branched supramolecular structure preventing further compaction of the network leading to a larger fiber diameter of CA-3 compared to CA-7, CA-10, CA-E, and CA-PE. In higher pH systems, like that of the CA-7 and CA-10, crosslinking solutions, alginate chains experience repulsion forces between deprotonated carboxylate groups which allow the chains to rearrange leading to syneresis and shrinkage of the overall material structure.[175] However, repulsion forces may also explain the higher fiber diameter for CA-10 and CA-7 despite equivalent mass retention.

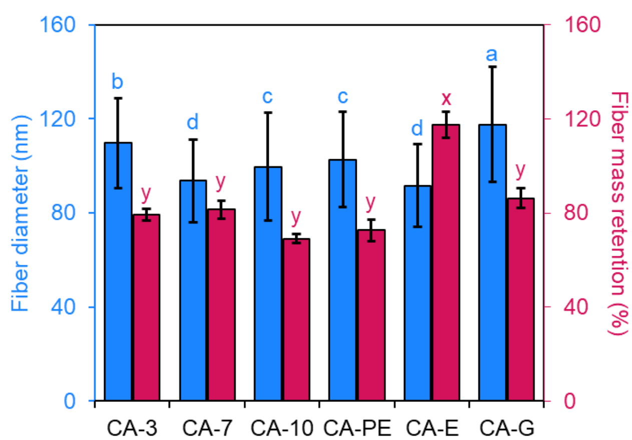

Figure 19: Relative fiber diameter (left axis) and fiber mass retention (right axis) of crosslinked nanofibers. The relative fiber diameter was calculated using **Equation 1**, whereas the fiber mass retention was calculated using **Equation 3**. Error bars represent mean ± standard error. When the same letter (a, b, or c for relative fiber diameter; x or y for fiber mass retention) is present above multiple data columns, it indicates that those samples are significantly equivalent ($p<0.05$). Data for samples CA-3, CA-7, CA-10, CA-PE, and CA-G are reproduced with permission from ref. **[112]**. Copyright 2023 American Chemical Society.

CA-PE and CA-E crosslinking systems also occurred in higher pH environments. Both samples were statistically different in both mass retention and fiber diameter.

Alginate is insoluble in ethanol. Therefore, the presence of ethanol can help compact the nanofiber together during crosslinking to help keep its mass.[41] Besides the ethanol pretreatment step, CA-PE spent 10 s in the ethanol:water crosslinking solution that contained $CaCl_2$, whereas CA-E was crosslinked in the same solution for 60 s. Increased crosslinking time has been shown to reduce the size and swelling behavior of calcium alginate hydrogels; thus, being consistent with a smaller fiber diameter in our case.[176,177]

While CA-G crosslinked fibers increased in mass after crosslinking, the crosslinked fiber diameters were still smaller than that of the as-spun fibers. The increase in fiber mass can be attributed to the diffusion of glycerol into the alginate-based nanofiber. In a study regarding the presence of glycerol in the crosslinking bath, Davarcı et al.[178] reported a decrease in alginate bead size due to the osmotic effect of glycerol in the crosslinking solution, which may apply to our study. Interestingly, Wang et al.[1] described that glycerol can have opposing effects on alginate structure size. On one hand, glycerol can replace the water molecules causing an increase in intermolecular distances between alginate chains. On the other hand, hydrogen bonding between glycerol and alginate chains can cause the overall structure to compact.

6.4.4. Chemical composition of crosslinked nanofibers via FTIR

A number of works[41,78,165] report the need for ethanol during the crosslinking of alginate-based nanofibers; however, these nanofibers differ in electrospinning recipes and parameters leading to variations in fiber properties like alginate content and fiber diameter. Alginate concentration has been found to affect the structure of alginate hydrogels.[180–182]. Adding solutions of alginate into calcium baths form alginate particles. Using low concentrations of alginate or calcium can need to oblong shapes rather than spherical particles. This work characterized the chemical and mass composition of our as-spun fibers as a reference point for other alginate crosslinking studies moving forward.

FTIR was used to detect the chemical compounds and calcium complexes present in the crosslinked nanofibers. Similar to the as-spun fibers, all crosslinked fibers showed characteristic peaks of SA, PEO, and PS80 indicating the presence of each of these components in all samples (**Figure 20**). For samples crosslinked in co-solvent systems, neither ethanol nor glycerol could be identified in the crosslinked fibers because the carbon bonds and hydroxyl groups found in ethanol and glycerol overlap with bonds seen in SA, PEO, and PS80 making them indistinguishable by FTIR.

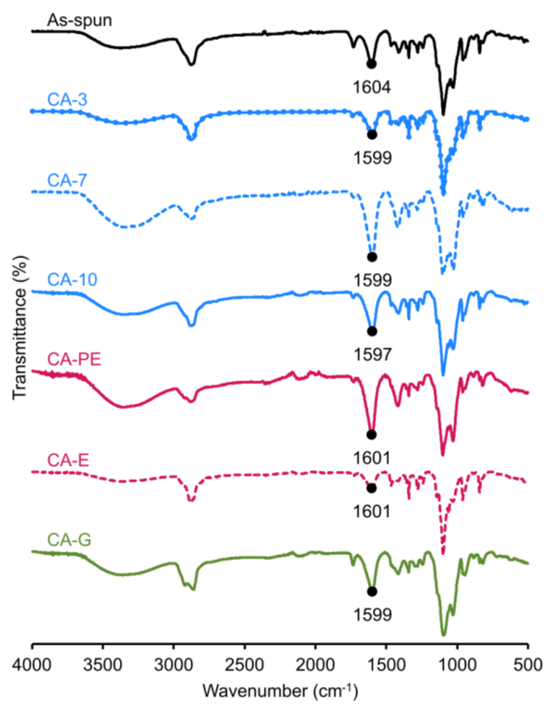

Figure 20: FTIR spectra of as-spun and crosslinked nanofibers. Data for as-spun, CA-3, CA-7, CA-10, CA-PE, and CA-G samples are reproduced with permission from ref. [112]. Copyright 2023 American Chemical Society.

To confirm chemical crosslinking, peaks assigned to the carboxylate group on the SA chains in each sample were marked and labeled in **Figure 20**. In crosslinked samples, this peak shifted from 1604 cm^{-1} in the as-spun sample to 1597 cm^{-1}-1601 cm^{-1} in the crosslinked samples due to the stronger interaction between alginate and calcium ions than the interaction between alginate and sodium. These results agree with other reports studying the FTIR analysis of calcium crosslinked alginate structures.[160] Given the limitation of our FTIR equipment, no correlation could be made between the wavenumber shift and the extent of crosslinking; furthermore, the quantity of SA, PEO, or PS80 in the nanofibers cannot be quantified by FTIR.

6.4.5. Mass composition of crosslinked nanofibers via TGA

The TGA data of crosslinked nanofibers displayed in **Figure 21** and reported in **Table 8** revealed a change in mass composition after crosslinking. The CA-3, CA-PE, CA-E, and CA-G crosslinked fiber mats experienced two major degradation events, but the CA-7 and CA-10 only exhibited one major degradation event. The different degradation events indicate different mass compositions for each crosslinked fiber. This led us to hypothesize that pH value and co-solvent systems can facilitate or hinder the diffusion of water-soluble components into and out of the crosslinked nanofibers.

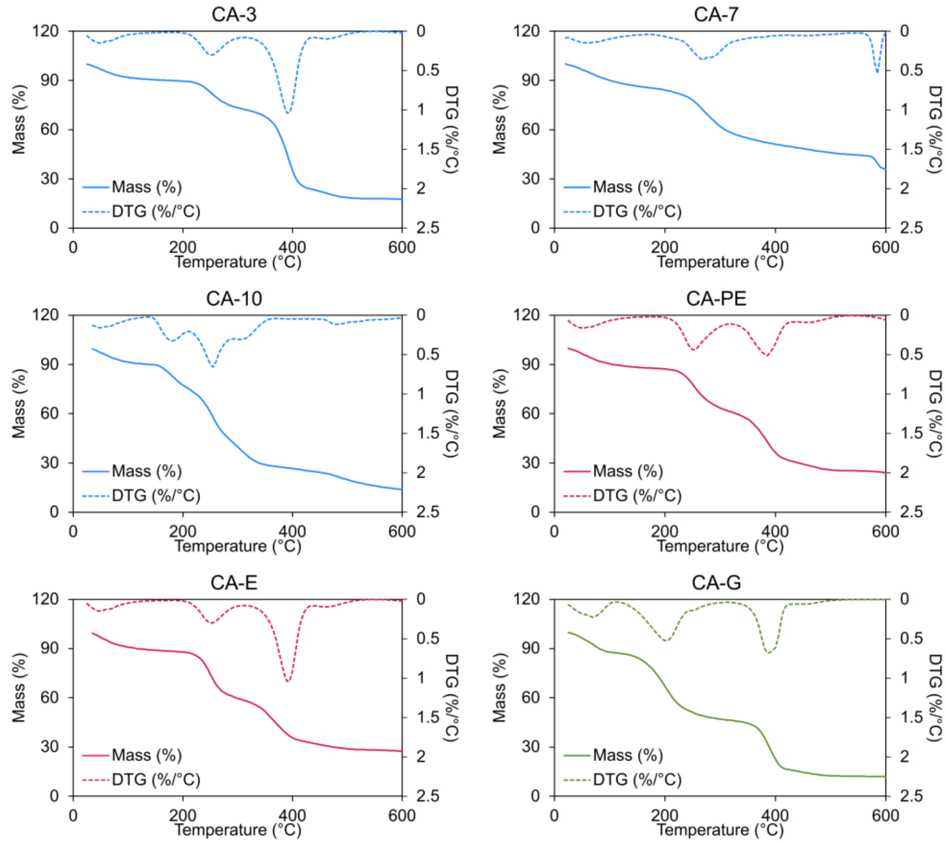

Figure 21: TGA thermograms of crosslinked nanofibers. Data for CA-3, CA-7, CA-10, CA-PE, and CA-G samples are reproduced with permission from ref. [112]. Copyright 2023 American Chemical Society.

Table 8: Thermal degradation data of crosslinked alginate-based nanofibers. This table is reproduced with permission from ref. [112]. Copyright 2023 American Chemical Society.

Sample	Water loss (%)	Residue (%)	Range (°C)[a]	Peak (°C)[b]	Mass loss (%)[c]	Reason for mass loss
CA-3	10.0	18.0	225-285 365-410	250 390	17.6 48.9	Alginate degradation[25,107,144] C-O-C bond breaking[107,142,143]
CA-7	14.3	50.1	230-330	270	35.5	Alginate degradation[25,107,144]
CA-10	13.9	31.4	210-315	255	54.7	Alginate degradation[25,107,144]
CA-PE	12.3	30.5	230-290 350-410	250 385	26.4 30.8	Alginate degradation[25,107,144] C-O-C bond breaking[107,142,143]
CA-E	11.5	32.3	230-275 330-400	250 360	29.3 26.9	Alginate degradation[25,107,144] C-O-C bond breaking[107,142,143]
CA-G	12.7	15.7	160-240 365-410	200 385	40.7 30.9	Alginate and glycerol degradation [25,107,144,159,183] C-O-C bond breaking[107,142,143]

[a] Degradation temperature ranges are reported from the onset temperature to offset temperature.[146]

[b] Peak degradation temperature represents the temperature of maximum mass loss as determined by local maxima on the first derivative thermogram.[142,146]

[c] Mass loss (%) refers to the change in mass between the onset and offset temperatures.[106]

6.4.6. TGA of crosslinked fibers with multiple degradation events

In CA-3, CA-PE, and CA-G crosslinked nanofibers, the first degradation peaks occurred at 250°C, 250°C, and 200°C, respectively, which is within the degradation range of SA.[25,107,144] Interestingly, the glycosidic bond degradation temperature in CA-G fibers shifted to a lower temperature of 200°C. It has previously been reported that glycerol decreased the thermal stability of alginate films by interrupting intermolecular forces between alginate chains and decreasing the crystallinity of the hydrogel.[159,183] The second degradation peaks of CA-3, CA-PE, CA-E, and CA-G occurred at 390°C, 385°C, 360°C, and 385°C, respectively, resembling the degradation of the C-O-C bonds found in PEO and PS80.[142,143]

The intermolecular interactions present in CA-3, CA-PE, CA-E, and CA-G crosslinking systems could have hindered or reduced the diffusion of PEO and PS80 out of the fibers. As previously mentioned, alginate under acidic conditions becomes protonated, also referred to as alginic acid. Upon the introduction of calcium ions, additional stability is provided by the combination of hydrogen bonding between carboxylic acids along the alginate chain, as well as by ionic crosslinking with calcium ions. In the case of the CA-PE and CA-E crosslinking systems, the ethanol (in the pretreatment and/or in the crosslinking solution) packed the alginate chains together before and during crosslinking as alginate is insoluble in ethanol.[41] The network of hydrogen-bonded or precipitated alginate along with the calcium crosslinks may prevent PEO and/or PS80 from diffusing out. Similarly, alginate and glycerol can also form hydrogen bonds, which might prevent the other components from diffusing out while simultaneously attracting glycerol to the fiber.[184]

6.4.7. TGA of crosslinked fibers with single degradation events

The degradation of CA-7 and CA-10 occurred in a singular event with peak degradation at 270°C and 255°C, respectively, which was again attributed to the degradation of SA. Notably, the degradation of CA-10 fibers occurred in multiple, less-defined steps within the range of alginate degradation. Similar to our findings, Liu et al.[144] found that barium crosslinked alginate films exhibited a multistep degradation with the first step corresponding to decarboxylation and the second step corresponding to glycosidic bond breaking, dehydration, and decarbonylation. In comparison with the as-spun fibers and other crosslinked fibers, the TGA data of CA-7 and CA-10 fibers did not exhibit degradation in the temperature range of PEO/PS80. As PEO and PS80 are water-soluble, submersion of the as-spun fibers into aqueous solution, like that of the crosslinking systems, can lead to the diffusion of PEO and PS80 out of the fibers as consistent with the work by Bonino et al.[41] In the CA-7 and CA-10 crosslinking systems, the alginate chains have more freedom for rearrangement, as previously discussed, which would also allow PEO and PS80 to diffuse out. Thus, the TGA of CA-7 and CA-10 only detected the presence of calcium alginate.

In summary, the TGA data suggests that CA-7 and CA-10 nanofibers were solely composed of calcium alginate (**Table 8**). The composition of CA-3, CA-PE, and CA-E fibers was suspected to be 17.6% SA and 30.8% PEO/PS80 with 18.0% residue; 26.4% SA and 30.8% PEO/PS80 with 12.3% residue; and 29.3% SA and 26.9% PEO/PS80 with 32.3% residue, respectively. Lastly, the composition of the CA-G fibers was 40.7% SA/glycerol and 30.9% PEO/PS80, with 15.7% residue. As previously stated in Section 4.4.5, residue may be attributed to the alginate component within these nanofibers.

6.4.8. Chemical stability of crosslinked alginate nanofibers

The crosslinked fibers were submerged in HCl/KCl acid buffer (pH 2.0), DI water (pH 5.5), and PBS buffer (pH 7.4) solutions for 120 min to test their stability in solutions having different pH values and salt solutions. HCl/KCl acid buffer and PBS buffer are also microbiologically and physiologically relevant media.[77,120] In general, fiber morphology was retained post-submersion in the acidic buffer (**Figure 22**) and DI water (**Figure 23**) with fiber diameter listed in **Table 9**. Fiber fusion and aggregation were common in crosslinked fibers submerged in the HCl/KCl solution, especially for CA-3, CA-7, and CA-10 nanofibers; however, distinct fibers were visible across all time points during submersion in the acidic buffer. These observations are consistent with literature wherein alginate hydrogels tend to contract in lower pH environments due to hydrogen bonding between protonated carboxylic acid groups.[64,104,145] When exposed to DI water, the CA-3, CA-7, and CA-10 fibers retained their distinct morphology. In contrast, CA-PE and CA-G fibers became slightly webbed in DI water after 120 min.

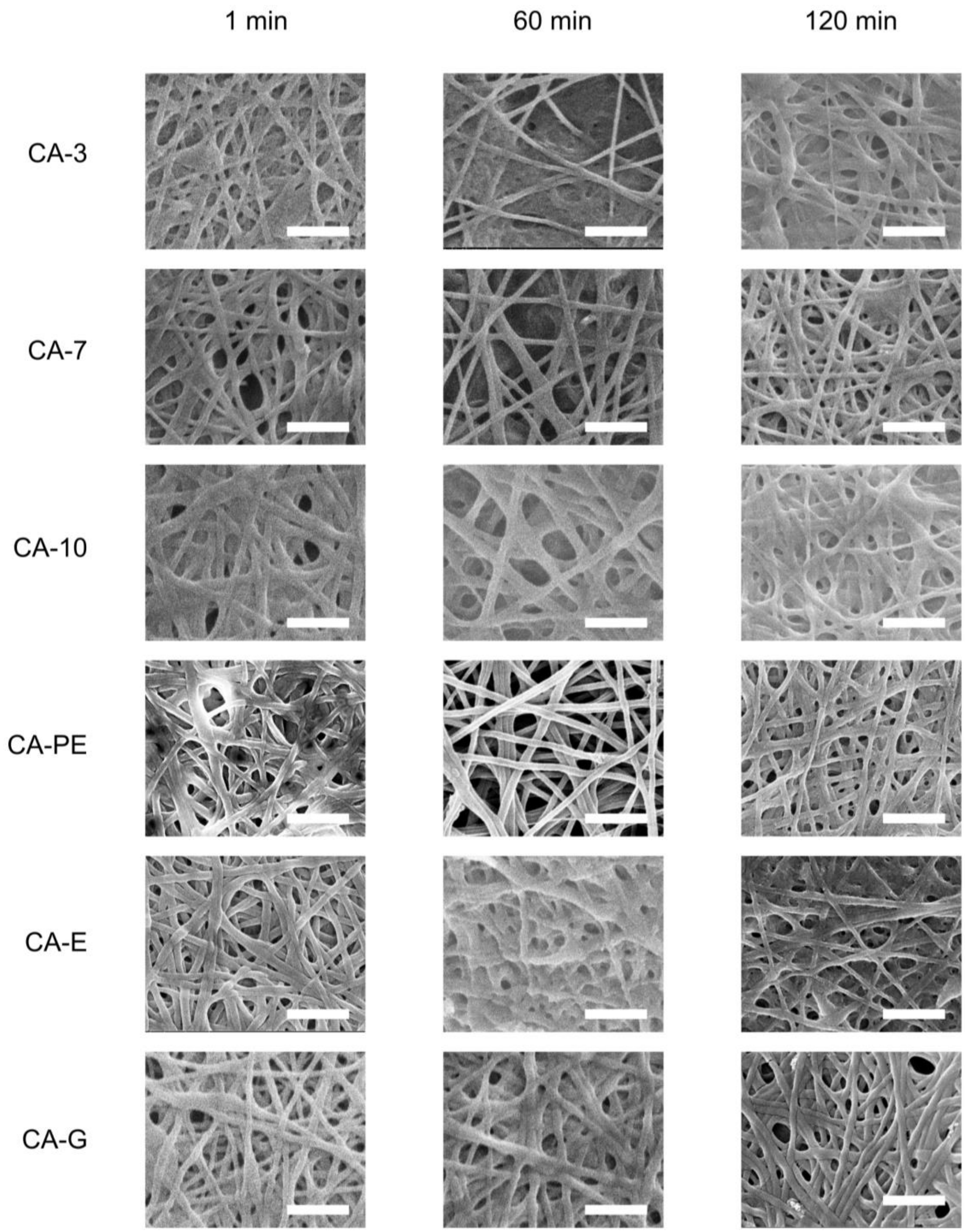

Figure 22: SEM micrographs of crosslinked alginate-based nanofibers after submersion in HCl/KCl acid buffer over 120 min. Scale bars are 1 μm. Panels for CA-3, CA-7, CA-10, CA-PE, and CA-G samples are reproduced with permission from ref. [112]. Copyright 2023 American Chemical Society.

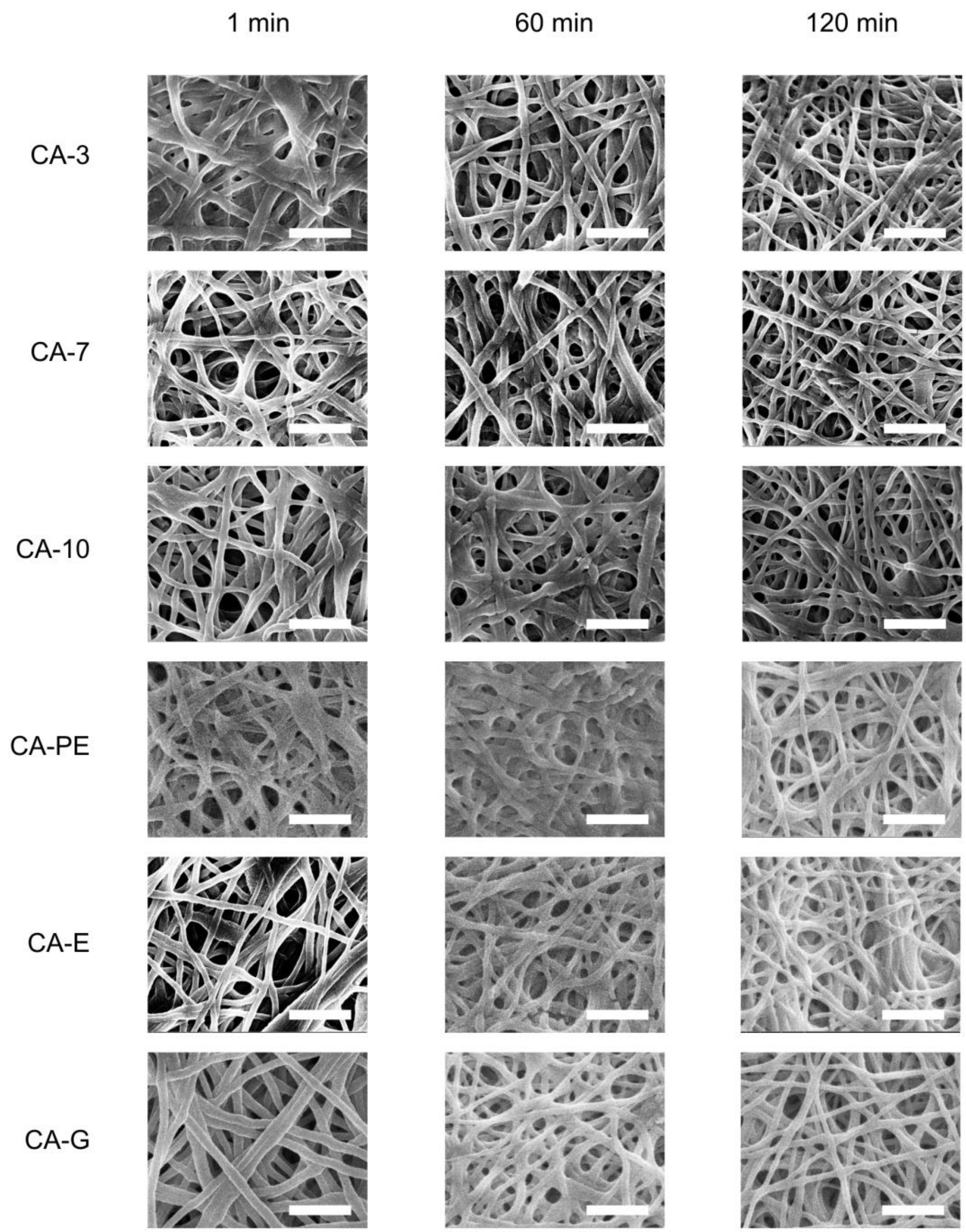

Figure 23: SEM micrographs of crosslinked alginate-based nanofibers after submersion in DI water over 120 min. Scale bars are 1 µm. Panels for CA-3, CA-7, CA-10, CA-PE, and CA-G samples are reproduced with permission from ref. [112]. Copyright 2023 American Chemical Society.

Table 9: Characteristics of as-spun and crosslinked alginate-based nanofibers. Data for CA-3, CA-7, CA-10, CA-PE, and CA-G samples were reproduced with permission from ref. [112]. Copyright 2023 American Chemical Society.

Sample name	After crosslinking (nm)	Acid			DI Water			PBS		
		1 min (nm)	1 hr (nm)	2 hr (nm)	1 min (nm)	1 hr (nm)	2 hr (nm)	1 min (nm)	1 hr (nm)	2 hr (nm)
As-spun	146.4 ± 18.1	n/a	n/a	n/a	n/a	n/a	n/a	n/a	n/a	n/a
CA-3	109.8 ± 19.1	111.5 ± 21.3	100.1 ± 16.4	88.1 ± 29.3	120.2 ± 27.6	127.0 ± 25.2	81.8 ± 21.5	111.2 ± 30.5	191.4 ± 46.0	509.4 ± 69.1
CA-7	93.7 ± 17.5	99.3 ± 17.0	106.9 ± 25.4	92.4 ± 19.9	86.5 ± 20.9	116.0 ± 26.3	82.8 ± 18.9	163.0 ± 40.2	n/a	n/a
CA-10	99.7 ± 22.9	125.8 ± 29.5	110.8 ± 28.2	107.6 ± 29.7	120.5 ± 23.8	133.2 ± 44.9	91.2 ± 23.4	107.8 ± 33.9	n/a	n/a
CA-PE	102.81 ± 20.2	125.9 ± 28.7	119.0 ± 45.8	92.7 ± 18.7	104.9 ± 30.9	103.8 ± 28.6	89.1 ± 21.2	159.7 ± 32.9	195.1 ± 34.0	244.8 ± 46.5
CA-E	91.66 ± 17.5	113.60 ± 17.6	123.65 ± 32.6	83.32 ± 20.3	105.74 ± 19.2	100.76 ± 20.1	121.21 ± 20.8	127.76 ± 23.5	n/a	n/a
CA-G	117.6 ± 24.5	106.6 ± 18.5	121.8 ± 30.9	121.2 ± 20.8	133.0 ± 31.2	99.7 ± 22.6	95.6 ± 19.0	107.9 ± 32.9	215.0 ± 34.5	266.9 ± 73.5

After being subjected to PBS, fibers swelled as shown by the fiber diameter analysis in **Table 9** or merge into a film as shown in **Figure 24**. After 1 min in PBS, CA-3 fibers appeared flat, whereas, after 60 min, their fiber outline remained visible. At 120 min, the CA-3 fibers were very swollen and textured. Similarly, CA-PE and CA-G fibers became textured after 60 min and continued to swell after 120 min of submersion in PBS. The observed texture could indicate either surface erosion due to the dissolution of materials from the nanofibers or mineralization due to the calcium ions within the nanofiber and phosphate ions from the buffer.[185,186] In addition to having a higher pH value than the HCl/KCl acidic buffer and DI water which destabilized crosslinked alginate structures, PBS also contains a complex salt system including phosphate ions known for binding to calcium ions. The calcium ions will either be sequestered by phosphate ions which contribute to the degradation of the fibers or act as a nucleation site for the precipitation of phosphate and other inorganic minerals onto the surface of the fibers.[186,187]

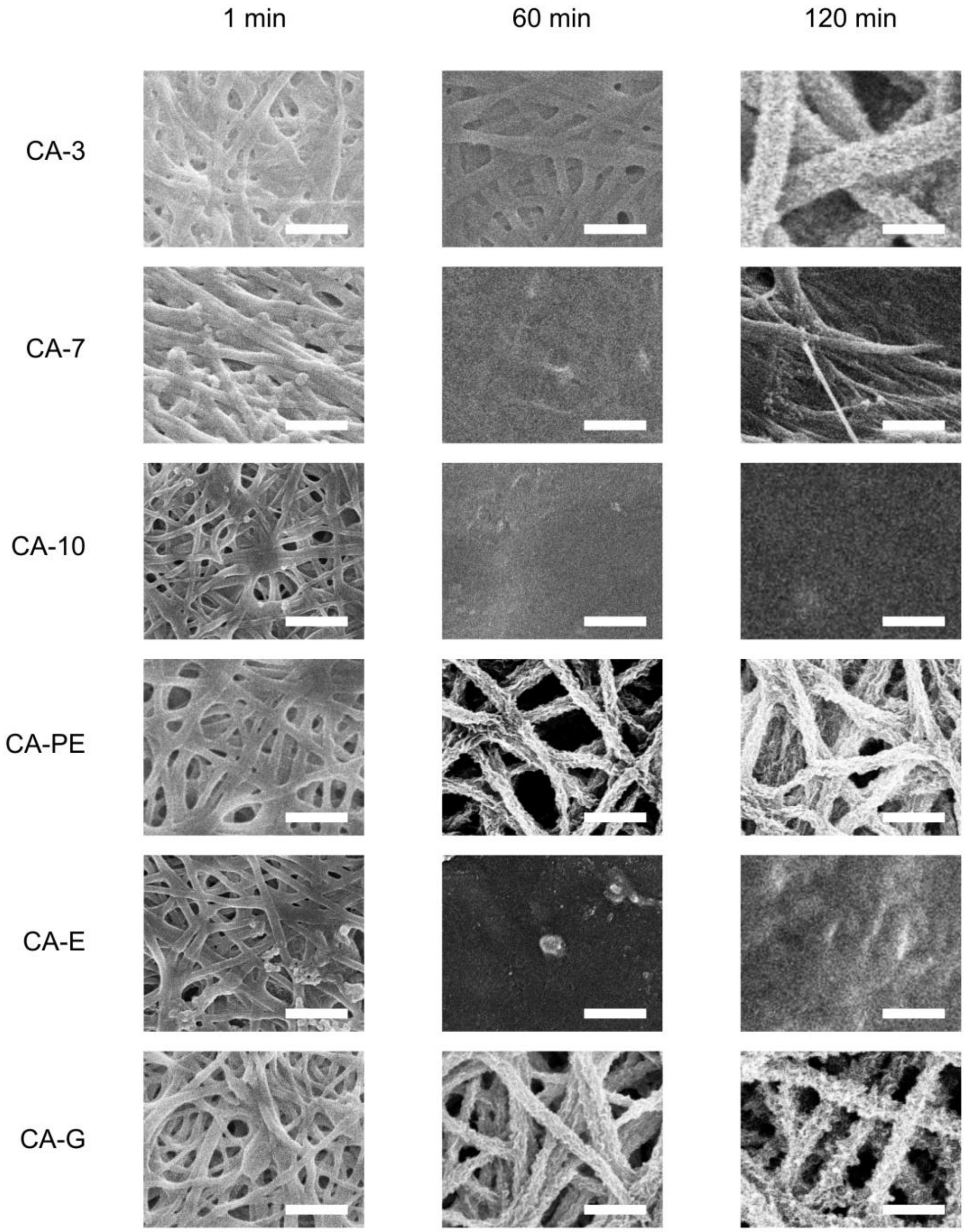

Figure 24: SEM micrographs of crosslinked alginate-based nanofibers submerged in PBS over 120 min. Scale bars are 1 µm. Panels for CA-3, CA-7, CA-10, CA-PE, and CA-G samples are reproduced with permission from ref. [112]. Copyright 2023 American Chemical Society.

6.5 Conclusion

Electrospun, alginate-based nanofibers were crosslinked using aqueous solutions of $CaCl_2$ prepared at acidic, neutral, and basic pH values, as well as using glycerol as a co-solvent for the $CaCl_2$ solution. These crosslinked fibers were compared to the current literature method that involves ethanol pretreatment and co-solvent. Ethanol can help prevent the dissolution of alginate-based nanofibers during crosslinking due to the insolubility of alginate in ethanol. Unfortunately, ethanol can be detrimental to biological materials. In the acidic crosslinking solution, hydrogen bonding between carboxylic acids binds alginate chains together preventing the dissolution of the alginate-based nanofiber in the aqueous crosslinking solution. Additionally, these bonds hinder the diffusion of PEO and PS80 from the nanofiber.

All crosslinked nanofibers retained their morphology after crosslinking. It is important to note that other studies reporting the dissolution of electrospun alginate nanofibers in the aqueous crosslinking solution utilize different precursor solutions and electrospinning parameters leading different alginate compositions in the electrospun fiber. FTIR and TGA were used to characterize the chemical and mass composition of the crosslinked nanofibers. Both methods confirm the presence of alginate in the nanofiber mats for all five crosslinking methods. Under acidic crosslinking conditions, the nanofibers maintained some composition of alginate, PEO, and PS80. In neutral and basic crosslinking solutions without co-solvents, the TGA data indicated that deprotonated carboxylate groups allow PEO and PS80 to diffuse out of the fiber leaving behind a solely calcium alginate nanofiber. As an alternative co-solvent system that would be more compatible with a variety of biological materials, a glycerol co-solvent system was used. Glycerol forms hydrogen bonds with alginate chains to aid in maintaining the electrospun nanofiber morphology as well as alginate, PEO, and PS80 composition in the crosslinked nanofibers.

SEM showed that the distinct nanofiber structure was maintained after crosslinking and throughout submersion in HCl/KCl acid buffer and DI water. In PBS where the pH value was higher and phosphate salt interactions were present, the crosslinked nanofibers tended to swell or merge into a film. The stability of the fiber in acidic environments and swelling in higher pH environments can be beneficial for the targeted release of active ingredients into the intestines for optimal performance in the body.

CHAPTER 7

APPLICATIONS OF BACTERIA-LOADED, ALGINATE-BASED NANOFIBERS

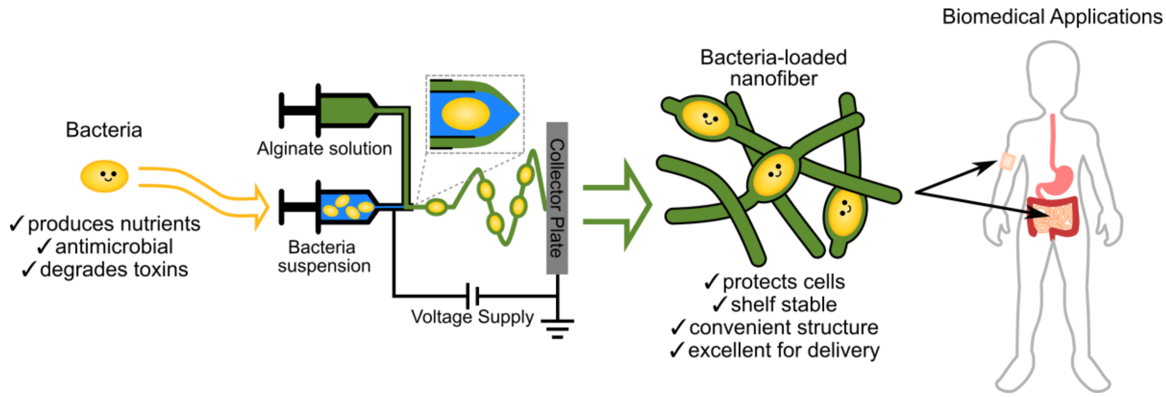

Adapted from:

Diep, E.; Schiffman, J. D. Electrospinning Living Bacteria: A Review of Applications from Agriculture to Health Care. *ACS Appl. Bio Mater*. 2023, *6* (3), 951-964. https://doi.org/10.1021/acsabm.2c01055.

7.1 Abstract

Probiotic bacteria can benefit a host or an environment by producing nutrients or producing antimicrobial compounds. Encapsulation technologies protect the bacteria against harmful agents to maintain bacterial viability and incur beneficial effects. Electrospinning bacteria encapsulates the cells in functional polymer nanofibers with excellent drug delivery properties as well as flexibility and porosity. As an encapsulation material, alginate is advantageous due to its biocompatibility and gelation with calcium ions under mild conditions. In this study, the effects of crosslinking the alginate-based nanofibers on the viability of bacteria was determined. In particular, crosslinking systems that utilized ethanol to maintain nanofiber structures were found to be antagonistic to encapsulated bacteria thus reducing their effectiveness. Instead, we proposed ethanol-free

crosslinking systems that could crosslink alginate nanofibers, while maintaining bacteria viability and loading. Gut probiotics, *E. coli* Nissle and *L. lactis*, were coaxially electrospun into alginate-based nanofibers to obtain high loadings (10^6-10^9 CFU/g). When nanofibers containing *L. lactis* were applied to surfaces inoculated with clinically relevant MRSA strains, their growth was inhibited. These scaffolds hold strong potential for use as wound dressings. Additionally, adding antacid into the formulation of the fibers improved the acid survivability of encapsulated bacteria. While this work demonstrated the use of bacteria-loaded nanofibers in two biomedical applications, future applications of these encapsulated probiotics can be expanded to other biomedical applications as well as environmental applications like water remediation and plant growth promotion.

7.2 Introduction

Bacteria offer a wide range of beneficial functions from producing nutrients to degrading harmful agents like toxins found in waste waters. In the gut, a complex community of bacteria, called the gut microbiota or microbiome, influences human health by producing antimicrobial chemicals that the body against pathogenic attack, digesting complex fibers found in various foods, and chemically signaling the immune and nervous system.[188–190] Modulation of the gut microbiota via oral delivery of probiotic bacteria has effectively treated illnesses like Clostridium difficile infection in the gastrointestinal tract.[191] Oral administration of probiotics to infants have also been found to decrease the likelihood of developing attention deficit hyperactivity disorder and Aspergers syndrome manifestations later in life suggesting gut probiotics have effects beyond the digestive tract.

A major challenge for the gut delivery of probiotics is deactivation of probiotic bacteria by stomach acid.[55,69,87] Bacteria membranes are primarily negatively charged. Positively charged protons in acidic environments can disrupt the cell membrane to kill the bacteria.[192,193] Therefore, processes like extrusion, emulsion, spray drying, freeze drying, fluidized bed, etc. have been employed to encapsulated probiotics in materials including rice proteins, alginate, chitosan, cellulose, and other biopolymers.[11,194]

After encapsulation, probiotics can be applied to a variety of environments beyond the typical oral probiotic application. Probiotic commercial products include plant supplement, lotion, toothpaste, sanitary napkin, shampoo, household cleaner, and bedding.[195,196] Encapsulation technologies improve the viability and stability of the probiotics in these products.[197] Like oral probiotics, plant supplements and cosmetic products like lotion utilize probiotics to enrich the environment. Other products like cleaners and bedding use probiotics to remove allergens or alter the microbial community.[198–200] Probiotics produce antimicrobial compounds that inhibit the growth of pathogenic bacteria and prevent infection.[201]

Many studies have already been dedicated to utilizing the antimicrobial abilities of probiotic for the treatment of wounds.[90,202,203] For example, *Lactobacillus plantarum* was co-emulsified with Vitamin E and lyophilized onto a Spanish Broom structure to create an antioxidant and antimicrobial wound dressing.[202] Spanish broom is a fibrous material with the necessary properties of flexibility and breathability as traditional cotton bandages. After the incorporation of probiotics, the Spanish broom wound dressing was effective at inhibiting the growth of *Staphylococcus aureus* and *Pseudomonas aeruginosa*. In addition to flexibility and breathability, electrospun nanofibers are excellent scaffolds for promoting cell adhesion during healing. A study by Khan et al.[90] electrospun *Enterococcus mundtii* into poly (vinyl alcohol)/ polyvinylpyrrolidone/ glycerol bioscaffolds. In a mouse model, these scaffolds improved wound closure over time compared to untreated wounds.

Electrospinning provides a dual functional encapsulation system: the encapsulation can protect bacteria against environmental factors while the nanofiber structure is a functional matrix that can be used as drug delivery systems, wound dressings, filtration membranes, tissue scaffolds, etc.[28,35] In many of these applications, the nanofibers come into contact with water and would benefit from chemical stabilization. In Chapter 5, known probiotics *E. coli* Nissle and *L. lactis* were electrospun into alginate-based nanofibers. In Chapter 6, ethanol-free crosslinking systems were developed to stabilize the nanofibers. In this chapter, the viability of encapsulated bacteria after crosslinking was determined. *L. lactis* produces nisin, an antimicrobial that inhibits the growth of Gram-positive bacteria. After crosslinking, the antimicrobial properties of the encapsulated *L. lactis* were evaluated against three strains of *S. aureus* including the clinically relevant strain, MRSA. For application of these nanofibers to deliver probiotics into the gut, the antacid calcium carbonate was formulated into the nanofibers to improve the survivability of the encapsulated *L. lactis* in a simulated gastrointestinal tract.

7.3 All Materials and Methods are described in Chapter 3.

7.4 Results and Discussion

7.4.1. Effects of crosslinking on bacterial viability

Both *E. coli* Nissle and *L. lactis* were coaxially electrospun as described in **Section 5.4.4**. To provide additional stability to the nanofiber matrix for the application of the fibers to any wet environment, the coaxially electrospun bacteria-alginate systems were crosslinked in systems outlined in **Table 3**. The viability of encapsulated bacteria (i.e., the amount of live cells relative to the total number of cells calculated by **Equation 2**) was determined via fluorescence microscopy. Free (unencapsulated) and encapsulated *E. coli* Nissle were subjected to either DI water (control) or to each crosslinking method to determine the effects of crosslinking chemicals on bacterial viability. (**Figure 25**) Control samples of free bacteria which were subjected to DI water instead of any crosslinking solution showed a viability of 95%. Free bacteria (blue) subjected to CA-3, CA-7, CA-10, CA-E, and CA-G crosslinking systems maintained high levels of viability. However, the viability of the unencapsulated bacteria decreased to 4% in the CA-PE crosslinking system. The submersion in 200 proof ethanol for 1 min as a pretreatment played a key role in deactivating bacteria since the CA-E crosslinking system did not significantly affect the viability of bacteria as compared to the control sample. Bacteria within CA-3, CA-7, CA-10, and CA-G nanofibers maintained significantly higher viability than bacteria exposed to the CA-PE crosslinking system. Interestingly, the bacteria viability within the CA-E nanofibers was significantly lower compared to that of free bacteria. These results show that the alternative crosslinking systems that avoid the use ethanol enable higher viability of encapsulated bacteria.

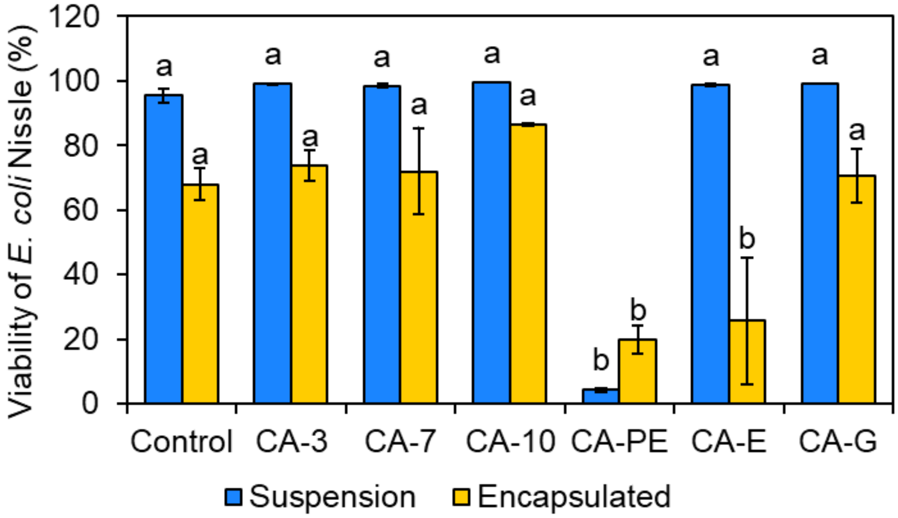

Figure 25: Viability of suspensions (blue) and coaxially electrospun (yellow) *E. coli* Nissle in SA/PEO/PS80 nanofibers after exposure to crosslinking systems detailed in **Table 3**. Data is reported as mean ± standard error of technical triplicates. Letters indicate statistically equivalent samples ($\mathbf{p < 0.05}$).

7.4.2. Bacteria loading in crosslinked nanofibers

The fluorescence analysis was not conducted on *L. lactis* because these bacteria lacked a fluorescent protein. Instead, *L. lactis* loaded nanofibers were crosslinked and plated on agar to determine the number of viable bacteria present within crosslinked nanofibers. CA-10 and CA-G were chosen as representative crosslinking systems that succeeded in maintaining bacterial viability as discussed in the previous section. As a literature control, the CA-PE crosslinking system was also studied though no bacteria growth was observed after crosslinking in the CA-PE system. For CA-10 and CA-G crosslinking systems, the bacteria loading before and after crosslinking was found to be statistically equivalent to as-spun loading. (**Figure 26**) Numerical values of bacteria loading within electrospun alginate-based nanofibers are listed in **Appendix B**. Tan et al.[204] found that divalent ions can have a detrimental (i.e. lethal) effect on bacteria particularly during the crosslinking of bacteria-loaded alginate hydrogels. Additionally, the bacteria-loading could be lowered by mass loss that occurs during crosslinking.

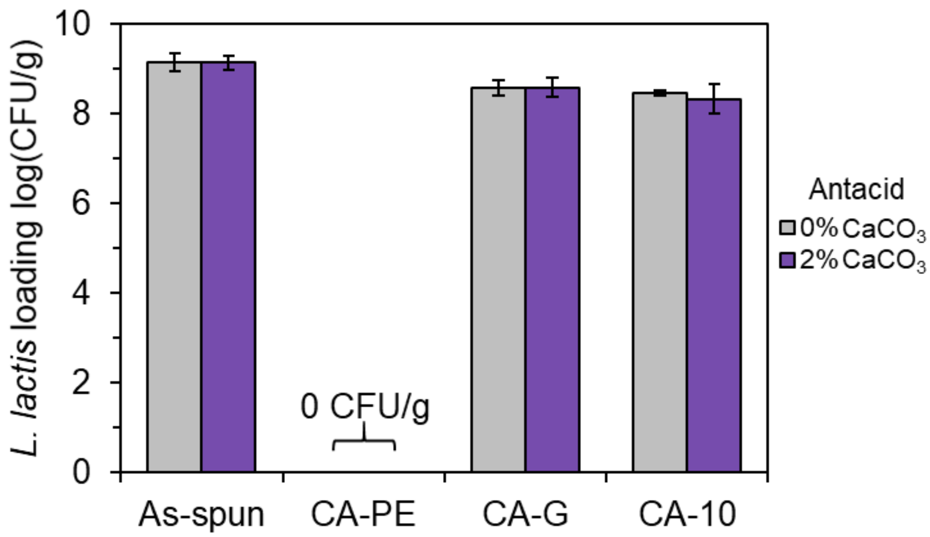

Figure 26: *L. lactis* was coaxially electrospun into alginate-based nanofibers without antacid (grey) and with 2% calcium carbonate antacid (purple). Bacterial loading before (As-spun) and after crosslinking (CA-G, and CA-10) is reported as mean ± standard error of three technical replicates. No viable cells were grown from CA-PE nanofibers; thus, these samples were labeled "0 CFU/g." All samples were determined to be statistically equivalent in *L. lactis* loading.

The antacid calcium carbonate ($CaCO_3$) was formulated into the SA/PEO/PS80 shell solution prior to electrospinning to improve the acid survivability of encapsulated bacteria. The addition of the 2 wt% of antacid did not significantly affect the bacteria-loading of as-spun or crosslinked nanofibers as compared to antacid-free fibers also shown in **Figure 26**. Overall, the as-spun and crosslinked nanofibers with and without antacid contained high loadings of *L. lactis* with over 10^8 CFU/g of electrospun mat.

7.4.3. Electrospun *L. lactis* for antimicrobial wound dressings

7.4.3.1. Motivation

MRSA is a pathogenic bacteria which can enter the body from an open wound, travel through the blood stream, and infect other parts of the body leading to lethal consequences.[205,206] While bacterial infections is usually treated with antibiotics, MRSA has developed resistant to many antibiotics making these infection difficult to treat. The rise of antibiotic resistant bacteria encourages the study of alternative methods to address bacterial infection prevention.[207] One solution includes the use of probiotics in place of antibiotics to prevent the growth of pathogenic bacteria. Additionally, electrospun probiotics could be used as antimicrobial wound dressings to protect open wounds from infection while promoting healing.[35,90]

In this section, the antimicrobial activity of *L. lactis* encapsulated within as-spun and crosslinked alginate-based nanofibers against *S. aureus* 12600, *S. aureus* SH1000 also known as Methicillin-sensitive *S. aureus* (MSSA), and MRSA were determined by an overlay assay. *L. lactis* produces the bacteriocin, nisin, that can inhibit the growth of other gram-positive bacteria such as *S. aureus*.[208] However, the inhibitory effects of nisin may be dependent on the overlay strain being tested. A study by Ramezani et al.[209] reported a lower minimal inhibitory concentration (MIC) of nisin was required to inhibition the growth of MRSA compared with the MIC required to inhibit MSSA.

7.4.3.2. Antimicrobial properties of encapsulated *L. lactis* determined via overlay assay

Overlay assays were conducted in 6-well plates. Each well plate was prepared by adding 5 mL of molten agar into each well and cooling down until solidified. A sample of either an *L. lactis s*uspension or *L. lactis* encapsulated within an electrospun fiber mat was incubated in separate wells. Next, soft agar containing *S. aureus* 12600, MSSA, or MRSA was poured into each well to create the overlay. Since controls did not contain any *L. lactis*, strains of *S. aureus* grew uninhibited and formed an opaque overlay as shown in **Figure 27**. Larger images of overlay assay results can be found in **Appendix B**. Typically, antimicrobial samples would inhibit the growth of the overlay strain causing a transparent area to appear around the sample known as the zone of inhibition or ZOI. Zones containing *L. lactis* may appear more transparent than the control; however, close inspection showed either single colonies in these zones or the zones appear slightly transparent. Therefore, these zones will be referred to as zones of reduced populations as (1) it is unclear whether single colonies are *L. lactis* or *S. aureus* and (2) slightly transparent zones indicated a reduced concentration of *S. aureus* in that area.

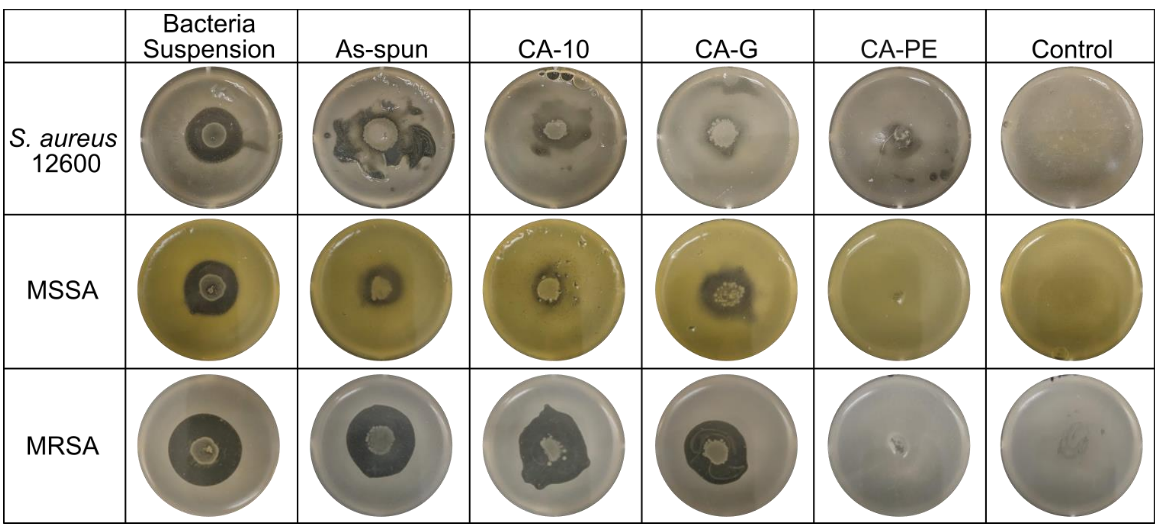

Figure 27: Digital images of the overlay assay results. The inhibitory activity of *L. lactis* was assessed as a bacterial suspension, encapsulated within as-spun nanofibers, encapsulated in CA-10 nanofibers, encapsulated in CA-G nanofibers, encapsulated in CA-PE nanofibers, and as negative control without *L. lactis* against *S. aureus* 12600, MSSA, and MRSA.

For suspensions of *L. lactis,* a droplet of bacterial suspension was added to the agar surface in the well. The circular nature of the droplet led to a circular biofilm of *L. lactis* and a circular zone. The *L. lactis* suspension produced the largest zone of reduced population against MRSA. Though encapsulated *L. lactis* samples were punched into uniform, 6 mm circles, crosslinking caused some samples to warp or fold over leading to nonuniform growth of *L. lactis* and non-circular zones of reduced population. The diffusion properties along the surfaces of the agar may account for other irregularities in zone shape. Similar to the *L. lactis* suspensions, the encapsulated *L. lactis* showed the most inhibition against MRSA for as-spun, CA-10, and CA-G samples. Notably, antimicrobial activity was not observed for the CA-PE nanofibers likely due to the depletion of viable *L. lactis* cells during crosslinking. Overall, the inhibitory effects of both the *L. lactis* suspension and electrospun *L. lactis* was the most effective against MRSA than the other *S. aureus* strains. Ethanol-free crosslinking systems were necessary for inhibitory activity of the bacteria-loaded, alginate-based nanofibers as CA-10 and CA-G samples showed zones of inhibition or reduced populations depending on the strain of *S. aureus* tested.

7.4.4. Targeted delivery of bacteria into the intestines

7.4.4.1.Motivation

While acid, enzymes, bile salts, and mechanical digestion in the stomach help convert food into nutrients for the body, they are also damaging to orally delivered probiotics on their way to the gut microbiota located in the intestines.[119] In particular, positively charged protons present in the acidic environment of the stomach can disrupt the bacteria cell membrane causing deactivation. Probiotic encapsulations for the oral delivery of probiotics into the gut can be designed to protect the bacteria particularly from acid insult.[10,11] For the targeted delivery of materials into the intestines, alginate is advantageous as it contracts due to hydrogen bonding in acid environments and swells in higher pH environments like the intestines.[103]

7.4.4.2. Proof-of-concept: Encapsulation and release of fluorescent beads using a simulated GIT model

Crosslinked alginate-based nanofibers that are stable in low pH solutions and exhibit swelling behavior in high pH environments would be useful for targeted delivery of cargo in the intestines. As a proof-of-concept study, FMG – green fluorescent polymer microspheres (green fluorescent beads) purchased from Cospheric LLC (Goleta, CA) had diameters ranging from 1 to 5 μm and a density of 1.3 g/cc (1,300 kg/m^3), as reported by the manufacturer. The green fluorescent beads as model cargo were encapsulated into the as-spun nanofiber mats via blend electrospinning (**Figure 28**). Though the diameters of the beads were much larger than that of the fiber, electrospinning pulls cargo into a sink-like flow allowing the beads to be encapsulated within the polymer nanofiber.[18] After crosslinking, bead-encapsulated fiber samples were submerged in a simulated GIT model featuring an acidic stomach stage (KCl/HCl acidic buffer of pH = 2; 2 hr)[120] followed by an intestinal stage (PBS of pH = 7.4; 4 hr).[65]

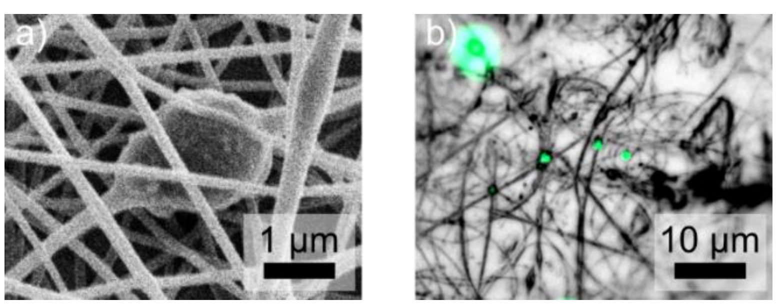

Figure 28: Representative micrographs acquired using (a) SEM and (b) an upright fluorescence microscope of green fluorescent beads encapsulated within as-spun SA/PEO/PS80 nanofiber mats. Scale bars are 1 µm and 10 µm. This figure is reproduced with permission from ref. [112]. Copyright 2023 American Chemical Society.

Release profiles of green fluorescent beads from crosslinked nanofibers into simulated GIT are presented in **Figure 29** as calculated by **Equation 4**. In the stomach stage of the simulated GIT, no cargo was released from the alginate-based nanofibers suggesting that the beads remain encapsulated within the fibers. In the intestinal stage of the simulated GIT, green fluorescent beads were quickly released within the first hour of submersion. Bead concentration was sustained for the rest of the submersion time (from 3 hr timepoint in the simulated GIT including the stomach phase onward) for all crosslinked fibers. The fast release from calcium alginate structures could be attributed to the swelling of the alginate, as found in a study by Mei et al.[103] on alginate beads. CA-3, CA-10, and CA-G fibers exhibited a more gradual release: less than 52% of total encapsulated beads were released within 5 min of submersion in PBS and over 72% were released over 45 min of submersion. Comparatively, over 70% of encapsulated green fluorescent beads were released from CA-7 and CA-PE fibers within the initial 5 min of submersion.

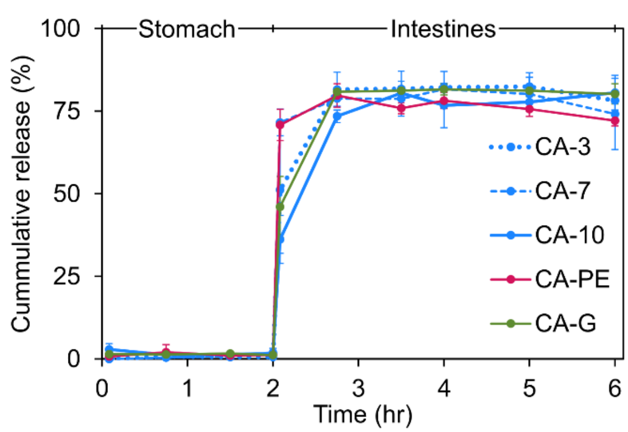

Figure 29: Release profiles of green fluorescent beads from crosslinked alginate-based nanofibers in a simulated GIT model. The stomach phase consisted of KCl/HCl acidic buffer of pH 2 whereas PBS (pH = 7.4) was used to represent the intestinal phase. Error bars represent standard error. This figure is reproduced with permission from ref. [112].

Electrospun nanofibers, especially those composed of PVA or PEO, have been extensively studied in the context of drug delivery applications.[33,156] Typically, a biphasic release wherein a burst release is followed by sustained release like the profiles seen in this paper are exhibited by electrospun nanofibers. The high surface area-to-volume ratio of electrospun nanofibers promotes ample surface interaction and erosion that lead to the rapid release of encapsulated cargo via diffusion or degradation mechanisms.[185] Cui et al.[51] found that thinner electrospun nanofibers (212 nm) with subsequently higher surface area-to-volume ratio had a greater total release of the analgesic drug, paracetamol, from the nanofibers compared to thicker nanofibers (551 nm). In regards to the effects of glycerol on the release of cargo from alginate, one study[65] found that the presence of glycerol in calcium alginate microbeads improved their stability and extended the release times of a drug, theophylline, into a buffer solution that had a pH value of 7.4.

In PBS, the release profiles appeared independent of the fiber morphology. Though CA-10 fibers merged into a film immediately upon submersion in PBS, the release of encapsulated green fluorescent beads from the CA-10 was similar to that of CA-G which had a swollen fiber structure in PBS. These results indicate swelling, regardless of the material's morphology, was a main contributor to release in this system. The maximum cumulative release from each sample ranged from 80-87%. We hypothesize that the mass loss that occurred during crosslinking (see **Figure 29**) contained some amount of the green fluorescent beads, which is preventing us from observing a 100% cumulative release into the simulated gastrointestinal solutions. Overall, our crosslinking systems have proven to be effective in enabling intestinal-targeted release from alginate-based nanofibers.

7.4.4.3. Bacteria survivability after acid exposure

To demonstrate the application of crosslinked alginate-based nanofibers for the delivery of probiotics into the gut, bacteria-loaded nanofibers were subjected to submersion in KCl/HCl acidic buffer for 2 hr, resembling the acidic environment and residence times of food in the stomach. As shown in **Figure 26**, a suspension of *L. lactis* of 10^6 CFU/mL of acidic buffer was completely deactivated after 2 hr. Unfortunately, neither encapsulated *E. coli* Nissle nor *L. lactis* exhibited growth after exposure to acid commonly seen in literature.[55,69,87] Even after crosslinking, the pore sizes can allow the penetration of protons throughout the structure and cause insult to encapsulants.[69]

Formulations for probiotics include antacids to improve bacterial survivability by neutralizing acid penetration into the encapsulation matrix.[69] **Figure 26** shows the *L. lactis* loading in coaxially electrospun nanofibers when calcium carbonate (2%) was adapted into the outer precursor solution. After subjecting these fibers to acidic buffer for 2 hr, the 2% calcium carbonate formulation was effective improving bacterial survivability compared to the formulation without antacid (**Figure 30**).

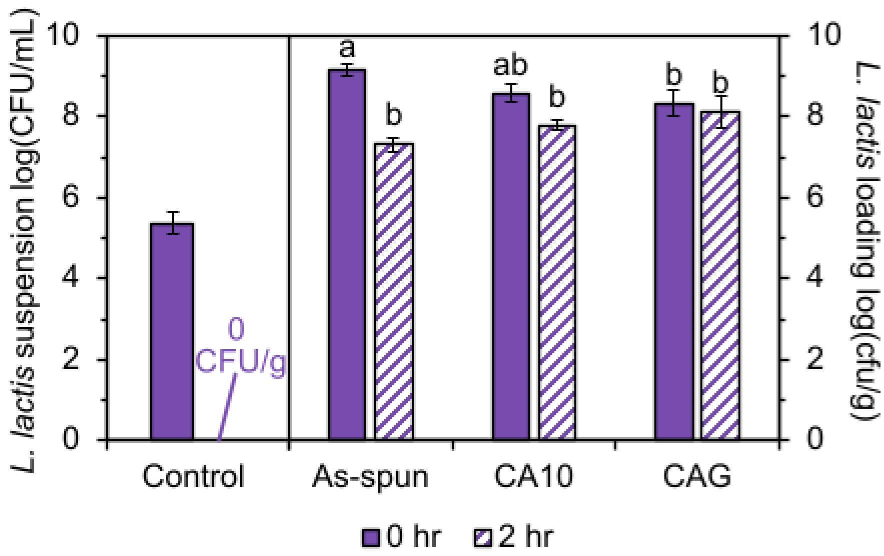

Figure 30: Survivability of *L. lactis* suspension and coaxially electrospun *L. lactis* in alginate-based nanofibers formulated with 2% calcium carbonate before (0 hr, solid, purple) and after submersion in acidic buffer for 2 hr (striped, purple) reported as mean ± standard error of technical triplicates. No viable cells were detected after the bacterial suspension was subjected to the acidic buffer; thus, the sample was labeled "0 CFU/g." Similar letters above each bar denoted statistically equivalent samples excluding the control sample.

7.4.4.3.1. Change in pH due to electrospun antacid

Calcium carbonate acts as an antacid by dissolving in acidic environments to reduce pH.[69] The pH of the acidic buffer was measured after submersion of bacteria-loaded, alginate-based nanofibers electrospun with $CaCO_3$. All samples increased the pH value of the acidic buffer from 2.0 to 2.21 ± 0.01 for as-spun nanofibers, 2.23 ± 0.01 for CA-10 nanofibers, and 2.20 ± 0.02 for CA-G nanofiber samples. These pH values are well within the normal pH range of the stomach (2.0-3.0).[118]

7.4.4.4. Bacteria release in simulated gastrointestinal tract

Next, the fibers containing *L. lactis* and antacid were subjected to a simulated gastrointestinal tract consisting of both a stomach phase and an intestinal phase (**Figure**

31; numerical values can be found in **Appendix B**). In this study, a simplified GIT system was used to highlight the pH-dependent behavior of the electrospun alginate nanofibers.[103] The stomach phase, made by adding HCl to DI water to reach a pH value of 2.5, was sampled after initial addition and after 2 hr of submersion of probiotic-loaded nanofibers. Viable bacteria were not detected at either time points in the stomach phase.

After 2 hr in the stomach phase, the fibers were transferred to the intestinal phase created by adding NaOH to DI water until a pH of 7.0. In the simulated intestines, the electrospun mat released over 10^5 CFU per g of mat in the first half hour of submersion. The concentration of bacteria remained steady for the rest of the duration in the intestinal tract. Therefore, both pH-dependent delivery and probiotic viability in the intestines were demonstrated. Notably, the concentration of probiotics released into the simulated gastrointestinal tract was lower than the concentration that survived acid insult from the previous section (**Section 7.4.4.2**). In the previous section, the bacteria-loaded mats were immediately plated on nutrient-rich agar after acid submersion. The environment of the intestinal phase lacked any nutritional compounds for the *L. lactis* cells which may have led to a lower number of viable cells detected.

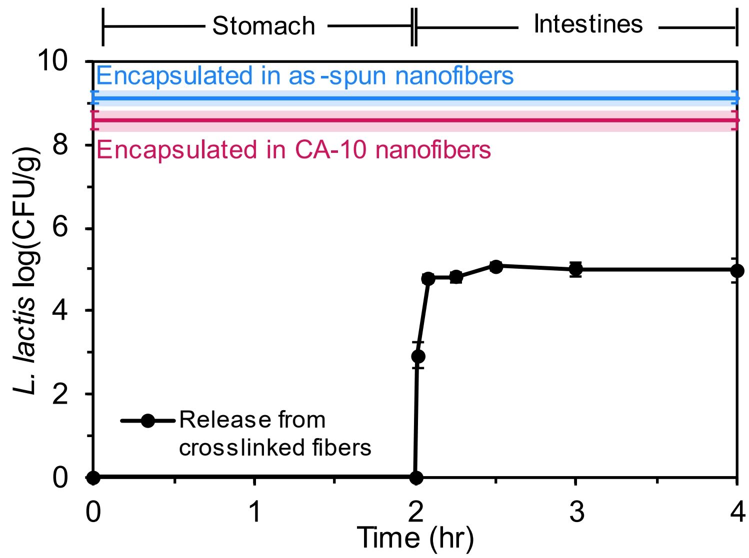

Figure 31: *L. lactis* was coaxially electrospun in alginate-based nanofibers containing 2% calcium carbonate as an antacid. The bacteria-loaded nanofibers were crosslinked using the CA-10 crosslinking system detailed in **Table 3**: Names and crosslinking compositions used to create the five crosslinked alginate nanofibers explored in this study, as well as the as-spun fibers. This table is reproduced with permission from ref. [112]. Copyright 2023 American Chemical Society. The bacterial release from crosslinked nanofibers in a simulated gastrointestinal tract (black circles) was reported as mean ± standard error from technical triplicates. Loading in as-spun fiber (blue dotted line representing average and shaded blue area as standard error) and in CA-10 crosslinked fiber (pink dotted line representing average and shaded pink area as standard error) are included for comparison.

7.5 Conclusion

The encapsulation of probiotics is necessary for the protection of cells in environments where they are useful from inside the gut to the outer layer of the skin. Here, probiotics *E. coli* Nissle and *L. lactis* were coaxially electrospun into alginate-based nanofibers and crosslinked using biocompatible calcium ions. Though ethanol-based crosslinking systems have been used in literature, ethanol significantly decreased the bacteria viability and loading in the alginate-based nanofibers. Therefore, the ethanol-free crosslinking systems developed in the previous chapter enabled the encapsulation of viable bacteria within crosslinked alginate nanofibers such that live probiotics could be delivered to various environments. For example, the encapsulation of *L. lactis* within crosslinked alginate-based nanofibers can be incorporated into antimicrobial wound dressings. Using an overlay assay, the bacteria-loaded nanofibers inhibited the growth of pathogenic MSSA and MRSA. Though encapsulation within alginate nanofibers was not sufficient to protect the encapsulated bacteria against acid insult, the formulation of 2 % calcium carbonate antacid into the outer precursor solution improved the survival of encapsulated *L. lactis* in a simulated gastrointestinal tract.

CHAPTER 8

CONCLUSIONS AND OUTLOOK

Sections adapted from:

Diep, E.; Schiffman, J. D. Electrospinning Living Bacteria: A Review of Applications from Agriculture to Health Care. *ACS Appl. Bio Mater*. 2023, *6* (3), 951-964. https://doi.org/10.1021/acsabm.2c01055.

8.1 Summary

Probiotic bacteria are useful for a variety of applications. Encapsulation technologies are necessary for maintaining viable bacteria such that they can be applied to different environments. This dissertation investigated the formation, crosslinking, and encapsulation of probiotics within electrospun alginate-based nanofibers. The initial objective of this work was the targeted gut delivery of probiotics which expanded to the use of probiotic-loaded nanofibers as an antimicrobial wound dressing. There are still many avenues to explore regarding this application and technology as the usefulness of probiotics within and beyond the human body is still being explored.

8.2 Immediate next steps

8.2.1. Further understanding precursor concentration effects on fiber composition

In Chapter 4, an alginate/PEO/PS80 precursor was used to electrospin alginate-based nanofibers. Though a systematic study was conducted on the influence of surfactant concentration on the formation of smooth nanofibers, the field of electrospinning alginate would also benefit from the study of precursor solution concentration on the final composition of the nanofibers. Exploring a wider range of electrospinnable, precursor solution concentrations would help determine if there was a maximum composition of alginate achievable by electrospinning examined via FTIR and TGA. In turn, this maximum alginate fiber composition may influence the stability and mechanical properties of the fibers before and after crosslinking.

8.2.2. Further understanding precursor concentration effects on bacteria loading

On the other hand, the concentration of alginate in the precursor solution affects its solution properties including the ability to disperse encapsulants throughout the electrospun nanofibers. Additionally, bacterial concentration in the precursor solution can impact the electrospinnabilty of the solution as mentioned in Chapter 5. There is likely a trade-off between the alginate composition and bacteria loading in electrospun nanofiber that has yet to be investigated.

The study of precursor concentration effects on bacteria loading would also be relevant for the coaxial electrospinning. During coaxially electrospinning, differences between core and shell solutions influence mixing that occurs at the needle tip. Therefore, bacterial suspensions were mixed with alginate solutions to avoid interfacial interference. However, the optimal properties for the inner precursor solution to maximize encapsulation was not studied. Deeper analysis of surface tension, viscosity, and interfacial interactions should be considered to understand mixing phenomena and how it may be relevant to encapsulation.

8.2.3. Improved gut viability with prebiotics

After determining the significance of core solution properties on encapsulation, adjustments to the core solution can be made. Namely, the co-encapsulation of prebiotics as a nutrient resource for encapsulated bacteria could improve the storage and viability of the probiotic upon delivery. From Chapter 7, lack of nutrients may have reduced the amount of viable bacteria detected in the simulated gastrointestinal tract. A number of polysaccharides and carbohydrates have been identified as prebiotics which are selectively digested by bacteria.[210] Inulin, in particular, is commonly used with *L. lactis*. The inclusion of prebiotics in microencapsulation as well as electrospun nanofibers can improve the viability of encapsulated bacteria during storage.[211] It would be interesting to study the effects of prebiotics in various applications of probiotic-loaded nanofibers including gut delivery. Future work on coaxial electrospinning systems or coacervate electrospinning will expand the materials that can be electrospun which may allow for nutrients like carbohydrates or proteins to form the encapsulating fiber as well as act as a nutrient source.[53,211,212] Improved viability and loading may also aid in the study of *L. lactis* nanofibers for antimicrobial wound dressing.

8.2.4. Continuation of antimicrobial, probiotic nanofibers

Since zones of inhibition were not confirmed by overlay assay, the following are recommendations for future antimicrobial testing. After the final incubation of the overlay assay, samples from within the transparent to slightly transparent zones can be extracted with a cork borer commonly used in agar diffusion assays. Homogenization of the sampled agar would release the bacteria for incubation. If the *S. aureus* overlay strain growth was inhibited, those cells may not be revived during incubation to confirm or deny the zone of inhibition. Furthermore, nisin content may be determined via liquid chromatography analysis of the released agar.

8.2.5. Mechanical testing of crosslinked nanofibers

Chapter 6 focused on the development of ethanol-free crosslinking systems and the chemical stability of crosslinked fibers. However, the mechanical properties of the electrospun fibers are also relevant to their applications. In the gut, mechanical forces help break down food. It would be important to determine if the nanofibers could withstand that mechanism and keep probiotics encapsulated. Tensile tests should be conducted on as-spun and crosslinked fibers. This data could be compared studies regarding the mechanical forces of the gut as well as tensile properties of bandages.

8.3 Future work

8.3.1. Recommended improvements for gastrointestinal tract model

The alginate-based nanofibers developed in this work were capable of the targeted release of green-fluorescent beads and *L. lactis* in gastrointestinal tract models based primarily on the pH of stomach and the intestines. A more realistic model should include mouth phase, as well as relevant electrolytes and enzymes in each stage that may affect the encapsulated probiotics and the fibers. The most realistic determination of the survivability and colonization of probiotics would be in a live gastrointestinal tract like that of a mouse model. Germ-free mice may help us determine if these probiotics can effectively colonize in the gut. In mice with established gut microbiota, interactions between gut bacteria and delivered probiotics can be investigated. An in vivo model would also allow us to study the mucoadhesive properties of alginate and PEO in the nanofiber and their influence on the colonization of probiotics via interaction with the mucosal layer. However, the gut microbiota of mice and humans differs significantly. Thus, clinical studies would need to be conducted eventually.

8.3.2. Future exploration of electrospun probiotics

The encapsulated probiotic strains in this dissertation were either lab standard (*E. coli* K12) or gut probiotic (*E. coli* Nissle and *L. lactis*) strains. Though Gram-negative, Gram-positive, aerobic, and anaerobic bacteria of various shapes and sizes have been successfully electrospun, it is unclear how and what other properties, like electroactivity, can make one strain of bacteria more robust toward electrospinning than another strain. The encapsulation of various strains of bacteria would help illuminate the genetic factors that enable the improved survivability of some strains with respect to others.

Current formulations for probiotic supplements contain several billion CFUs and may include multiple strains of bacteria though few guarantee the survival of these bacteria in the body. Probiotics for the gut mainly consist of lactic acid bacteria easily derived from fermented foods. However, the gut is host to several hundreds of strains of bacteria. Electrospinning can be conducted in a glove box in the absence of oxygen beneficial for the encapsulation of anaerobic gut bacteria. Electrospinning can also be used to develop personal dosages by layering mats of various bacterial strains together which can consist of bacteria from fermented foods or health guts.

Biocompatible polymers and aqueous solvents are generally safe for the electrospinning of the cells. Much research has been conducted encapsulating bacteria into PVA and PEO nanofibers. Bacteria encapsulated within water-soluble, biocompatible polymers are quickly released upon contact with moisture for the treatment of an open wound or to rebalance the vaginal microbiome. In this study, the targeted delivery of the encapsulated gut probiotics was achieved through the use of alginate and its pH-dependent behavior that could selectively release materials into the intestines. Alginate and PEO also have mucoadhesive for integration with the intestinal mucosal layer. Future work should investigate if this property improves the efficacy of encapsulated probiotics. Other materials may be used to create the nanofibers with other benefits such as a gradual release. It would also be interesting to see if probiotics could be electrospun into other nutrients for the body (other carbohydrates, proteins, dietary fibers, etc.) or for bacteria (prebiotics).

In addition to studying the electrospinning of different gut bacteria, strains that promote plant growth or are used in wastewater treatments should be encapsulated. The electrospinning of bacteria for industrial and environmental use is currently much less explored than for the electrospinning of gut probiotics. Furthermore, these bacteria may benefit from different encapsulation materials. For plant growth promotion, the bacteria may be released into soil or a soil model similar to my work on gut release. On the other hand, water waste treatment may require the bacteria to stay encapsulated during treatment for regeneration and reuse.

8.4 Emerging applications

Coaxial electrospinning is promising for creating water-stable, bacteria-loaded nanofibers; the bacteria suspended in biocompatible solvents in the inner needle is simultaneously extruded with a spinnable precursor solution in the outer needle. The bacterial suspension is then “pulled along” by the spinnable precursor allowing for the formation of the electrospun fiber. Notably, a polymer dissolved in an organic solvent has been used to create a water-insoluble fiber containing living bacteria cells. For significant advances toward “real-world” applications, the performance of the bacteria or the physical properties of the fibers might need to be improved by the incorporation of additives, such as pharmaceuticals or other functional agents.

Few researchers have focused on environmental applications, such as plant growth. Electrospun coatings on plant seeds prevented fungal infection while promoting root growth. It will be interesting to see how electrospun bacteria can evolve for the coating of grown plants or even food products to help with other fungal and mold issues. Perhaps, future fibers engineered for environmental applications will explore multi-shell fibers that can degrade toxins while releasing nutrients that will repair the soil environment. Bacteria also play a role in the composting process. Integration of such bacteria into composable products may improve its degradability in less-than-optimal environments.

Barely any attention has been paid to bioremediation and microbial fuel cell applications. And in the future, a life-cycle analysis of these materials will be needed to determine the influence of the encapsulated bacteria on the soil microbial communities and the reusability of bacteria-loaded fibers in bioremediation and microbial fuel cell applications. In tandem with the enormous efforts being made to develop permeable, porous, and stable polymer nanofiber scaffolds that provide an optimized environment for microorganisms, exciting developments in synthetic biology have been emerging; we are excited to learn about future bacteria-loaded polymer fibers biotechnologies.

CHAPTER 9

SCIENTIFIC CONTRIBUTIONS

The work in this thesis has culminated in various publications, which are listed in this section. Additionally, dissemination of this work has taken place through various conference presentations and on-campus presentations within different organizations.

- **Publications**

    1. **Diep, E.;** Schiffman, J. D. Designing a biocompatible matrix for delivery of living bacteria. Emerging Trends in Polymer and Material Science, 2019, Amherst, MA.
    2. **Diep, E.;** Schiffman, J. D. Encapsulating Bacteria in Alginate-Based Electrospun Nanofibers. *Biomater*. *Sci*. **2021**, *9* (12), 4364–4373. https://doi.org/10.1039/D0BM02205E.
    3. **Diep, E.;** Schiffman, J. D.; Kurtz, I. S. Interfacing Electrospun Nanofibers with Microorganisms: Applications from Killing to Repelling to Delivering Living Microbes. In Applications of Polymer Nanofibers; Andrady, A. L., Khan, S. A., Eds.; John Wiley & Sons, Inc. U.S.A., 2022.
    4. **Diep, E.;** Schiffman, J. D. Electrospinning Living Bacteria: A Review of Applications from Agriculture to Health Care. ACS Appl. Bio Mater. **2023**, *6* (3), 951-964. https://doi.org/10.1021/acsabm.2c01055.
    5. **Diep, E.;** Schiffman, J. D. Ethanol-free Cross-Linking of Alginate Nanofibers Enables Controlled Released into a Simulated Gastrointestinal Tract Model. *Biomacromolecules*. **2023**, *24* (6), 2908-2917. https://doi.org/10.1021/acs.biomac.3c00274.

6. Hancock, S.N.; Yuntawattana, N.; **Diep, E.**; Maity, A.; Tran, A.; Schiffman, J.D.; Michaudel, Q. ROMP of *N*-methyl Pyridinium-fused Norborenes for the Precise Synthesis of Antibacterial Main-Chain Cationic Polymers. *PNAS*. **2023**. (Under revision)

- **Posters**

1. **Diep, E.;** Schiffman, J. D. Electrospinning of bacteria into alginate-based nanofibers. Polymer Event Virtual Poster Session, 2020, Amherst, MA.
2. **Diep, E.;** Schiffman, J. D. Electrospinning of bacteria into alginate-based nanofibers. Biofilm Technologies: Pathways to Product Development Virtual Meeting, 2021, Bozeman, MT.
3. **Diep, E.;** Schiffman, J. D. Facilitation of electrospun alginate-based nanofiber for the encapsulation and delivery of live bacteria into the gut. *MIT Polymer Day (Virtual)*, 2021, Boston, MA.
4. **Diep, E.;** Schiffman, J. D.; Kurtz, I. S. Interfacing Electrospun Nanofibers with Microorganisms: Applications from Killing to Repelling to Delivering Living Microbes. In Applications of Polymer Nanofibers; Andrady, A. L., Khan, S. A., Eds.; John Wiley & Sons, Inc. U.S.A., 2022.
5. **Diep, E.;** Schiffman, J. D. Facilitation of electrospun alginate-based nanofiber for the encapsulation and delivery of live bacteria into the gut. *AIChE Annual Meeting*, 2022, Pheonix, AZ.
6. **Diep, E.;** Schiffman, J. D. Electrospinning living probiotics into alginate-based nanofibers antimicrobial wound dressings. BASF 2023 North American Research Forum and Sustainability Challenge, 2023, Wyandotte, MI.

7. **Diep, E.;** Schiffman, J. D. Electrospinning living probiotics into alginate-based nanofibers antimicrobial wound dressings. 6th Stevens Conference on Bacteria-Materials Interactions, 2023, Hoboken, NJ.

APPENDIX A

EFFECTS OF MOLECULAR WEIGHT OF PEO

The influence of PEO molecular weight on the formation was briefly studied. High molecular weight PEO (1,000 kDa) was purchased from Sigma Aldrich (St. Louis, MO). Notably, high molecular weight PEO has been preferred by other researchers to form electrospun alginate/PEO nanofibers.[76,132] The molecular weight of a polymer can be correlated to the length of its chain where longer polymers are more easily entangled. In addition, higher molecular weight polymer solutions increase more rapidly in viscosity which can reducing beading of the electrospun nanofiber.[135]

A.1 High molecular weight PEO

SA was mixed with high molecular weight PEO (1000 kDa) in a 70:30 ratio with 1 wt% PS80. Despite varying electrospinning parameters, no fibers were observed. Differences in the alginate and surfactant used in this study and other studies[41,76] may have prevented fiber formation despite other studies using this composition to form electrospun fibers. The deformation of the electrospinning droplet was not visibly observed using 1000 kDa PEO during electrospinning even in the presence of a surfactant. While viscosity stabilizes the nanofiber during electrospun, exceedingly high viscosity has been known to clog the electrospinning needle and hinder fiber formation.[45] I concluded the high viscosity deterred jet and fiber formation thereby preventing electrospinning.[45]

A.2 Low molecular weight PEO

To reduce viscosity, the sodium alginate to PEO ratio was decreased to 60:40 which was another composition that was shown to produce fibers.[76] However, fiber density was still sparse for electrospun mats and large beads capable of dissolving fibers upon collection were also observed. Lowering the molecular weight of the PEO polymer would also reduce solution viscosity.[46] Therefore, 600 kDa PEO was primarily used throughout this work.

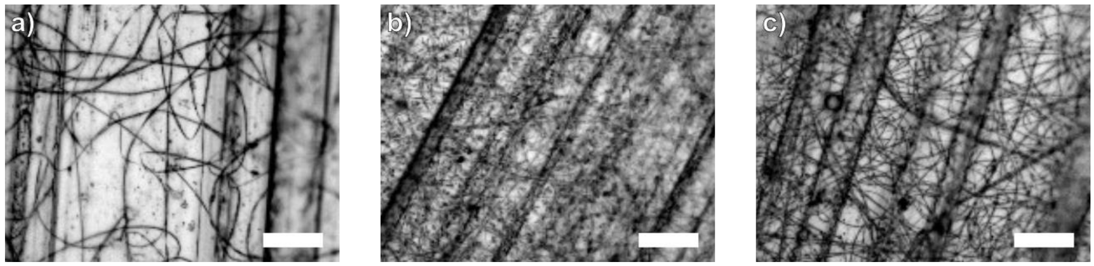

Figure 32: Brightfield images of a systematic investigation into electrospinning fibers using (a) 2.4/1.6/2 wt%, (b) 2.8/1.2/2 wt%, and (c) 2.8/1.2/3 wt% SA/PEO/PS80. All precursor solutions were made using 600 kDa PEO. Scale bar represents 20 μm.

APPENDIX B

SUPPLEMENTAL INFORMATION FOR CHAPTER 5 & 7

Figures generally report log(CFU) data as common for microbiological studies. Bacteria count reported as scientific notation without logarithmic conversion are listed in this Appendix to provide more information.

Table 10: Loading of bacteria electrospun into alginate-based nanofibers using both single needle and coaxial setups and varying precursor solution recipes.

Bacteria	Electrospinning Setup	Precursor solution	Flow rate (mL/hr)	Loading (CFU/g)
E. coli K12	Single needle	10^8 CFU/mL in 2.5/1.5/3% SA/PEO/PS80	2.00 mL/hr	2.74×10^5
E. coli Nissle	Single needle	10^8 CFU/mL in 2.5/1.5/3% SA/PEO/PS80	2.00 mL/hr	8.47×10^5
E. coli Nissle	Single needle	10^8 CFU/mL in 2.5/1.5/3% SA/PEO/PS80 with 1% glycerol	2.00 mL/hr	1.51×10^6
E. coli Nissle	Coaxial needle	Core: 5.0×10^9 CFU/mL in 2.5% SA Shell: 2.5/1.5/3% SA/PEO/PS80	0.35/0.70 core/shell 0.70/0.70 core/shell 0.70/0.35 core/shell	6.78×10^5 9.05×10^6 5.21×10^6
L. lactis	Coaxial needle	Core: 5.0×10^9 CFU/mL in 2.5% SA Shell: 2.5/1.5/3% SA/PEO/PS80	0.35/0.70 core/shell 0.70/0.70 core/shell 0.70/0.35 core/shell	1.41×10^9 1.53×10^9 1.18×10^9
L. lactis	Coaxial needle	Core: 5.0×10^9 CFU/mL in 2.5% SA Shell: 2.5/1.5/3% SA/PEO/PS80 with 2% calcium carbonate	0.35/0.70 core/shell 0.70/0.70 core/shell	1.35×10^9 1.03×10^9

Table 11: Loading of *L. lactis* in coaxially electrospun alginate-based nanofibers after crosslinking and submersion in KCl/HCl acid buffer for 2 hr. Crosslinking systems are outlined in Table 3. Shell solution contained 2.5/1.5/3% SA/PEO/PS80 formulated with and without calcium carbonate.

Crosslinking system	Calcium carbonate (wt%)	*L. lactis* loading after crosslinking (CFU/g)	*L. lactis* loading after acid submersion (CFU/g)
CA-PE	0.00	0	n/a
CA-10	0.00	2.86×10^8	0
CA-G	0.00	3.73×10^8	0
CA-PE	2.00	0	n/a
CA-10	2.00	3.79×10^8	6.10×10^7
CA-G	2.00	2.09×10^8	1.33×10^8

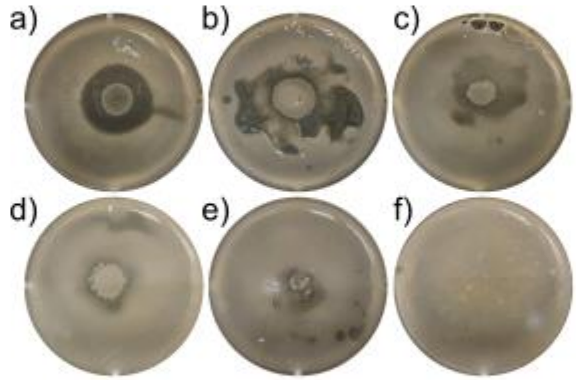

Figure 33: Results of overlay assay assessing the inhibitory activity of *L. lactis* as (a) a bacterial suspension, (b) encapsulated within as-spun nanofibers, (c) encapsulated in CA-10 nanofibers, (d) encapsulated in CA-G nanofibers, (e) encapsulated in CA-PE nanofibers, and (f) a negative control without *L. lactis* against *S. aureus* 12600.

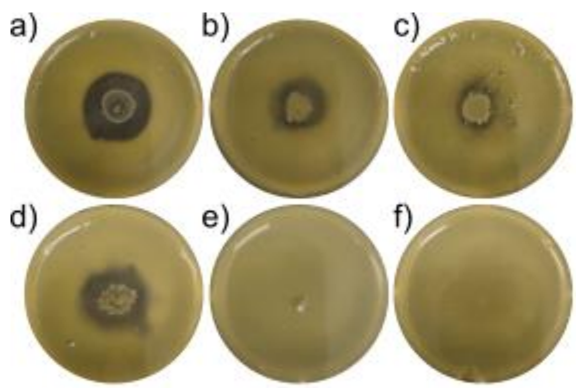

Figure 34: Results of overlay assay assessing the inhibitory activity of *L. lactis* as (a) a bacterial suspension, (b) encapsulated within as-spun nanofibers, (c) encapsulated in CA-10 nanofibers, (d) encapsulated in CA-G nanofibers, (e) encapsulated in CA-PE nanofibers, and (f) a negative control without *L. lactis* against MSSA.

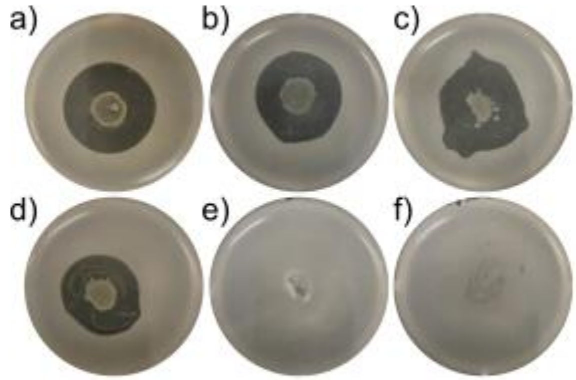

Figure 35: Results of overlay assay assessing the inhibitory activity of *L. lactis* as (a) a bacterial suspension, (b) encapsulated within as-spun nanofibers, (c) encapsulated in CA-10 nanofibers, (d) encapsulated in CA-G nanofibers, (e) encapsulated in CA-PE nanofibers, and (f) a negative control without *L. lactis* against MRSA.

Table 12: Viable bacteria count of free *L. lactis* and coaxially electrospun *L. lactis* in SA/PEO/PS80 nanofibers with 2 wt% calcium carbonate before and after submersion in KCl/HCl acidic buffer.

Acid submersion time (hr)	**Sample**			
	Control	As-spun	CA-10	CA-G
0	5.36×10^5 CFU/mL	1.35×10^9 CFU/g	3.79×10^8 CFU/g	2.09×10^8 CFU/g
2	0	2.07×10^7 CFU/g	6.10×10^7 CFU/g	1.33×10^8 CFU/g

Table 13: *L. lactis* was coaxially electrospun in alginate-based nanofibers containing 2% calcium carbonate as an antacid and released into a simulated gastrointestinal tract.

Gastrointestinal Tract Phase	**Time (min)**	**Cumulative *L. lactis* released (CFU/g)**
Stomach	0	0.00
	120	0.00
Intestines	121	8.55×10^2
	125	6.06×10^4
	135	6.52×10^4
	150	1.20×10^5
	180	1.01×10^5
	240	9.42×10^4

APPENDIX C

(ROMP) OF *N*-METHYLPYRIDINIUM-FUSED NORBORENES FOR THE PRECISE SYNTEHSIS OF ANTIBACTERIAL MAIN-CHAIN CATIONIC POLYMERS

This work was conducted in collaboration with the Michaudel Group in the Department of Chemistry at Texas A&M University.

Adapted from:

Hancock, S. N.; Yuntawattana, N.; Diep, E.; Maity, A.; Tran, A.; Schiffman, J. D.; Michaudel, Q. Antibacterial Main-Chain Cationic Polymers via Controlled ROMP of *N*-methyl Pyridinium-fused Norborenes. *PNAS.* **2023**. (under revision)

C.1 Abstract

With the rise of antibiotic resistant bacteria, the development of antimicrobial polymers is imperative for the prevention or treatment of pathogenic infections. Here, synthesis and ring-opening metathesis polymerization (ROMP) of *N*-methylpyridinium-fused norborenes monomers created cationic homo- and co-polymers that exhibited antibacterial activity. Disk diffusion assays were conducted to qualitatively determine antibacterial susceptibility of monomers and polymers against lab standard *E. coli* and clinically relevant MRSA. Since monomers did not inhibit the growth of either of these strains, polymerization was deemed necessary for antibacterial activity. Broth microdilution assays were used to quantitatively determine minimal inhibitory concentrations (MIC) of polymers. For water-insoluble polymers, an assay with dilute dimethyl sulfoxide solvent was adapted. Homo- and co-polymers of varying molecular weights effectively inhibited the growth of both strains of bacteria with MICs of 25-50 μg/mL.

C.2 Materials

The bacterial strains used were *Escherichia coli* K12 Wildtype (*E. coli* K12) and clinical isolate methicillin-resistant *Staphylococcus aureus* (MRSA) IDRL-6169. Mueller Hinton broth (MHB), bovine serum albumin (BSA), and dimethyl sulfoxide (DMSO) were purchased from Sigma Aldrich (St. Louis, MO). Acetic acid (AA; percent purity ≥99.7%), agar, and hydrochloric acid (HCl; percent purity = 36.5-38.0%) were purchased from Fisher Scientific (Hampton, NH). Deionized (DI) water was obtained from a Barnstead Nanopure Infinity water purification system (Thermo Fisher Scientific, Waltham, MA) and sterilized via autoclave (120°C, 1 bar, 15 min). Monomers and in-house synthesized polymers were used as received from the Michaudel Lab at Texas A&M University. A list of monomers and polymers and their properties is provided in **Table 14**.

Table 14: Polymer properties and solvents

Polymer	Polymer properties	Solvent stock solution
1-H^{+}	MW=307.29 g/mol	DI water or DMSO
1-^{t}**Bu**$^{+}$	MW=363.4 g/mol	DI water or DMSO
poly(**1-H**$^{+}$)$_{40}$	Dp^{theo} = 40 M_n^{exp}= 11.7 kg/mol	DI water
poly(**1-**^{t}**Bu**$^{+}$)$_{10}$	Dp^{theo} = 10 M_n^{exp}= 6.3 kg/mol	DMSO
poly(**1-**^{t}**Bu**$^{+}$)$_{20}$	Dp^{theo} = 20 M_n^{exp}= 6.3 kg/mol	DMSO
poly(**1-**^{t}**Bu**$^{+}$)$_{40}$	Dp^{theo} = 40 M_n^{exp}= 6.3 kg/mol	DMSO
poly(**1-**^{t}**Bu**$^{+}$)-*b*-(**1-H**$^{+}$)	Dp^{theo} = 20 (n=m=10) M_n^{exp}= 6.9 kg/mol	DMSO
poly(**1-H**$^{+}$)-*r*-(**1-**^{t}**Bu**$^{+}$)	Dp^{theo} = 20 (n=m=10) M_n^{exp}= 6.9 kg/mol	DMSO

C.3 Methods

C.3.1 Antibacterial susceptibility using disk diffusion assay

Disk diffusion assays were conducted based off a previously published method[50] and Clinical and Laboratory Standard Institute (CSLI) guidelines.[65] Whatman filter paper

(Grade 3) was punched into 6 mm diameter disks using a hole puncher and sterilized via autoclave.[66] Stock solutions of water-soluble monomers or polymers were made by dissolving the sample in either sterile DI water or DMSO, while stock solutions of water-insoluble polymers were made by dissolving the sample in DMSO. Two-fold serial dilutions were made by diluting the stock solution with its respective solvent. Test samples were prepared by pipetting 20 µL of a polymer dilution onto a filter disk, whereas the controls were loaded with 20 µL of solvent (no polymer). *E. coli* and MRSA were incubated in MHB at 37 °C with shaking (250 rpm) for 4–6 hr until their logarithmic growth phase was reached in accordance with standards set by the CLSI. The liquid cultures of bacteria were diluted to an optical density (Genesys 10S UV-Vis, Thermo Fisher Scientific, Waltham, MA; λ = 600 nm) of 0.1, which was approximately 10^8 CFU/mL and 10^7 CFU/mL, for *E. coli* and MRSA, respectively. Using a sterile cotton swab (tifanso, Guanzhou, China), the bacterial suspension was streaked in three panes across the Mueller Hinton Agar plate (21 g/L MHB and 17 g/L agar in DI water autoclaved for 15 min at 120 °C). Agar plates were divided into six partitions for one control and five polymer dilutions.[67] Control disks and inoculated disks were placed within each partition using flame-sterilized forceps. Agar plates containing samples were incubated for 16 hr at 37 °C before the detection of a ZOI was used to determine the antibacterial susceptibility of a given polymer concentration.

C.3.2 MIC determination by broth microdilution assay

Standardized broth microdilution protocols were followed for the needs of each of the different polymers.[59, 67] For water-soluble monomer and polymers, stock solutions were serial diluted with MHB in a 1:9 ratio before serial diluting the solutions two-fold with MHB in 10 columns of a polypropylene 96-well plate. Each well contained a final volume of 50 µL of polymer solution. The bacteria suspension was diluted to a concentration of 10^6 CFU/mL before inoculating each well with 50 µL of bacteria. For water-insoluble polymers, the polymers were dissolved in DMSO before diluting with MHB in a 1:9 ratio. In the well plate, stock solutions were serial diluted two-fold in the first column with MHB followed by a serial two-fold dilution with 5% DMSO in MHB in subsequent columns.

The last two columns of the well plate contained a growth control of bacteria inoculated in MHB and a sterile control of MHB without bacteria, respectively. The well plates were incubated (37 °C) in a BioTek Synergy HTX Multimode microplate reader for 16 hr with continuous orbital shaking. The absorbance at λ = 600 nm was measured every 20 min. The MIC was determined as the lowest concentration that prevented the growth of bacteria.

C.4 Results

C.4.1 Antibacterial susceptibility determined by disk diffusion assay

C.4.1.1 1-H$^+$ and 1-^{t}Bu$^+$ monomers

Disk diffusion assays were performed as preliminary studies to determine the inhibitory potential of monomers and in-house synthesized polymers.[213,214] This method rapidly assesses antibacterial susceptibility rather than a quantitative determination of a minimal inhibitory concentration (MIC).[50-52] To assess the antimicrobial activity, Gram-negative, common laboratory strain of *E. coli* K12 and Gram-positive, clinically relevant strain of MRSA were selected. These results are summarized in **Table 15** & **Table 16**. Monomers did not produce any ZOI for both bacteria and solvents. (Figure 36: Disk diffusion assays against *E. coli* and MRSA for: (a) 1-H+ dissolved in water, (b) 1-H+ dissolved in DMSO,

(c) 1-tBu+ dissolved in water, and (d) 1-tBu+ dissolved in DMSO.**Figure 36**) Thus, further investigations excluded monomers.

Table 15: Antimicrobial activity determined by disk diffusion assay.

Sample type	Sample Name	Solvent	Testing concentrations (µg/mL)	Disk Diffusion MIC	
				E. coli	**MRSA**
Monomer	**1-H**$^{+}$	DI water	400 to 6,400	<400	<400
		DMSO	400 to 6,400	<400	<400
	1-^{t}**Bu**$^{+}$	DI water	400 to 6,400	<400	<400
		DMSO	400 to 6,400	<400	<400
Polymer	poly(**1-H**$^{+}$)$_{20}$	DI water	400 to 6,400	1,600	1,600
		DMSO	400 to 6,400	1,600	800
	poly(**1-**^{t}**Bu**$^{+}$)$_{20}$	DMSO	400 to 6,400	1,600	400
	poly(**1-**^{t}**Bu**$^{+}$)-*b*-(**1-H**$^{+}$)	DMSO	400 to 6,400	3,200	3,200
	poly(**1-H**$^{+}$)-*r*-(**1-**^{t}**Bu**$^{+}$)	DMSO	400 to 6,400	6,400	3,200

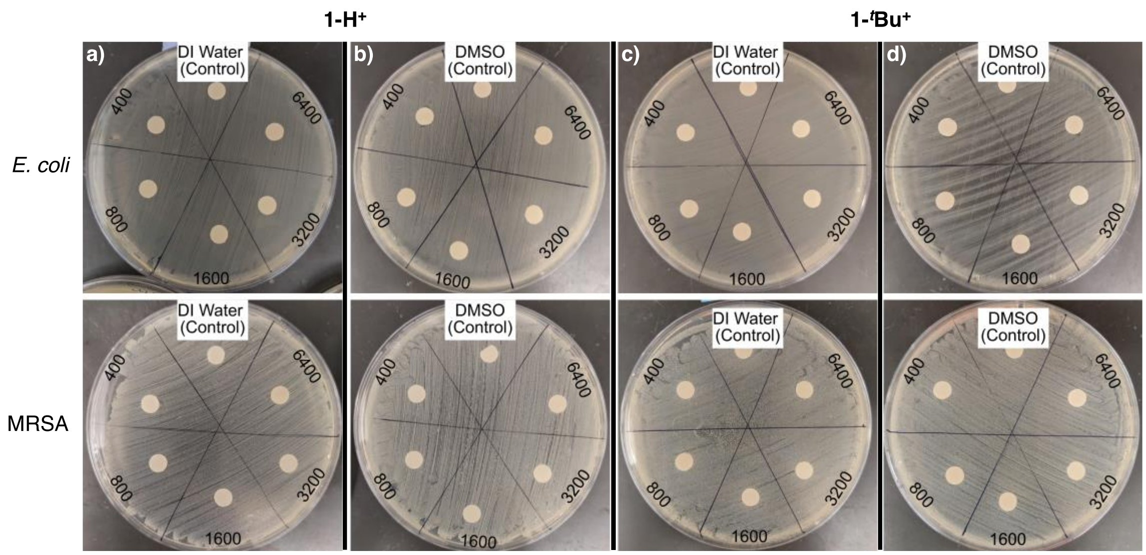

Figure 36: Disk diffusion assays against *E. coli* and MRSA for: (a) 1-H^{+} dissolved in water, (b) 1-H^{+} dissolved in DMSO, (c) 1-^{t}Bu^{+} dissolved in water, and (d) 1-^{t}Bu^{+} dissolved in DMSO.

C.4.1.2 Poly(1-H^{+}) and poly(1-^{t}Bu^{+}) homopolymers

For the assessment of the antimicrobial susceptibility of in-house synthesized polymers, poly(**1-H**$^{+}$) could be dissolved in water or DMSO before being diluted with MHB. Since poly(**1-**^{t}**Bu**$^{+}$) and copolymers poly(**1-**^{t}**Bu**$^{+}$)-*b*-(**1-H**$^{+}$) and poly(**1-H**$^{+}$)-*r*-(**1-**^{t}**Bu**$^{+}$) were not water-soluble, DMSO was selected as a solvent due to its relatively low toxicity to cells, in contrast to most organic solvents.[53] Other literature[54] has cited its successful use in disk diffusion assays for antibacterial susceptibility testing. In parallel to testing the cationic polymers, a control disk, that was only exposed to the relevant solvent used (i.e. water or DMSO without polymers) was also tested.

Poly(**1-H**$^{+}$)$_{20}$ dissolved in water produced ZOIs at a concentration of 1600 μg/mL for both bacteria (**Figure 37.a**). When DMSO was used to dissolve poly(**1-H**$^{+}$)$_{20}$, the concentration needed to inhibit growth of *E. coli* was similar to that of the aqueous solution. The lowest concentration with a ZOI for MRSA was 800 μg/mL **Figure 37.b**). Notably, both of the control disks (containing water or DMSO) exhibited no ZOI. The difference in inhibitory concentrations for poly(**1-H**$^{+}$)$_{20}$ dissolved in water and in DMSO may be caused by the differences in the diffusion of the cationic polymer and solvent along the hydrophilic agar plate. Meanwhile *tert*-butyl substituted poly(**1-^{t}Bu**$^{+}$)$_{20}$ dissolved in DMSO exhibited ZOIs at concentrations of 1600 μg/mL against *E. coli*, and 400 μg/mL against MRSA (**Figure 37.c**). These results indicated the importance of the polycationic structure for antibacterial activity.

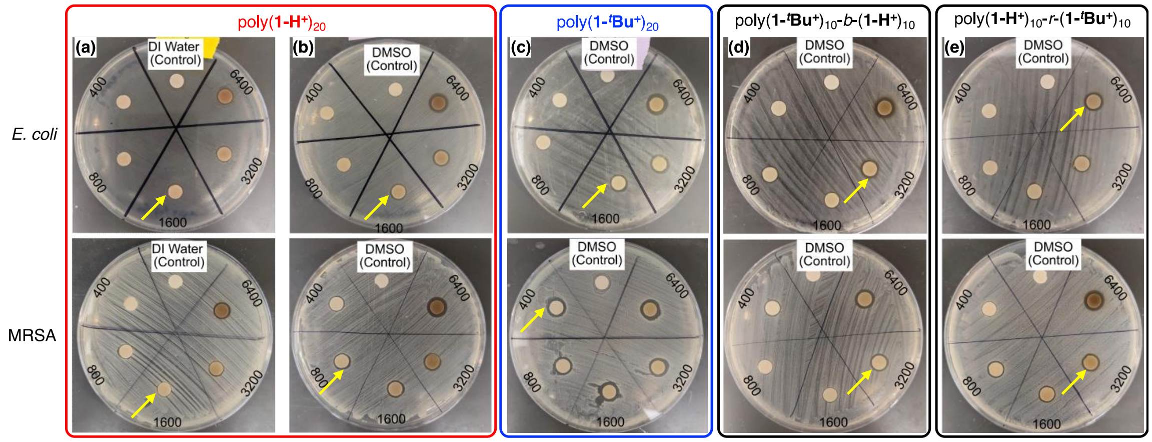

Figure 37: Disk diffusion assays against *E. coli* and MRSA (with arrows indicating lowest concentration in which a ZOI is observed) for: (a) poly(**1-H**$^+$)$_{20}$ dissolved in water, (b) poly(**1-H**$^+$)$_{20}$ dissolved in DMSO, (c) poly(**1-**^{t}**Bu**$^+$)$_{20}$ dissolved in DMSO, (d) poly(**1-**^{t}**Bu**$^+$)$_{10}$-*b*-(**1-H**$^+$)$_{10}$ dissolved in DMSO, and (e) poly(**1-H**$^+$)$_{10}$-*r*-(**1-**^{t}**Bu**$^+$)$_{10}$ dissolved in DMSO. The polymer concentration tested (μg/mL) is provided along the outside edge of the petri dish. Control samples containing relevant solvent (no cationic polymers) were also tested.

C.4.1.3 Poly(1-^{t}Bu$^+$)$_{10}$-(1-H$^+$)$_{10}$ co-polymers

The antibacterial activity of block and random copolymers, poly(**1-**^{t}**Bu**$^+$)$_{10}$-*b*-(**1-H**$^+$)$_{10}$ and poly(**1-H**$^+$)$_{10}$-*r*-(**1-**^{t}**Bu**$^+$)$_{10}$, respectively, was determined to explore the effect of varying the steric bulk and hydrophobicity surrounding the pyridinium group. Block copolymer poly(**1-**^{t}**Bu**$^+$)$_{10}$-*b*-(**1-H**$^+$)$_{10}$ showed ZOIs at 3200 μg/mL for both bacteria (**Figure 37.d**), while random copolymer poly(**1-H**$^+$)$_{10}$-*r*-(**1-**^{t}**Bu**$^+$)$_{10}$ exhibited ZOIs at 6400 and 3200 μg/mL for *E. coli* and MRSA, respectively **Figure 37.e**). The difference in lowest concentrations necessary for a ZOI against *E. coli* between the copolymers suggests that the spatial arrangement of repeating units bearing hydrophobic groups nearby the pyridinium is important to the bactericidal activity of the polymers.

C.4.2 MIC determination by broth microdilution assays

After initial disk diffusion assays confirmed initial antibacterial activity of poly(**1-H$^+$**) and (**1-^{t}Bu$^+$**) against *E. coli* and MRSA, broth microdilution assays were conducted to determine the MIC values of the polymers. This method provides quantitative MICs since the disk diffusion assay cannot quantify the amount of the antibacterial agent that diffuses along the agar surface.[51] In addition to investigating the effect of chemical structure on the antibacterial activity of poly(**1-H$^+$**) and (**1-^{t}Bu$^+$**), the influence of the length of the polymers was also studied. While it was beyond the scope of this study to identify the exact mechanism of bacterial inactivation, we note that some studies have shown that higher molecular weight polymers with more cationic charges inactivate and disrupt bacterial cell membranes via surface contact.[55-57] In contrast, other compounds have to permeate into the cell membrane in order to inactivate the bacteria; in that case, higher molecular weight polymers might exhibit poorer diffusion into the cell membrane, thus reducing their antibacterial efficacy.[56,58]

C.4.2.1 Effects of chain length on MIC of poly(1-H$^+$)

Polymers with shorter chain length (DP = 10; poly(**1$^+$**)$_{10}$) and higher chain length (DP = 40; poly(**1$^+$**)$_{40}$) were compared to poly(**1$^+$**)$_{20}$ that was studied in the disk diffusion assays. An MIC value of 50 µg/mL against both *E. coli* and MRSA was measured for all tested poly(**1-H$^+$**) independent of their DP (**Table 16**). This MIC is markedly lower than the concentrations needed for bacterial inhibition in the disk diffusion assays. Notably, inconsistencies between disk diffusion and broth dilution evaluations have been reported and attributed to the ability of the polymer to interact with and diffuse from the filter disk.[59-61]

Table 16: Comparison of the MIC of various homo- and copolymers

Sample	Stock solution solvent	Testing concentrations (μg/mL)	MIC (μg/mL) *E. coli*	MIC (μg/mL) MRSA
poly(**1-H$^+$**)$_{10}$	DI water	0.195 to 100	50	50
poly(**1-H$^+$**)$_{20}$	DI water	0.195 to 100	50	50
poly(**1-H$^+$**)$_{40}$	DI water	0.195 to 100	50	50
poly(**1-^{t}Bu$^+$**)$_{10}$	DMSO	0.195 to 100	25	50
poly(**1-^{t}Bu$^+$**)$_{20}$	DMSO	0.195 to 100	50	50
poly(**1-^{t}Bu$^+$**)$_{40}$	DMSO	0.195 to 100	50	50
poly(**1-^{t}Bu$^+$**)$_{10}$-*b*-(**1-H$^+$**)$_{10}$	DMSO	0.195 to 100	25	50
poly(**1-H$^+$**)$_{10}$-*r*-(**1-^{t}Bu$^+$**)$_{10}$	DMSO	0.195 to 100	50	50

C.4.2.2 Effects of chain length on MIC of poly(1-^{t}Bu$^+$)

A similar study was conducted with *tert*-butyl substituted poly(**1-^{t}Bu$^+$**), as well as copolymers poly(**1-^{t}Bu$^+$**)$_{10}$-*b*-(**1-H$^+$**)$_{10}$ and poly(**1-H$^+$**)$_{10}$-*r*-(**1-^{t}Bu$^+$**)$_{10}$. However, because of the poor water solubility of these polymers, all samples were first dissolved in DMSO prior to dilution with Mueller Hinton Broth (MHB), which afforded MHB/polymer solutions with 5% DMSO content. Though high concentrations of organic solvents are generally incompatible with the growth of bacteria, low concentrations of DMSO (5%) are known not to inhibit the growth of *E. coli* or MRSA.[59, 62] This was further confirmed by monitoring the bacterial growth curves of growth controls run with 5% DMSO in MHB (not shown). For this second series of cationic polymers, the broth microdilution assays were also found to be more sensitive to polymer concentrations than the disk diffusion assays. The MIC of poly(**1-^{t}Bu$^+$**)$_{20}$ and poly(**1-^{t}Bu$^+$**)$_{40}$ was 50 μg/mL for both bacteria (**Table 16**). Interestingly, the MIC of poly(**1-^{t}Bu$^+$**)$_{10}$ differed for *E. coli* (25 μg/mL) and MRSA (50 μg/mL).

C.4.2.3 Effects of chain length on MIC of co-polymers

Similar to poly(**1-^{t}Bu$^+$**)$_{10}$, the block copolymer poly(**1-^{t}Bu$^+$**)$_{10}$-*b*-(**1-H$^+$**)$_{10}$ also resulted in MIC values of 25 and 50 μg/mL for *E. coli* and MRSA, respectively, whereas the random copolymer poly(**1-H$^+$**)$_{10}$-*r*-(**1-^{t}Bu$^+$**)$_{10}$ had an MIC value of 50 μg/mL for both bacteria.

Differences in MIC values observed with Gram-negative and Gram-positive bacteria in the presence of antibacterial polymers are common and are typically ascribed to the specific outer membrane of each strain, which has been reported to impact the ability of bioactive compounds to interact with and/or diffuse into cellular membranes.[58, 63, 64]

REFERENCES

(1) Singleton, P. *Bacteria in Biology, Biotechnology, and Medicine.*, Fourth edition.; J. Wiley & Sons, 1997.

(2) Furst, A. L.; Hoepker, A. C.; Francis, M. B. Quantifying Hormone Disruptors with an Engineered Bacterial Biosensor. *ACS Cent. Sci.* **2017**, *3* (2), 110–116. https://doi.org/10.1021/acscentsci.6b00322.

(3) Asaithambi, N.; Singh, S. K.; Singha, P. Current Status of Non-Thermal Processing of Probiotic Foods: A Review. *Journal of Food Engineering* **2021**, *303*, 110567. https://doi.org/10.1016/j.jfoodeng.2021.110567.

(4) Finkel, S. E. Long-Term Survival during Stationary Phase: Evolution and the GASP Phenotype. *Nat Rev Microbiol* **2006**, *4* (2), 113–120. https://doi.org/10.1038/nrmicro1340.

(5) Sehrawat, R.; Abdullah, S.; Khatri, P.; Kumar, L.; Kumar, A.; Mujumdar, A. S. Role of Drying Technology in Probiotic Encapsulation and Impact on Food Safety. *Drying Technology* **2022**, *40* (8), 1562–1581. https://doi.org/10.1080/07373937.2022.2044844.

(6) Goderska, K. *Different Methods of Probiotics Stabilization*; IntechOpen, 2012. https://doi.org/10.5772/50313.

(7) Hubálek, Z. Protectants Used in the Cryopreservation of Microorganisms. *Cryobiology* **2003**, *46* (3), 205–229. https://doi.org/10.1016/S0011-2240(03)00046-4.

(8) Cook, M. T.; Tzortzis, G.; Charalampopoulos, D.; Khutoryanskiy, V. V. Microencapsulation of Probiotics for Gastrointestinal Delivery. *Journal of Controlled Release* **2012**, *162* (1), 56–67. https://doi.org/10.1016/j.jconrel.2012.06.003.

(9) Lahtinen, S. J.; Ouwehand, A. C.; Salminen, S. J.; Forssell, P.; Myllärinen, P. Effect of Starch- and Lipid-based Encapsulation on the Culturability of Two Bifidobacterium Longum Strains. *Lett. Appl. Microbiol.* **2007**, *44* (5), 500–505. https://doi.org/10.1111/j.1472-765X.2007.02110.x.

(10) Vidyalakshmi, R.; Bhakyaraj, R.; Subhasree, R. S. Encapsulation "The Future of Probiotics"-A Review. *Adv Biol Res* **2009**, *3*, 96–103.

(11) Huq, T.; Khan, A.; Khan, R. A.; Riedl, B.; Lacroix, M. Encapsulation of Probiotic Bacteria in Biopolymeric System. *Crit. Rev. Food Sci. Nutr.* **2013**, *53* (9), 909–916. https://doi.org/10.1080/10408398.2011.573152.

(12) Moumita, S.; Goderska, K.; Johnson, E. M.; Das, B.; Indira, D.; Yadav, R.; Kumari, S.; Jayabalan, R. Evaluation of the Viability of Free and Encapsulated Lactic Acid Bacteria Using In-Vitro Gastro Intestinal Model and Survivability Studies of Synbiotic Microcapsules in Dry Food Matrix during Storage. *LWT* **2017**, *77*, 460–467. https://doi.org/10.1016/j.lwt.2016.11.079.

(13) Butorac, K.; Novak, J.; Bellich, B.; Terán, L. C.; Banić, M.; Leboš Pavunc, A.; Zjalić, S.; Cescutti, P.; Šušković, J.; Kos, B. Lyophilized Alginate-Based Microspheres Containing Lactobacillus Fermentum D12, an Exopolysaccharides Producer, Contribute to the Strain's Functionality in Vitro. *Microb Cell Fact* **2021**, *20*, 85. https://doi.org/10.1186/s12934-021-01575-6.

(14) Alkayyali, T.; Cameron, T.; Haltli, B.; Kerr, R. G.; Ahmadi, A. Microfluidic and Cross-Linking Methods for Encapsulation of Living Cells and Bacteria - A Review. *Analytica Chimica Acta* **2019**, *1053*, 1–21. https://doi.org/10.1016/j.aca.2018.12.056.

(15) Rodrigo-Navarro, A.; Sankaran, S.; Dalby, M. J.; del Campo, A.; Salmeron-Sanchez, M. Engineered Living Biomaterials. *Nat Rev Mater* **2021**, *6* (12), 1175–1190. https://doi.org/10.1038/s41578-021-00350-8.

(16) Tromp, R. H.; Vink, C.; Stijnman, A. C. Encapsulation by Electrospinning of Live Bacteria Used in the Food Industry. In *Gums and Stabilisers for the Food Industry 16*; Williams, P. A., Phillips, G. O., Eds.; Royal Soc Chemistry: Cambridge, 2012; Vol. 335, pp 247–255. http://dx.doi.org/10.1039/9781849734554-00247.

(17) Nagy, Zs. K.; Wagner, I.; Suhajda, A.; Tobak, T.; Harasztos, A. H.; Vigh, T.; Soti, P. L.; Pataki, H.; Molnar, K.; Marosi, Gy. Nanofibrous Solid Dosage Form of Living Bacteria Prepared by Electrospinning. *Express Polym. Lett.* **2014**, *8* (5), 352–361. https://doi.org/10.3144/expresspolymlett.2014.39.

(18) Salalha, W.; Kuhn, J.; Dror, Y.; Zussman, E. Encapsulation of Bacteria and Viruses in Electrospun Nanofibres. *Nanotechnology* **2006**, *17* (18), 4675–4681. https://doi.org/10.1088/0957-4484/17/18/025.

(19) Zupančič, Š.; Škrlec, K.; Kocbek, P.; Kristl, J.; Berlec, A. Effects of Electrospinning on the Viability of Ten Species of Lactic Acid Bacteria in Poly(Ethylene Oxide) Nanofibers. *Pharmaceutics* **2019**, *11* (9), 483. https://doi.org/10.3390/pharmaceutics11090483.

(20) Weinbreck, F.; Bodnár, I.; Marco, M. L. Can Encapsulation Lengthen the Shelf-Life of Probiotic Bacteria in Dry Products? *Int. J. Food Microbiol.* **2010**, *136* (3), 364–367. https://doi.org/10.1016/j.ijfoodmicro.2009.11.004.

(21) Bhattarai, D. P.; Aguilar, L. E.; Park, C. H.; Kim, C. S. A Review on Properties of Natural and Synthetic Based Electrospun Fibrous Materials for Bone Tissue Engineering. *Membranes* **2018**, *8* (3), 62. https://doi.org/10.3390/membranes8030062.

(22) López-Rubio, A.; Sanchez, E.; Sanz, Y.; Lagaron, J. M. Encapsulation of Living Bifidobacteria in Ultrathin PVOH Electrospun Fibers. *Biomacromolecules* **2009**, *10* (10), 2823–2829. https://doi.org/10.1021/bm900660b.

(23) Diep, E.; Schiffman, J. D. Encapsulating Bacteria in Alginate-Based Electrospun Nanofibers. *Biomater. Sci.* **2021**, *9* (12), 4364–4373. https://doi.org/10.1039/D0BM02205E.

(24) Li, T. X.; Ding, X.; Sui, X.; Tian, L. L.; Zhang, Y.; Hu, J. Y.; Yang, X. D. Sustained Release of Protein Particle Encapsulated in Bead-on-String Electrospun Nanofibers. *Journal of Macromolecular Science, Part B* **2015**, *54* (8), 887–896. https://doi.org/10.1080/00222348.2015.1051210.

(25) Castellano, M.; Alloisio, M.; Darawish, R.; Dodero, A.; Vicini, S. Electrospun Composite Mats of Alginate with Embedded Silver Nanoparticles: Synthesis and Characterization. *J Therm Anal Calorim* **2019**, *137* (3), 767–778. https://doi.org/10.1007/s10973-018-7979-z.

(26) Bölgen, N.; Vargel, İ.; Korkusuz, P.; Menceloğlu, Y. Z.; Pişkin, E. In Vivo Performance of Antibiotic Embedded Electrospun PCL Membranes for Prevention of Abdominal Adhesions. *Journal of Biomedical Materials Research Part B: Applied Biomaterials* **2007**, *81B* (2), 530–543. https://doi.org/10.1002/jbm.b.30694.

(27) De Silva, R. T.; Dissanayake, R. K.; Mantilaka, M. M. M. G. P. G.; Wijesinghe, W. P. S. L.; Kaleel, S. S.; Premachandra, T. N.; Weerasinghe, L.; Amaratunga, G. A. J.; de Silva, K. M. N. Drug-Loaded Halloysite Nanotube-Reinforced Electrospun Alginate-Based Nanofibrous Scaffolds with Sustained Antimicrobial Protection. *ACS Appl. Mater. Interfaces* **2018**, *10* (40), 33913–33922. https://doi.org/10.1021/acsami.8b11013.

(28) Pillay, V.; Dott, C.; Choonara, Y. E.; Tyagi, C.; Tomar, L.; Kumar, P.; du Toit, L. C.; Ndesendo, V. M. K. A Review of the Effect of Processing Variables on the Fabrication of Electrospun Nanofibers for Drug Delivery Applications. *J. Nanomater.* **2013**, *2013*, 1–22. https://doi.org/10.1155/2013/789289.

(29) Kataria, K.; Gupta, A.; Rath, G.; Mathur, R. B.; Dhakate, S. R. In Vivo Wound Healing Performance of Drug Loaded Electrospun Composite Nanofibers Transdermal Patch. *International Journal of Pharmaceutics* **2014**, *469* (1), 102–110. https://doi.org/10.1016/j.ijpharm.2014.04.047.

(30) Sill, T. J.; von Recum, H. A. Electrospinning: Applications in Drug Delivery and Tissue Engineering. *Biomaterials* **2008**, *29* (13), 1989–2006. https://doi.org/10.1016/j.biomaterials.2008.01.011.

(31) Ghorani, B.; Tucker, N. Fundamentals of Electrospinning as a Novel Delivery Vehicle for Bioactive Compounds in Food Nanotechnology. *Food Hydrocoll.* **2015**, *51*, 227–240. https://doi.org/10.1016/j.foodhyd.2015.05.024.

(32) Zheng, Y. 3 - Fabrication on Bioinspired Surfaces. In *Bioinspired Design of Materials Surfaces*; Zheng, Y., Ed.; Materials Today; Elsevier, 2019; pp 99–146. https://doi.org/10.1016/B978-0-12-814843-3.00003-X.

(33) Haider, A.; Haider, S.; Kang, I.-K. A Comprehensive Review Summarizing the Effect of Electrospinning Parameters and Potential Applications of Nanofibers in Biomedical and Biotechnology. *Arab. J. Chem.* **2018**, *11* (8), 1165–1188. https://doi.org/10.1016/j.arabjc.2015.11.015.

(34) Reneker, D. H.; Yarin, A. L. Electrospinning Jets and Polymer Nanofibers. *Polymer* **2008**, *49* (10), 2387–2425. https://doi.org/10.1016/j.polymer.2008.02.002.

(35) Diep, E.; Schiffman, J. D. Electrospinning Living Bacteria: A Review of Applications from Agriculture to Health Care. *ACS Appl. Bio Mater.* **2023**, *6* (3), 951–964. https://doi.org/10.1021/acsabm.2c01055.

(36) Ramakrishna, S.; Fujihara, K.; Teo, W.-E.; Lim, T.-C.; Ma, Z. *An Introduction to Electrospinning and Nanofibers*; World Scientific Publishing Co. Pte. Ltd., 2005. https://doi.org/10.1142/5894.

(37) Bhardwaj, N.; Kundu, S. C. Electrospinning: A Fascinating Fiber Fabrication Technique. *Biotechnol. Adv.* **2010**, *28* (3), 325–347. https://doi.org/10.1016/j.biotechadv.2010.01.004.

(38) Elveren, B.; Kurečič, M.; Maver, T.; Maver, U. Cell Electrospinning: A Mini-Review of the Critical Processing Parameters and Its Use in Biomedical Applications. *Advanced Biology* **2023**, *n/a* (n/a), 2300057. https://doi.org/10.1002/adbi.202300057.

(39) Deitzel, J. M.; Kleinmeyer, J.; Harris, D.; Beck Tan, N. C. The Effect of Processing Variables on the Morphology of Electrospun Nanofibers and Textiles. *Polymer* **2001**, *42* (1), 261–272. https://doi.org/10.1016/S0032-3861(00)00250-0.

(40) Regev, O.; Vandebril, S.; Zussman, E.; Clasen, C. The Role of Interfacial Viscoelasticity in the Stabilization of an Electrospun Jet. *Polymer* **2010**, *51* (12), 2611–2620. https://doi.org/10.1016/j.polymer.2010.03.061.

(41) Bonino, C. A.; Krebs, M. D.; Saquing, C. D.; Jeong, S. I.; Shearer, K. L.; Alsberg, E.; Khan, S. A. Electrospinning Alginate-Based Nanofibers: From Blends to Crosslinked Low Molecular Weight Alginate-Only Systems. *Carbohydr. Polym.* **2011**, *85* (1), 111–119. https://doi.org/10.1016/j.carbpol.2011.02.002.

(42) Nie, H.; He, A.; Wu, W.; Zheng, J.; Xu, S.; Li, J.; Han, C. C. Effect of Poly(Ethylene Oxide) with Different Molecular Weights on the Electrospinnability of Sodium Alginate. *Polymer* **2009**, *50* (20), 4926–4934. https://doi.org/10.1016/j.polymer.2009.07.043.

(43) Taemeh, M. A.; Shiravandi, A.; Korayem, M. A.; Daemi, H. Fabrication Challenges and Trends in Biomedical Applications of Alginate Electrospun Nanofibers. *Carbohydrate Polymers* **2020**, *228*, 115419. https://doi.org/10.1016/j.carbpol.2019.115419.

(44) Ballengee, J. B.; Pintauro, P. N. Morphological Control of Electrospun Nafion Nanofiber Mats. *J. Electrochem. Soc.* **2011**, *158* (5), B568. https://doi.org/10.1149/1.3561645.

(45) Chung, S.; Moghe, A. K.; Montero, G. A.; Kim, S. H.; King, M. W. Nanofibrous Scaffolds Electrospun from Elastomeric Biodegradable Poly(L-Lactide-Co-$\upepsilon$-Caprolactone) Copolymer. *Biomed. Mater.* **2009**, *4* (1), 015019. https://doi.org/10.1088/1748-6041/4/1/015019.

(46) Zhang, C.; Yuan, X.; Wu, L.; Han, Y.; Sheng, J. Study on Morphology of Electrospun Poly(Vinyl Alcohol) Mats. *Eur. Polym. J.* **2005**, *41* (3), 423–432. https://doi.org/10.1016/j.eurpolymj.2004.10.027.

(47) Bosworth, L. A.; Downes, S. Acetone, a Sustainable Solvent for Electrospinning Poly(ε-Caprolactone) Fibres: Effect of Varying Parameters and Solution Concentrations on Fibre Diameter. *J Polym Environ* **2012**, *20* (3), 879–886. https://doi.org/10.1007/s10924-012-0436-3.

(48) Tripatanasuwan, S.; Zhong, Z.; Reneker, D. H. Effect of Evaporation and Solidification of the Charged Jet in Electrospinning of Poly(Ethylene Oxide) Aqueous Solution. *Polymer* **2007**, *48* (19), 5742–5746. https://doi.org/10.1016/j.polymer.2007.07.045.

(49) De Vrieze, S.; Van Camp, T.; Nelvig, A.; Hagström, B.; Westbroek, P.; De Clerck, K. The Effect of Temperature and Humidity on Electrospinning. *J Mater Sci* **2009**, *44* (5), 1357–1362. https://doi.org/10.1007/s10853-008-3010-6.

(50) Diep, E.; Schiffman, J. D.; Kurtz, I. S. Interfacing Electrospun Nanofibers with Microorganisms: Applications from Killing to Repelling to Delivering Living Microbes. In *Applications of Polymer Nanofibers*; Andrady, A. L., Khan, S. A., Eds.; John Wiley & Sons, Inc. U.S.A., 2022.

(51) Cui, W.; Li, X.; Zhu, X.; Yu, G.; Zhou, S.; Weng, J. Investigation of Drug Release and Matrix Degradation of Electrospun Poly(Dl-Lactide) Fibers with Paracetanol Inoculation. *Biomacromolecules* **2006**, *7* (5), 1623–1629. https://doi.org/10.1021/bm060057z.

(52) Škrlec, K.; Zupančič, Š.; Prpar Mihevc, S.; Kocbek, P.; Kristl, J.; Berlec, A. Development of Electrospun Nanofibers That Enable High Loading and Long-Term Viability of Probiotics. *Eur J Pharm Sci* **2019**, *136*, 108–119. https://doi.org/10.1016/j.ejpb.2019.01.013.

(53) Rathore, P.; Schiffman, J. D. Beyond the Single-Nozzle: Coaxial Electrospinning Enables Innovative Nanofiber Chemistries, Geometries, and Applications. *ACS Appl. Mater. Interfaces* **2021**, *13* (1), 48–66. https://doi.org/10.1021/acsami.0c17706.

(54) Jiang, H.; Hu, Y.; Zhao, P.; Li, Y.; Zhu, K. Modulation of Protein Release from Biodegradable Core–Shell Structured Fibers Prepared by Coaxial Electrospinning. *J. Biomed. Mater. Res.* **2006**, *79B* (1), 50–57. https://doi.org/10.1002/jbm.b.30510.

(55) Anselmo, A. C.; McHugh, K. J.; Webster, J.; Langer, R.; Jaklenec, A. Layer-by-Layer Encapsulation of Probiotics for Delivery to the Microbiome. *Advanced Materials* **2016**, *28* (43), 9486–9490. https://doi.org/10.1002/adma.201603270.

(56) Deng, L.; Zhang, H. Recent Advances in Probiotics Encapsulation by Electrospinning. *ES Food Agrofor.* **2020**. https://doi.org/10.30919/esfaf1120.

(57) Mendes, A. C.; Chronakis, I. S. Electrohydrodynamic Encapsulation of Probiotics: A Review. *Food Hydrocolloids* **2021**, *117*, 106688. https://doi.org/10.1016/j.foodhyd.2021.106688.

(58) Desitti, C.; Beliavski, M.; Tarre, S.; Avrahami, R.; Zussman, E.; Green, M. Durable Electrospun Microtubes for Encapsulation of Bacteria in Atrazine Bioremediation. *Journal of Water Process Engineering* **2017**, *19*, 205–211. https://doi.org/10.1016/j.jwpe.2017.08.004.

(59) Liu, Y.; Liu, B.; Li, D.; Hu, Y.; Zhao, L.; Zhang, M.; Ge, S.; Pang, J.; Li, Y.; Wang, R.; Wang, P.; Huang, Y.; Huang, J.; Bai, J.; Ren, F.; Li, Y. Improved Gastric Acid Resistance and Adhesive Colonization of Probiotics by Mucoadhesive and Intestinal Targeted Konjac Glucomannan Microspheres. *Adv. Funct. Mater.* **2020**, *30* (35), 2001157. https://doi.org/10.1002/adfm.202001157.

(60) Varum, F. J. O.; Veiga, F.; Sousa, J. S.; Basit, A. W. Mucoadhesive Platforms for Targeted Delivery to the Colon. *International Journal of Pharmaceutics* **2011**, *420* (1), 11–19. https://doi.org/10.1016/j.ijpharm.2011.08.006.

(61) Patel, P. Edible Packaging. *ACS Cent Sci* **2019**, *5* (12), 1907–1910. https://doi.org/10.1021/acscentsci.9b01251.

(62) Sen, D. J. Cross Linking of Calcium Ion in Alginate Produce Spherification in Molecular Gastronomy by Pseudoplastic Flow. *World J. Phamr. Sci.* **2017**, 1–10.

(63) Bruchet, M.; Melman, A. Fabrication of Patterned Calcium Cross-Linked Alginate Hydrogel Films and Coatings through Reductive Cation Exchange. *Carbohydr. Polym.* **2015**, *131*, 57–64. https://doi.org/10.1016/j.carbpol.2015.05.021.

(64) Lee, K. Y.; Mooney, D. J. Alginate: Properties and Biomedical Applications. *Prog. Polym. Sci.* **2012**, *37* (1), 106–126. https://doi.org/10.1016/j.progpolymsci.2011.06.003.

(65) Ahirrao, S.; Gide, P.; Shrivastav, B.; Sharma, P. Extended Release of Theophylline Through Sodium Alginate Hydrogel Beads: Effect of Glycerol on Entrapment Efficiency, Drug Release. *Particulate Science and Technology* **2014**, *32* (2), 105–111. https://doi.org/10.1080/02726351.2013.809396.

(66) Takka, S.; Ocak, O. H.; Acartürk, F. Formulation and Investigation of Nicardipine HCl-Alginate Gel Beads with Factorial Design-Based Studies. *Eur J Pharm Sci* **1998**, *6* (3), 241–246. https://doi.org/10.1016/s0928-0987(97)10005-7.

(67) Liu, J.; Pang, Y.; Zhang, S.; Cleveland, C.; Yin, X.; Booth, L.; Lin, J.; Lucy Lee, Y.-A.; Mazdiyasni, H.; Saxton, S.; Kirtane, A. R.; Erlach, T. von; Rogner, J.; Langer, R.; Traverso, G. Triggerable Tough Hydrogels for Gastric Resident Dosage Forms. *Nat Commun* **2017**, *8* (1), 124. https://doi.org/10.1038/s41467-017-00144-z.

(68) Anal, A. K.; Singh, H. Recent Advances in Microencapsulation of Probiotics for Industrial Applications and Targeted Delivery. *Trends Food Sci. Technol.* **2007**, *18* (5), 240–251. https://doi.org/10.1016/j.tifs.2007.01.004.

(69) Gu, M.; Zhang, Z.; Pan, C.; Goulette, T. R.; Zhang, R.; Hendricks, G.; McClements, D. J.; Xiao, H. Encapsulation of Bifidobacterium Pseudocatenulatum G7 in Gastroprotective Microgels: Improvement of the Bacterial Viability under Simulated Gastrointestinal Conditions. *Food Hydrocoll.* **2019**, *91*, 283–289. https://doi.org/10.1016/j.foodhyd.2019.01.040.

(70) Pestovsky, Y. S.; Martínez-Antonio, A. The Synthesis of Alginate Microparticles and Nanoparticles. *DDIPIJ* **2019**, *3* (1), 293–327.

(71) Moumita, S.; Das, B.; Hasan, U.; Jayabalan, R. Effect of Long-Term Storage on Viability and Acceptability of Lyophilized and Spray-Dried Synbiotic Microcapsules in Dry Functional Food Formulations. *LWT* **2018**, *96*, 127–132. https://doi.org/10.1016/j.lwt.2018.05.030.

(72) Chávarri, M.; Marañón, I.; Ares, R.; Ibáñez, F. C.; Marzo, F.; Villarán, M. del C. Microencapsulation of a Probiotic and Prebiotic in Alginate-Chitosan Capsules Improves Survival in Simulated Gastro-Intestinal Conditions. *Int. J. Food Microbiol.* **2010**, *142* (1), 185–189. https://doi.org/10.1016/j.ijfoodmicro.2010.06.022.

(73) Picot, A.; Lacroix, C. Encapsulation of Bifidobacteria in Whey Protein-Based Microcapsules and Survival in Simulated Gastrointestinal Conditions and in Yoghurt. *Int. Dairy J.* **2004**, *14* (6), 505–515. https://doi.org/10.1016/j.idairyj.2003.10.008.

(74) Ungphaiboon, S.; Attia, D.; d'Ayala, G. G.; Sansongsak, P.; Cellesi, F.; Tirelli, N. Materials for Microencapsulation: What Toroidal Particles ("Doughnuts") Can Do Better than Spherical Beads. *Soft Matter* **2010**, *6* (17), 4070–4083. https://doi.org/10.1039/C0SM00150C.

(75) Mokhena, T. C.; Mochane, M. J.; Mtibe, A.; John, M. J.; Sadiku, E. R.; Sefadi, J. S. Electrospun Alginate Nanofibers Toward Various Applications: A Review. *Materials* **2020**, *13* (4), 934. https://doi.org/10.3390/ma13040934.

(76) Saquing, C. D.; Tang, C.; Monian, B.; Bonino, C. A.; Manasco, J. L.; Alsberg, E.; Khan, S. A. Alginate–Polyethylene Oxide Blend Nanofibers and the Role of the Carrier Polymer in Electrospinning. *Ind. Eng. Chem. Res.* **2013**, *52* (26), 8692–8704. https://doi.org/10.1021/ie302385b.

(77) Leung, V.; Hartwell, R.; Elizei, S. S.; Yang, H.; Ghahary, A.; Ko, F. Postelectrospinning Modifications for Alginate Nanofiber-Based Wound Dressings. *J. Biomed. Mater. Res.* **2014**, *102* (3), 508–515. https://doi.org/10.1002/jbm.b.33028.

(78) Shen, W.; Hsieh, Y.-L. Biocompatible Sodium Alginate Fibers by Aqueous Processing and Physical Crosslinking. *Carbohydr. Polym.* **2014**, *102*, 893–900. https://doi.org/10.1016/j.carbpol.2013.10.066.

(79) Yilmaz, M. T.; Taylan, O.; Karakas, C. Y.; Dertli, E. An Alternative Way to Encapsulate Probiotics within Electrospun Alginate Nanofibers as Monitored under Simulated Gastrointestinal Conditions and in Kefir. *Carbohydr. Polym.* **2020**, *244*, 116447. https://doi.org/10.1016/j.carbpol.2020.116447.

(80) Kurečič, M.; Rijavec, T.; Hribernik, S.; Lapanje, A.; Kleinschek, K. S.; Maver, U. Novel Electrospun Fibers with Incorporated Commensal Bacteria for Potential Preventive Treatment of the Diabetic Foot. *Nanomedicine* **2018**, *13* (13), 1583–1594. https://doi.org/10.2217/nnm-2018-0014.

(81) Baumgarten, P. K. Electrostatic Spinning of Acrylic Microfibers. *J. Colloid Interface Sci.* **1971**, *36* (1), 71–79. https://doi.org/10.1016/0021-9797(71)90241-4.

(82) Hirsch, E.; Pantea, E.; Vass, P.; Domján, J.; Molnár, M.; Suhajda, Á.; Andersen, S. K.; Vigh, T.; Verreck, G.; Marosi, G. J.; Nagy, Z. K. Probiotic Bacteria Stabilized in Orally Dissolving Nanofibers Prepared by High-Speed Electrospinning. *Food and Bioproducts Processing* **2021**, *128*, 84–94. https://doi.org/10.1016/j.fbp.2021.04.016.

(83) Xie, S. Genetically Engineering of Escherichia Coli and Immobilization on Electrospun Fibers for Drug Delivery Purposes. *Journal of Materials Chemistry B* **2016**, 10.

(84) Feng, K.; Zhai, M.-Y.; Zhang, Y.; Linhardt, R. J.; Zong, M.-H.; Li, L.; Wu, H. Improved Viability and Thermal Stability of the Probiotics Encapsulated in a Novel Electrospun Fiber Mat. *J. Agric. Food Chem.* **2018**, *66* (41), 10890–10897. https://doi.org/10.1021/acs.jafc.8b02644.

(85) Reznik, S. N.; Yarin, A. L.; Zussman, E.; Bercovici, L. Evolution of a Compound Droplet Attached to a Core-Shell Nozzle under the Action of a Strong Electric Field. *Phys. Fluids* **2006**, *18* (6), 062101. https://doi.org/10.1063/1.2206747.

(86) Vass, P.; Pantea, E.; Domokos, A.; Hirsch, E.; Domján, J.; Németh, Á.; Molnár, M.; Fehér, C.; Andersen, S. K.; Vigh, T.; Verreck, G.; Csontos, I.; Marosi, G.; Nagy, Z. K. Electrospun Solid Formulation of Anaerobic Gut Microbiome Bacteria. *AAPS PharmSciTech* **2020**, *21* (6), 214. https://doi.org/10.1208/s12249-020-01769-y.

(87) Atraki, R.; Azizkhani, M. Survival of Probiotic Bacteria Nanoencapsulated within Biopolymers in a Simulated Gastrointestinal Model. *Innovative Food Science & Emerging Technologies* **2021**, *72*, 102750. https://doi.org/10.1016/j.ifset.2021.102750.

(88) Ghorbani, S.; Azizkhani, M. Encapsulation of Lactic Acid Bacteria and Bifidobacteria Using Starch-Sodium Alginate Nanofibers to Enhance Viability in Food Model. *Journal of Food Processing and Preservation* **2021**, *45* (12), e16048. https://doi.org/10.1111/jfpp.16048.

(89) Fareed, F.; Saeed, F.; Afzaal, M.; Imran, A.; Ahmad, A.; Mahmood, K.; Shah, Y. A.; Hussain, M.; Ateeq, H. Fabrication of Electrospun Gum Arabic–Polyvinyl Alcohol Blend Nanofibers for Improved Viability of the Probiotic. *J Food Sci Technol* **2022**, *59* (12), 4812–4821. https://doi.org/10.1007/s13197-022-05567-1.

(90) Khan, M. A.; Hussain, Z.; Ali, S.; Qamar, Z.; Imran, M.; Hafeez, F. Y. Fabrication of Electrospun Probiotic Functionalized Nanocomposite Scaffolds for Infection Control and Dermal Burn Healing in a Mice Model. *ACS Biomater. Sci. Eng.* **2019**, *5* (11), 6109–6116. https://doi.org/10.1021/acsbiomaterials.9b01002.

(91) Silva, J. A.; De Gregorio, P. R.; Rivero, G.; Abraham, G. A.; Nader-Macías, M. E. F. Immobilization of Vaginal Lactobacillus in Polymeric Nanofibers for Its Incorporation in Vaginal Probiotic Products. *European Journal of Pharmaceutical Sciences* **2021**, *156*, 105563. https://doi.org/10.1016/j.ejps.2020.105563.

(92) Stojanov, S.; Kristl, J.; Zupančič, Š.; Berlec, A. Influence of Excipient Composition on Survival of Vaginal Lactobacilli in Electrospun Nanofibers. *Pharmaceutics* **2022**, *14* (6), 1155. https://doi.org/10.3390/pharmaceutics14061155.

(93) Mukiri, C.; Raja, K.; Senthilkumar, M.; Subramanian, K. S.; Govindaraju, K.; Pradeep, D.; Ranjan, S. Immobilization of Beneficial Microbe Methylobacterium Aminovorans in Electrospun Nanofibre as Potential Seed Coatings for Improving Germination and Growth of Groundnut Arachis Hypogaea. *Plant Growth Regul* **2022**, *97* (2), 419–427. https://doi.org/10.1007/s10725-021-00737-1.

(94) De Gregorio, P. R.; Michavila, G.; Muller, L. R.; Borges, C. de S.; Pomares, M. F.; Sá, E. L. S. de; Pereira, C.; Vincent, P. A. Beneficial Rhizobacteria Immobilized in Nanofibers for Potential Application as Soybean Seed Bioinoculants. *PLOS ONE* **2017**, *12* (5), e0176930. https://doi.org/10.1371/journal.pone.0176930.

(95) Damasceno, R.; Roggia, I.; Pereira, C.; de Sá, E. Rhizobia Survival in Seeds Coated with Polyvinyl Alcohol (PVA) Electrospun Nanofibres. *Can. J. Microbiol.* **2013**, *59* (11), 716–719. https://doi.org/10.1139/cjm-2013-0508.

(96) Hussain, Z.; Khan, M. A.; Iqbal, F.; Raffi, M.; Hafeez, F. Y. Electrospun Microbial-Encapsulated Composite-Based Plasticized Seed Coat for Rhizosphere Stabilization and Sustainable Production of Canola (Brassica Napus L.). *J. Agric. Food Chem.* **2019**, *67* (18), 5085–5095. https://doi.org/10.1021/acs.jafc.8b06505.

(97) Sarioglu, O. F.; Keskin, N. O. S.; Celebioglu, A.; Tekinay, T.; Uyar, T. Bacteria Encapsulated Electrospun Nanofibrous Webs for Remediation of Methylene Blue Dye in Water. *Colloids and Surfaces B: Biointerfaces* **2017**, *152*, 245–251. https://doi.org/10.1016/j.colsurfb.2017.01.034.

(98) San Keskin, N. O.; Celebioglu, A.; Sarioglu, O. F.; Uyar, T.; Tekinay, T. Encapsulation of Living Bacteria in Electrospun Cyclodextrin Ultrathin Fibers for Bioremediation of Heavy Metals and Reactive Dye from Wastewater. *Colloids and Surfaces B: Biointerfaces* **2018**, *161*, 169–176. https://doi.org/10.1016/j.colsurfb.2017.10.047.

(99) Massaglia, G.; Sacco, A.; Chiodoni, A.; Pirri, C. F.; Quaglio, M. Living Bacteria Directly Embedded into Electrospun Nanofibers: Design of New Anode for Bio-Electrochemical Systems. *Nanomaterials* **2021**, *11* (11), 3088. https://doi.org/10.3390/nano11113088.

(100) Sanchez, J.-L.; Laberty-Robert, C. A Novel Microbial Fuel Cell Electrode Design: Prototyping a Self-Standing One-Step Bacteria-Encapsulating Bioanode with Electrospinning. *J. Mater. Chem. B* **2021**, *9* (21), 4309–4318. https://doi.org/10.1039/D1TB00680K.

(101) Jacobsen, N. M. Y.; Caglayan, I.; Caglayan, A.; Bar-Shalom, D.; Müllertz, A. Achieving Delayed Release of Freeze-Dried Probiotic Strains by Extrusion, Spheronization and Fluid Bed Coating - Evaluated Using a Three-Step in Vitro Model. *International Journal of Pharmaceutics* **2020**, *591*, 120022. https://doi.org/10.1016/j.ijpharm.2020.120022.

(102) Cheow, W. S.; Kiew, T. Y.; Hadinoto, K. Controlled Release of Lactobacillus Rhamnosus Biofilm Probiotics from Alginate-Locust Bean Gum Microcapsules. *Carbohydrate Polymers* **2014**, *103*, 587–595. https://doi.org/10.1016/j.carbpol.2014.01.036.

(103) Mei, L.; He, F.; Zhou, R.-Q.; Wu, C.-D.; Liang, R.; Xie, R.; Ju, X.-J.; Wang, W.; Chu, L.-Y. Novel Intestinal-Targeted Ca-Alginate-Based Carrier for pH-Responsive Protection and Release of Lactic Acid Bacteria. *ACS Appl. Mater. Interfaces* **2014**, *6* (8), 5962–5970. https://doi.org/10.1021/am501011j.

(104) Su, Y.; Gu, L.; Zhang, Z.; Chang, C.; Li, J.; McClements, D. J.; Yang, Y. Encapsulation and Release of Egg White Protein in Alginate Microgels: Impact of pH and Thermal Treatment. *Food Res. Int.* **2019**, *120*, 305–311. https://doi.org/10.1016/j.foodres.2019.02.048.

(105) Marounek, M.; Volek, Z.; Taubner, T.; Dušková, D.; Czauderna, M. Effect of Pancreatic Lipase Inhibitor and Sorbent of Lipids on Cholesterolaemia and Faecal Output of Fat in Rats. *bioRxiv* **2020**, 2020.08.06.239335. https://doi.org/10.1101/2020.08.06.239335.

(106) Kianfar, P.; Vitale, A.; Dalle Vacche, S.; Bongiovanni, R. Photo-Crosslinking of Chitosan/Poly(Ethylene Oxide) Electrospun Nanofibers. *Carbohydrate Polymers* **2019**, *217*, 144–151. https://doi.org/10.1016/j.carbpol.2019.04.062.

(107) Çaykara, T.; Demirci, S.; Eroğlu, M. S.; Güven, O. Poly(Ethylene Oxide) and Its Blends with Sodium Alginate. *Polymer* **2005**, *46* (24), 10750–10757. https://doi.org/10.1016/j.polymer.2005.09.041.

(108) Schindelin, J.; Arganda-Carreras, I.; Frise, E.; Kaynig, V.; Longair, M.; Pietzsch, T.; Preibisch, S.; Rueden, C.; Saalfeld, S.; Schmid, B.; Tinevez, J.-Y.; White, D. J.; Hartenstein, V.; Eliceiri, K.; Tomancak, P.; Cardona, A. Fiji: An Open-Source Platform for Biological-Image Analysis. *Nat. Methods* **2012**, *9* (7), 676–682. https://doi.org/10.1038/nmeth.2019.

(109) Thomas, P.; Sekhar, A. C.; Upreti, R.; Mujawar, M. M.; Pasha, S. S. Optimization of Single Plate-Serial Dilution Spotting (SP-SDS) with Sample Anchoring as an Assured Method for Bacterial and Yeast Cfu Enumeration and Single Colony Isolation from Diverse Samples. *Biotechnology Reports* **2015**, *8*, 45–55. https://doi.org/10.1016/j.btre.2015.08.003.

(110) Chao, Y.; Zhang, T. Optimization of Fixation Methods for Observation of Bacterial Cell Morphology and Surface Ultrastructures by Atomic Force Microscopy. *Appl Microbiol Biotechnol* **2011**, *92* (2), 381–392. https://doi.org/10.1007/s00253-011-3551-5.

(111) Becce, M.; Klöckner, A.; G. Higgins, S.; Penders, J.; Hachim, D.; J. Bashor, C.; M. Edwards, A.; M. Stevens, M. Assessing the Impact of Silicon Nanowires on Bacterial Transformation and Viability of Escherichia Coli. *Journal of Materials Chemistry B* **2021**, *9* (24), 4906–4914. https://doi.org/10.1039/D0TB02762F.

(112) Diep, E.; Schiffman, J. D. Ethanol-Free Cross-Linking of Alginate Nanofibers Enables Controlled Release into a Simulated Gastrointestinal Tract Model. *Biomacromolecules* **2023**, *24* (6), 2908–2917. https://doi.org/10.1021/acs.biomac.3c00274.

(113) Ma, G.; Fang, D.; Liu, Y.; Zhu, X.; Nie, J. Electrospun Sodium Alginate/Poly(Ethylene Oxide) Core–Shell Nanofibers Scaffolds Potential for Tissue Engineering Applications. *Carbohydr. Polym.* **2012**, *87* (1), 737–743. https://doi.org/10.1016/j.carbpol.2011.08.055.

(114) Fleming, H. P.; Etchells, J. L.; Costilow, R. N. Microbial Inhibition by an Isolate of Pediococcus from Cucumber Brines 1. *Appl Microbiol* **1975**, *30* (6), 1040–1042.

(115) Millette, M.; Smoragiewicz, W.; Lacroix, M. Antimicrobial Potential of Immobilized Lactococcus Lactis Subsp. Lactis ATCC 11454 against Selected Bacteria. *Journal of Food Protection* **2004**, *67* (6), 1184–1189. https://doi.org/10.4315/0362-028X-67.6.1184.

(116) Bailey, D. N.; Briggs, J. R. The Effect of Ethanol and pH on the Adsorption of Drugs From Simulated Gastric Fluid Onto Activated Charcoal. *Therapeutic Drug Monitoring* **2003**, *25* (3), 310.

(117) Chan, A. W.; Neufeld, R. J. Tuneable Semi-Synthetic Network Alginate for Absorptive Encapsulation and Controlled Release of Protein Therapeutics. *Biomaterials* **2010**, *31* (34), 9040–9047. https://doi.org/10.1016/j.biomaterials.2010.07.111.

(118) Minekus, M.; Alminger, M.; Alvito, P.; Ballance, S.; Bohn, T.; Bourlieu, C.; Carrière, F.; Boutrou, R.; Corredig, M.; Dupont, D.; Dufour, C.; Egger, L.; Golding, M.; Karakaya, S.; Kirkhus, B.; Feunteun, S. L.; Lesmes, U.; Macierzanka, A.; Mackie, A.; Marze, S.; McClements, D. J.; Ménard, O.; Recio, I.; Santos, C. N.; Singh, R. P.; Vegarud, G. E.; Wickham, M. S. J.; Weitschies, W.; Brodkorb, A. A Standardised Static in Vitro Digestion Method Suitable for Food – an International Consensus. *Food Funct.* **2014**, *5* (6), 1113–1124. https://doi.org/10.1039/C3FO60702J.

(119) Zhang, Z.; Zhang, R.; Xiao, H.; Bhattacharya, K.; Bitounis, D.; Demokritou, P.; McClements, D. J. Development of a Standardized Food Model for Studying the Impact of Food Matrix Effects on the Gastrointestinal Fate and Toxicity of Ingested Nanomaterials. *NanoImpact* **2019**, *13*, 13–25. https://doi.org/10.1016/j.impact.2018.11.002.

(120) Bailey, D. N.; Briggs, J. R. The Effect of Ethanol and pH on the Adsorption of Drugs from Simulated Gastric Fluid onto Activated Charcoal. *Ther Drug Monit* **2003**, *25* (3), 310–313. https://doi.org/10.1097/00007691-200306000-00011.

(121) Echalier, C.; Valot, L.; Martinez, J.; Mehdi, A.; Subra, G. Chemical Cross-Linking Methods for Cell Encapsulation in Hydrogels. *Materials Today Communications* **2019**, *20*, 100536. https://doi.org/10.1016/j.mtcomm.2019.05.012.

(122) Shenoy, S. L.; Bates, W. D.; Frisch, H. L.; Wnek, G. E. Role of Chain Entanglements on Fiber Formation during Electrospinning of Polymer Solutions: Good Solvent, Non-Specific Polymer–Polymer Interaction Limit. *Polymer* **2005**, *46* (10), 3372–3384. https://doi.org/10.1016/j.polymer.2005.03.011.

(123) Han, D.; Steckl, A. Coaxial Electrospinning Formation of Complex Polymer Fibers and Their Applications. *ChemPlusChem* **2019**, *84*. https://doi.org/10.1002/cplu.201900434.

(124) McKee, J. W. A.; Kavalieris, L.; Brasch, D. J.; Brown, M. T.; Melton, L. D. Alginate Content and Composition ofMacrocystis Pyrifera from New Zealand. *J Appl Phycol* **1992**, *4* (4), 357–369. https://doi.org/10.1007/BF02185794.

(125) Nie, H.; He, A.; Zheng, J.; Xu, S.; Li, J.; Han, C. C. Effects of Chain Conformation and Entanglement on the Electrospinning of Pure Alginate. *Biomacromolecules* **2008**, *9* (5), 1362–1365. https://doi.org/10.1021/bm701349j.

(126) Fang, D.; Liu, Y.; Jiang, S.; Nie, J.; Ma, G. Effect of Intermolecular Interaction on Electrospinning of Sodium Alginate. *Carbohydr. Polym.* **2011**, *85* (1), 276–279. https://doi.org/10.1016/j.carbpol.2011.01.054.

(127) Lu, J.-W.; Zhu, Y.-L.; Guo, Z.-X.; Hu, P.; Yu, J. Electrospinning of Sodium Alginate with Poly(Ethylene Oxide). *Polymer* **2006**, *47* (23), 8026–8031. https://doi.org/10.1016/j.polymer.2006.09.027.

(128) Islam, Md. S.; Karim, M. R. Fabrication and Characterization of Poly(Vinyl Alcohol)/Alginate Blend Nanofibers by Electrospinning Method. *Colloids Surf, A Physicochem Eng Asp* **2010**, *366* (1), 135–140. https://doi.org/10.1016/j.colsurfa.2010.05.038.

(129) Bhattarai, N.; Zhang, M. Controlled Synthesis and Structural Stability of Alginate-Based Nanofibers. *Nanotechnology* **2007**, *18* (45), 455601. https://doi.org/10.1088/0957-4484/18/45/455601.

(130) Hajiali, H.; Summa, M.; Russo, D.; Armirotti, A.; Brunetti, V.; Bertorelli, R.; Athanassiou, A.; Mele, E. Alginate–Lavender Nanofibers with Antibacterial and Anti-Inflammatory Activity to Effectively Promote Burn Healing. *J. Mater. Chem. B* **2016**, *4* (9), 1686–1695. https://doi.org/10.1039/C5TB02174J.

(131) Ma, Y.; Qi, P.; Ju, J.; Wang, Q.; Hao, L.; Wang, R.; Sui, K.; Tan, Y. Gelatin/Alginate Composite Nanofiber Membranes for Effective and Even Adsorption of Cationic Dyes. *Compos. B. Eng. COMPOS PART B-ENG* **2019**, *162*, 671–677. https://doi.org/10.1016/j.compositesb.2019.01.048.

(132) Mirtič, J.; Balažic, H.; Zupančič, Š.; Kristl, J. Effect of Solution Composition Variables on Electrospun Alginate Nanofibers: Response Surface Analysis. *Polymers* **2019**, *11* (4), 692. https://doi.org/10.3390/polym11040692.

(133) Vigani, B.; Rossi, S.; Milanesi, G.; Bonferoni, M. C.; Sandri, G.; Bruni, G.; Ferrari, F. Electrospun Alginate Fibers: Mixing of Two Different Poly(Ethylene Oxide) Grades to Improve Fiber Functional Properties. *Nanomaterials* **2018**, *8* (12), 971. https://doi.org/10.3390/nano8120971.

(134) Angammana, C. J.; Jayaram, S. H. Analysis of the Effects of Solution Conductivity on Electrospinning Process and Fiber Morphology. *IEEE Transactions on Industry Applications* **2011**, *47* (3), 1109–1117. https://doi.org/10.1109/TIA.2011.2127431.

(135) Fong, H.; Chun, I.; Reneker, D. H. Beaded Nanofibers Formed during Electrospinning. *Polymer* **1999**, *40* (16), 4585–4592. https://doi.org/10.1016/S0032-3861(99)00068-3.

(136) Kazsoki, A.; Szabó, P.; Domján, A.; Balázs, A.; Bozó, T.; Kellermayer, M.; Farkas, A.; Balogh-Weiser, D.; Pinke, B.; Darcsi, A.; Béni, S.; Madarász, J.; Szente, L.; Zelkó, R. Microstructural Distinction of Electrospun Nanofibrous Drug Delivery Systems Formulated with Different Excipients. *Mol. Pharmaceutics* **2018**, *15* (9), 4214–4225. https://doi.org/10.1021/acs.molpharmaceut.8b00646.

(137) Ćirin, D. M.; Poša, M. M.; Krstonošić, V. S. Interactions between Sodium Cholate or Sodium Deoxycholate and Nonionic Surfactant (Tween 20 or Tween 60) in Aqueous Solution. *Ind. Eng. Chem. Res.* **2012**, *51* (9), 3670–3676. https://doi.org/10.1021/ie202373z.

(138) Pérez-Rodríguez, M.; Prieto, G.; Rega, C.; Varela, L. M.; Sarmiento, F.; Mosquera, V. A Comparative Study of the Determination of the Critical Micelle Concentration by Conductivity and Dielectric Constant Measurements. *Langmuir* **1998**, *14* (16), 4422–4426. https://doi.org/10.1021/la980296a.

(139) Durand-Vidal, S.; Bernard, O.; Medoš, Ž.; Bešter-Rogač, M. Theoretical Interpretation of Conductivity Data below and above the CMC: The Case of Alkaline Ion Decanoate Solutions. *J. Mol. Liq.* **2020**, *309*, 112968. https://doi.org/10.1016/j.molliq.2020.112968.

(140) Sethupathy, M.; Sethuraman, V.; Jeyaraman, A. R.; Muthuraja, P.; Manisankar, P. Electrospun Polyethylene Oxide (PEO) Nanofiber Membranes Based Polymer Electrolyte for Dye Sensitized Solar Cell. *AIP Conf. Proc.* **2014**, *1620*, 253–257. https://doi.org/10.1063/1.4898250.

(141) Kim, B.; Yang, J.; Hwang, M.; Choi, J.; Kim, H.-O.; Jang, E.; Lee, J.; Ryu, S.; Suh, J.; Huh, Y.-M.; Haam, S. Aptamer-Modified Magnetic Nanoprobe for Molecular MR Imaging of VEGFR2 on Angiogenic Vasculature. *Nanoscale research letters* **2013**, *8*, 399. https://doi.org/10.1186/1556-276X-8-399.

(142) Jakić, M.; Vrandečić, N. S.; Klarić, I. Thermal Degradation of Poly(Vinyl Chloride)/Poly(Ethylene Oxide) Blends: Thermogravimetric Analysis. *Polymer Degradation and Stability* **2013**, *98* (9), 1738–1743. https://doi.org/10.1016/j.polymdegradstab.2013.05.024.

(143) Kishore, R. S. K.; Pappenberger, A.; Dauphin, I. B.; Ross, A.; Buergi, B.; Staempfli, A.; Mahler, H.-C. Degradation of Polysorbates 20 and 80: Studies on Thermal Autoxidation and Hydrolysis. *J. Pharm. Sci.* **2011**, *100* (2), 721–731. https://doi.org/10.1002/jps.22290.

(144) Liu, Y.; Zhang, C.-J.; Zhao, J.-C.; Guo, Y.; Zhu, P.; Wang, D.-Y. Bio-Based Barium Alginate Film: Preparation, Flame Retardancy and Thermal Degradation Behavior. *Carbohydrate Polymers* **2016**, *139*, 106–114. https://doi.org/10.1016/j.carbpol.2015.12.044.

(145) Soares, J. P.; Santos, J. E.; Chierice, G. O.; Cavalheiro, E. T. G. Thermal Behavior of Alginic Acid and Its Sodium Salt. *Ecl. Quím.* **2004**, *29* (2), 57–63. https://doi.org/10.1590/s0100-46702004000200009.

(146) Sun, N.; Liang, Y.; Xu, Z.; Li, H.; Shaohua, J.; Yibiao, L. The Thermal Degradation Behavior of Meta- and Para- Hetero-Amide Fibers by TGA-FTIR. *Journal of Polymer Engineering* **2013**, *33* (4), 337–344. https://doi.org/10.1515/polyeng-2012-0028.

(147) Canbolat, M. F.; Tang, C.; Bernacki, S. H.; Pourdeyhimi, B.; Khan, S. Mammalian Cell Viability in Electrospun Composite Nanofiber Structures. *Macromol Biosci* **2011**, *11* (10), 1346–1356. https://doi.org/10.1002/mabi.201100108.

(148) Dickson, J. S.; Koohmaraie, M. Cell Surface Charge Characteristics and Their Relationship to Bacterial Attachment to Meat Surfaces. *Appl Environ Microbiol* **1989**, *55* (4), 832–836.

(149) Townsend-Nicholson, A.; Jayasinghe, S. N. Cell Electrospinning: A Unique Biotechnique for Encapsulating Living Organisms for Generating Active Biological Microthreads/Scaffolds. *Biomacromolecules* **2006**, *7* (12), 3364–3369. https://doi.org/10.1021/bm060649h.

(150) Hülsheger, H.; Niemann, E.-G. Lethal Effects of High-Voltage Pulses on E. Coli K12. *Radiat Environ Biophys* **1980**, *18* (4), 281–288. https://doi.org/10.1007/BF01324271.

(151) Yu, D.-G.; Xu, Y.; Li, Z.; Du, L.-P.; Zhao, B.-G.; Wang, X. Coaxial Electrospinning with Mixed Solvents: From Flat to Round Eudragit L100 Nanofibers for Better Colon-Targeted Sustained Drug Release Profiles. *Journal of Nanomaterials* **2014**, *2014*, 1–8. https://doi.org/10.1155/2014/967295.

(152) Ching, S. H.; Bansal, N.; Bhandari, B. Alginate Gel Particles–A Review of Production Techniques and Physical Properties. *Critical Reviews in Food Science and Nutrition* **2017**, *57* (6), 1133–1152. https://doi.org/10.1080/10408398.2014.965773.

(153) Gurikov, P.; Smirnova, I. Non-Conventional Methods for Gelation of Alginate. *Gels* **2018**, *4* (1), 14. https://doi.org/10.3390/gels4010014.

(154) Ning, E.; Turnbull, G.; Clarke, J.; Picard, F.; Riches, P.; Vendrell, M.; Graham, D.; Wark, A. W.; Faulds, K.; Shu, W. 3D Bioprinting of Mature Bacterial Biofilms for Antimicrobial Resistance Drug Testing. *Biofabrication* **2019**, *11* (4), 045018. https://doi.org/10.1088/1758-5090/ab37a0.

(155) Rieger, K. A.; Birch, N. P.; Schiffman, J. D. Designing Electrospun Nanofiber Mats to Promote Wound Healing – a Review. *J. Mater. Chem. B* **2013**, *1* (36), 4531–4541. https://doi.org/10.1039/C3TB20795A.

(156) Zamani, M.; Prabhakaran, M. P.; Ramakrishna, S. Advances in Drug Delivery via Electrospun and Electrosprayed Nanomaterials. *Int J Nanomedicine* **2013**, *8*, 2997–3017. https://doi.org/10.2147/IJN.S43575.

(157) LeRoux, M. A.; Guilak, F.; Setton, L. A. Compressive and Shear Properties of Alginate Gel: Effects of Sodium Ions and Alginate Concentration. *Journal of Biomedical Materials Research* **1999**, *47* (1), 46–53. https://doi.org/10.1002/(SICI)1097-4636(199910)47:1<46::AID-JBM6>3.0.CO;2-N.

(158) Ahmad Raus, R.; Wan Nawawi, W. M. F.; Nasaruddin, R. R. Alginate and Alginate Composites for Biomedical Applications. *Asian Journal of Pharmaceutical Sciences* **2021**, *16* (3), 280–306. https://doi.org/10.1016/j.ajps.2020.10.001.

(159) Gao, C.; Pollet, E.; Avérous, L. Properties of Glycerol-Plasticized Alginate Films Obtained by Thermo-Mechanical Mixing. *Food Hydrocolloids* **2017**, *63*, 414–420. https://doi.org/10.1016/j.foodhyd.2016.09.023.

(160) Li, J.; He, J.; Huang, Y.; Li, D.; Chen, X. Improving Surface and Mechanical Properties of Alginate Films by Using Ethanol as a Co-Solvent during External Gelation. *Carbohydr. Polym.* **2015**, *123*, 208–216. https://doi.org/10.1016/j.carbpol.2015.01.040.

(161) Bhattarai, N.; Li, Z.; Edmondson, D.; Zhang, M. Alginate-Based Nanofibrous Scaffolds: Structural, Mechanical, and Biological Properties. *Adv. Mater.* **2006**, *18*, 1463–1467. https://doi.org/10.1002/adma.200502537.

(162) Dodero, A.; Vicini, S.; Alloisio, M.; Castellano, M. Sodium Alginate Solutions: Correlation between Rheological Properties and Spinnability. *J Mater Sci* **2019**, *54* (10), 8034–8046. https://doi.org/10.1007/s10853-019-03446-3.

(163) Jeong, S. I.; Krebs, M. D.; Bonino, C. A.; Khan, S. A.; Alsberg, E. Electrospun Alginate Nanofibers with Controlled Cell Adhesion for Tissue Engineeringa. *Macromolecular Bioscience* **2010**, *10* (8), 934–943. https://doi.org/10.1002/mabi.201000046.

(164) Wongkanya, R.; Chuysinuan, P.; Pengsuk, C.; Techasakul, S.; Lirdprapamongkol, K.; Svasti, J.; Nooeaid, P. Electrospinning of Alginate/Soy Protein Isolated Nanofibers and Their Release Characteristics for Biomedical Applications. *Journal of Science: Advanced Materials and Devices* **2017**, *2* (3), 309–316. https://doi.org/10.1016/j.jsamd.2017.05.010.

(165) Wang, H.; Wang, Y.; Li, C.; Jia, L. Fabrication of Eco-Friendly Calcium Crosslinked Alginate Electrospun Nanofibres for Rapid and Efficient Removal of Cu(II). *International Journal of Biological Macromolecules* **2022**, *219*, 1–10. https://doi.org/10.1016/j.ijbiomac.2022.07.221.

(166) Ingram, L. O. Ethanol Tolerance in Bacteria. *Critical Reviews in Biotechnology* **1989**, *9* (4), 305–319. https://doi.org/10.3109/07388558909036741.

(167) Kitagaki, H.; Araki, Y.; Funato, K.; Shimoi, H. Ethanol-Induced Death in Yeast Exhibits Features of Apoptosis Mediated by Mitochondrial Fission Pathway. *FEBS Letters* **2007**, *581* (16), 2935–2942. https://doi.org/10.1016/j.febslet.2007.05.048.

(168) Hoek, J. B.; Pastorino, J. G. Ethanol, Oxidative Stress, and Cytokine-Induced Liver Cell Injury. *Alcohol* **2002**, *27* (1), 63–68. https://doi.org/10.1016/S0741-8329(02)00215-X.

(169) Cartwright, M. M.; Smith, S. M. Increased Cell Death and Reduced Neural Crest Cell Numbers in Ethanol-Exposed Embryos: Partial Basis for the Fetal Alcohol Syndrome Phenotype. *Alcoholism: Clinical and Experimental Research* **1995**, *19* (2), 378–386. https://doi.org/10.1111/j.1530-0277.1995.tb01519.x.

(170) Remmer, H.; Kessler, W.; Einsele, H.; Hintze, Th.; De Toranzo, G. D.; Gharaibeh, A. M.; Frank, H. Ethanol Promotes Oxygen-Radical Attack on Proteins But Not on Lipids. *Drug Metabolism Reviews* **1989**, *20* (2–4), 219–232. https://doi.org/10.3109/03602538909103538.

(171) Guo, L.; Yang, J. Y.; Wu, C. F. Oxidative DNA Damage Induced by Ethanol in Mouse Peripheral Leucocytes. *Basic Clin Pharmacol Toxicol* **2008**, *103* (3), 222–227. https://doi.org/10.1111/j.1742-7843.2008.00258.x.

(172) Wang, Q.; Ju, J.; Tan, Y.; Hao, L.; Ma, Y.; Wu, Y.; Zhang, H.; Xia, Y.; Sui, K. Controlled Synthesis of Sodium Alginate Electrospun Nanofiber Membranes for Multi-Occasion Adsorption and Separation of Methylene Blue. *Carbohydrate Polymers* **2019**, *205*, 125–134. https://doi.org/10.1016/j.carbpol.2018.10.023.

(173) Stone, S. A.; Gosavi, P.; Athauda, T. J.; Ozer, R. R. In Situ Citric Acid Crosslinking of Alginate/Polyvinyl Alcohol Electrospun Nanofibers. *Mater. Lett.* **2013**, *112*, 32–35. https://doi.org/10.1016/j.matlet.2013.08.100.

(174) Zazzali, I.; Aguirre Calvo, T. R.; Pizones Ruíz-Henestrosa, V. M.; Santagapita, P. R.; Perullini, M. Effects of pH, Extrusion Tip Size and Storage Protocol on the Structural Properties of Ca(II)-Alginate Beads. *Carbohydr. Polym.* **2019**, *206*, 749–756. https://doi.org/10.1016/j.carbpol.2018.11.051.

(175) da Silva, M. A.; Bierhalz, A. C. K.; Kieckbusch, T. G. Alginate and Pectin Composite Films Crosslinked with Ca2+ Ions: Effect of the Plasticizer Concentration. *Carbohydrate Polymers* **2009**, *77* (4), 736–742. https://doi.org/10.1016/j.carbpol.2009.02.014.

(176) Smrdel, P.; Bogataj, M.; Mrhar, A. The Influence of Selected Parameters on the Size and Shape of Alginate Beads Prepared by Ionotropic Gelation. *Sci Pharm* **2008**, *76* (1), 77–89. https://doi.org/10.3797/scipharm.0611-07.

(177) Reddy, S.; Pandit, A.; Thakur, A. Effects of Crosslink Agents on Sodium Alginate and Lignosulphonic Acid Blends. *Polym-Korea.* **2016**. https://doi.org/10.7317/PK.2016.40.1.63.

(178) Davarcı, F.; Turan, D.; Ozcelik, B.; Poncelet, D. The Influence of Solution Viscosities and Surface Tension on Calcium-Alginate Microbead Formation Using Dripping Technique. *Food Hydrocolloids* **2017**, *62*, 119–127. https://doi.org/10.1016/j.foodhyd.2016.06.029.

(179) Wang, X.; Feng, Y.; Feng, T.; Wang, X.; Xia, S.; Zhang, X. Modulation Effect of Glycerol on Plasticization and Water Distribution of Vacuum-Dried Calcium Alginate Gel Beads Encapsulating Peppermint Oil/β-Cyclodextrin Complex. *Food Biosci.* **2021**, *41*, 100968. https://doi.org/10.1016/j.fbio.2021.100968.

(180) Chuang, J.-J.; Huang, Y.-Y.; Lo, S.-H.; Hsu, T.-F.; Huang, W.-Y.; Huang, S.-L.; Lin, Y.-S. Effects of pH on the Shape of Alginate Particles and Its Release Behavior. *International Journal of Polymer Science* **2017**, *2017*, e3902704. https://doi.org/10.1155/2017/3902704.

(181) Del Gaudio, P.; Colombo, P.; Colombo, G.; Russo, P.; Sonvico, F. Mechanisms of Formation and Disintegration of Alginate Beads Obtained by Prilling. *International Journal of Pharmaceutics* **2005**, *302* (1), 1–9. https://doi.org/10.1016/j.ijpharm.2005.05.041.

(182) Chan, E.-S.; Lim, T.-K.; Voo, W.-P.; Pogaku, R.; Tey, B. T.; Zhang, Z. Effect of Formulation of Alginate Beads on Their Mechanical Behavior and Stiffness. *Particuology* **2011**, *9* (3), 228–234. https://doi.org/10.1016/j.partic.2010.12.002.

(183) Azucena Castro-Yobal, M.; Contreras-Oliva, A.; Saucedo-Rivalcoba, V.; Rivera-Armenta, J. L.; Hernández-Ramírez, G.; Salinas-Ruiz, J.; Herrera-Corredor, A. Evaluation of Physicochemical Properties of Film-Based Alginate for Food Packing Applications. *e-Polymers* **2021**, *21* (1), 82–95. https://doi.org/10.1515/epoly-2021-0011.

(184) Giz, A. S.; Berberoglu, M.; Bener, S.; Aydelik-Ayazoglu, S.; Bayraktar, H.; Alaca, B. E.; Catalgil-Giz, H. A Detailed Investigation of the Effect of Calcium Crosslinking and Glycerol Plasticizing on the Physical Properties of Alginate Films. *Int. J. Biol. Macromol.* **2020**, *148*, 49–55. https://doi.org/10.1016/j.ijbiomac.2020.01.103.

(185) Cui, S.; Yao, B.; Gao, M.; Sun, X.; Gou, D.; Hu, J.; Zhou, Y.; Liu, Y. Effects of Pectin Structure and Crosslinking Method on the Properties of Crosslinked Pectin Nanofibers. *Carbohydrate Polymers* **2017**, *157*, 766–774. https://doi.org/10.1016/j.carbpol.2016.10.052.

(186) Lotsari, A.; Rajasekharan, A. K.; Halvarsson, M.; Andersson, M. Transformation of Amorphous Calcium Phosphate to Bone-like Apatite. *Nat Commun* **2018**, *9* (1), 4170. https://doi.org/10.1038/s41467-018-06570-x.

(187) Pillay, V.; Fassihi, R. In Vitro Release Modulation from Crosslinked Pellets for Site-Specific Drug Delivery to the Gastrointestinal Tract: I. Comparison of pH-Responsive Drug Release and Associated Kinetics. *J Control Release* **1999**, *59* (2), 229–242. https://doi.org/10.1016/S0168-3659(98)00196-5.

(188) Tlaskalová-Hogenová, H.; Štěpánková, R.; Kozáková, H.; Hudcovic, T.; Vannucci, L.; Tučková, L.; Rossmann, P.; Hrnčíř, T.; Kverka, M.; Zákostelská, Z.; Klimešová, K.; Přibylová, J.; Bártová, J.; Sanchez, D.; Fundová, P.; Borovská, D.; Šrůtková, D.; Zídek, Z.; Schwarzer, M.; Drastich, P.; Funda, D. P. The Role of Gut Microbiota (Commensal Bacteria) and the Mucosal Barrier in the Pathogenesis of Inflammatory and Autoimmune Diseases and Cancer: Contribution of Germ-Free and Gnotobiotic Animal Models of Human Diseases. *Cell Mol Immunol* **2011**, *8* (2), 110–120. https://doi.org/10.1038/cmi.2010.67.

(189) Wang, C.-Z.; Ma, X.-Q.; Yang, D.-H.; Guo, Z.-R.; Liu, G.-R.; Zhao, G.-X.; Tang, J.; Zhang, Y.-N.; Ma, M.; Cai, S.-Q.; Ku, B.-S.; Liu, S.-L. Production of Enterodiol from Defatted Flaxseeds through Biotransformation by Human Intestinal Bacteria. *BMC Microbiol* **2010**, *10* (1), 115. https://doi.org/10.1186/1471-2180-10-115.

(190) Medzhitov, R.; Janeway, Charles. J. Innate Immune Recognition: Mechanisms and Pathways. *Immunol Rev* **2000**, *173* (1), 89–97. https://doi.org/10.1034/j.1600-065X.2000.917309.x.

(191) Chapman, C. M. C.; Gibson, G. R.; Rowland, I. Health Benefits of Probiotics: Are Mixtures More Effective than Single Strains? *Eur J Nutr* **2011**, *50* (1), 1–17. https://doi.org/10.1007/s00394-010-0166-z.

(192) Sovadinová, I.; Kuroda, K.; Palermo, E. F. Unexpected Enhancement of Antimicrobial Polymer Activity against Staphylococcus Aureus in the Presence of Fetal Bovine Serum. *Molecules* **2021**, *26* (15), 4512. https://doi.org/10.3390/molecules26154512.

(193) Nguyen, L. T.; Haney, E. F.; Vogel, H. J. The Expanding Scope of Antimicrobial Peptide Structures and Their Modes of Action. *Trends in Biotechnology* **2011**, *29* (9), 464–472. https://doi.org/10.1016/j.tibtech.2011.05.001.

(194) Burgain, J.; Gaiani, C.; Linder, M.; Scher, J. Encapsulation of Probiotic Living Cells: From Laboratory Scale to Industrial Applications. *Journal of Food Engineering* **2011**, *104* (4), 467–483. https://doi.org/10.1016/j.jfoodeng.2010.12.031.

(195) Song, D.; Ibrahim, S.; Hayek, S.; Song, D.; Ibrahim, S.; Hayek, S. Recent Application of Probiotics in Food and Agricultural Science. In *Probiotics*; IntechOpen, 2012. https://doi.org/10.5772/50121.

(196) Foligné, B.; Daniel, C.; Pot, B. Probiotics from Research to Market: The Possibilities, Risks and Challenges. *Current Opinion in Microbiology* **2013**, *16* (3), 284–292. https://doi.org/10.1016/j.mib.2013.06.008.

(197) Kailasapathy, K. Microencapsulation of Probiotic Bacteria: Technology and Potential Applications. *Curr Issues Intest Microbiol* **2002**, *3* (2), 39–48.

(198) D'Accolti, M.; Soffritti, I.; Bonfante, F.; Ricciardi, W.; Mazzacane, S.; Caselli, E. Potential of an Eco-Sustainable Probiotic-Cleaning Formulation in Reducing Infectivity of Enveloped Viruses. *Viruses* **2021**, *13* (11), 2227. https://doi.org/10.3390/v13112227.

(199) Spök, A.; Arvanitakis, G.; McClung, G. Status of Microbial Based Cleaning Products in Statutory Regulations and Ecolabelling in Europe, the USA, and Canada. *Food and Chemical Toxicology* **2018**, *116*, 10–19. https://doi.org/10.1016/j.fct.2017.12.057.

(200) Stone, W.; Tolmay, J.; Tucker, K.; Wolfaardt, G. M. Disinfectant, Soap or Probiotic Cleaning? Surface Microbiome Diversity and Biofilm Competitive Exclusion. *Microorganisms* **2020**, *8* (11), 1726. https://doi.org/10.3390/microorganisms8111726.

(201) Gillor, O.; Etzion, A.; Riley, M. A. The Dual Role of Bacteriocins as Anti- and Probiotics. *Appl Microbiol Biotechnol* **2008**, *81* (4), 591–606. https://doi.org/10.1007/s00253-008-1726-5.

(202) Cerchiara, T.; Giordani, B.; Melgoza, L. M.; Prata, C.; Parolin, C.; Dalena, F.; Abruzzo, A.; Bigucci, F.; Luppi, B.; Vitali, B. New Spanish Broom Dressings Based on Vitamin E and Lactobacillus Plantarum for Superficial Skin Wounds. *Journal of Drug Delivery Science and Technology* **2020**, *56*, 101499. https://doi.org/10.1016/j.jddst.2020.101499.

(203) Valdéz, J. C.; Peral, M. C.; Rachid, M.; Santana, M.; Perdigón, G. Interference of Lactobacillus Plantarum with Pseudomonas Aeruginosa in Vitro and in Infected Burns: The Potential Use of Probiotics in Wound Treatment. *Clinical Microbiology and Infection* **2005**, *11* (6), 472–479. https://doi.org/10.1111/j.1469-0691.2005.01142.x.

(204) Tan, L. L.; Sampathkumar, K.; Wong, J. H.; Loo, S. C. J. Divalent Cations Are Antagonistic to Survivability of Freeze-Dried Probiotics Encapsulated in Cross-Linked Alginate. *Food and Bioproducts Processing* **2020**, *124*, 369–377. https://doi.org/10.1016/j.fbp.2020.09.013.

(205) *MRSA | CDC*. https://www.cdc.gov/mrsa/ (accessed 2023-04-20).

(206) Piewngam, P.; Khongthong, S.; Roekngam, N.; Theapparat, Y.; Sunpaweravong, S.; Faroongsarng, D.; Otto, M. Probiotic for Pathogen-Specific Staphylococcus Aureus Decolonisation in Thailand: A Phase 2, Double-Blind, Randomised, Placebo-Controlled Trial. *Lancet Microbe* **2023**, *4* (2), e75–e83. https://doi.org/10.1016/S2666-5247(22)00322-6.

(207) Silva, D. R.; Sardi, J. de C. O.; Pitangui, N. de S.; Roque, S. M.; Silva, A. C. B. da; Rosalen, P. L. Probiotics as an Alternative Antimicrobial Therapy: Current Reality and Future Directions. *Journal of Functional Foods* **2020**, *73*, 104080. https://doi.org/10.1016/j.jff.2020.104080.

(208) Spelhaug, S. R.; Harlander, S. K. Inhibition of Foodborne Bacterial Pathogens by Bacteriocins from Lactococcus Lactis and Pediococcus Pentosaceous. *Journal of Food Protection* **1989**, *52* (12), 856–862. https://doi.org/10.4315/0362-028X-52.12.856.

(209) Ramezani, M.; Rezazadeh Zarandi, E.; Zainodini, N.; Bahramabadi, R.; Assar, S. Effects of Nisin on the Expression of Virulence Genes of Methicillin-Resistant/Sensitive Staphylococcus Aureus. *Iran J Microbiol* **2022**, *14* (6), 874–880. https://doi.org/10.18502/ijm.v14i6.11262.

(210) Bamigbade, G. B.; Subhash, A. J.; Kamal-Eldin, A.; Nyström, L.; Ayyash, M. An Updated Review on Prebiotics: Insights on Potentials of Food Seeds Waste as Source of Potential Prebiotics. *Molecules* **2022**, *27* (18), 5947. https://doi.org/10.3390/molecules27185947.

(211) Rajam, R.; Anandharamakrishnan, C. Microencapsulation of Lactobacillus Plantarum (MTCC 5422) with Fructooligosaccharide as Wall Material by Spray Drying. *LWT - Food Science and Technology* **2015**, *60* (2, Part 1), 773–780. https://doi.org/10.1016/j.lwt.2014.09.062.

(212) Meng, X.; Du, Y.; Liu, Y.; Coughlin, E. B.; Perry, S. L.; Schiffman, J. D. Electrospinning Fibers from Oligomeric Complex Coacervates: No Chain Entanglements Needed. *Macromolecules* **2021**, *54* (11), 5033–5042. https://doi.org/10.1021/acs.macromol.1c00397.

(213) Bauer, A. W.; Kirby, W. M. M.; Sherris, J. C.; Turck, M. Antibiotic Susceptibility Testing by a Standardized Single Disk Method. *American Journal of Clinical Pathology* **1966**, *45* (4_ts), 493–496. https://doi.org/10.1093/ajcp/45.4_ts.493.

(214) Balouiri, M.; Sadiki, M.; Ibnsouda, S. K. Methods for in Vitro Evaluating Antimicrobial Activity: A Review. *Journal of Pharmaceutical Analysis* **2016**, *6* (2), 71–79. https://doi.org/10.1016/j.jpha.2015.11.005.